Impact of small organic molecules on the nucleation of calcium silicate hydrate

Lina Bouzouaid

Thèse de doctorat de l'établissement université Bourgogne Franche Comté préparée à l'université Bourgogne Franche Comté

Ecole doctorale n°553

Carnot Pasteur

Doctorat de spécialité chimie physique

Par

BOUZOUAID Lina

IMPACT OF SMALL ORGANIC MOLECULES ON THE NUCLEATION AND GROWTH OF C-S-H, THE MAIN HYDRATE OF CEMENT

Thèse présentée et soutenue à l'université Bourgogne Franche Comté, le 25 novembre 2021

Composition du jury :

Pirio Nadine	Professeure (ICMUB-CNRS, UBFC, Dijon)	Présidente du jury
Veesler Stéphane	Directeur de recherche (CINaM-CNRS, AMU, Marseille)	Rapporteur
Daval Damien	Chargé de recherche (ISTerre-CNRS, UGA, Grenoble)	Rapporteur
D'Espinose Jean-Baptiste	Professeur (SIMM-CNRS, Paris)	Examinateur
Wieland Erich	Chargé de recherche (PSI, Villigen)	Examinateur
Labbez Christophe	Chargé de recherche (ICB-CNRS, UBFC, Dijon)	Directeur de thèse
Fernandez-Martinez Alejandro	Chargé de recherche (ISTerre-CNRS, UGA, Grenoble)	Co-encadrant de thèse
Lothenbach Barbara	Professeure (EMPA, Dübendorf)	Co-encadrante de thèse

AKNOWLEDGMENTS

This thesis was carried out at the Carnot Interdisciplinary Laboratory in Burgundy (ICB), at the university of Grenoble (ISterre) and at the federal laboratory EMPA. This project was funded by Nanocem, a consortium of industrialists and academics who collaborate to improve their knowledge of building materials.

This thesis was made possible thanks to the help of several people to whom I would like to express my gratitude. First of all, I would like to express my gratitude to my pHD director Christophe Labbez, for his help, patience and availability. I would also like to thank my co-directors, Barbara Lothenbach and Alejandro Fernandez-Martinez for providing me the necessary tools I needed to facilitate my work.

I would like to especially thank and express my gratitude to Sarra, David, Karen, Luigi, Sarah for their precious help during my laboratory work. Sarra, thank you for giving me moral support throughout my journey, I will not forget it.

A big thank you to the industrial team who accompanied me during these years: Josephine H.Cheung, Vanessa Kocaba, Martin Mosquet, Patrick Juilland and of course Luis Pegado! Thank you again for your advices and help to improve myself.

I am also very thankfull to the examiners, Jean-Baptiste d'Espinose and Erich Wieland, but also the rapporteurs Damien Daval and Stephane Veesler. Thank you very much for accepting to report and examine the thesis.

Finally I would like to thank my family, particularly my parents and my older brother, Isshaq, who helped me a lot morally when I was stressed.

TABLE OF CONTENT

INTRODUCTION

This work is a continuation of Camille Nallet's PhD thesis on the influence of organic admixtures on the hydration of ordinary Portland cement (OPC). The present work is devoted to the study of the influence of small organic molecules on the nucleation of C-S-H and portlandite but also on the driving force of the nucleation. It was carried out at the *Laboratoire Interdisciplinaire Carnot de Bourgogne* (ICB - Dijon) in close collaboration with the *Swiss Federal Laboratories for Materials Science & Technology* (Empa - Duebendorf) and the *Institut des sciences de la Terre* (ISTerre– Grenoble) and was financed by Nanocem, a consortium of industrial and academic partners working together to improve their knowledge on building materials. The goal of the thesis project was twofold: first, to provide quantitative experimental data, which can serve as a basis for simulations at the atomic and mesoscopic scales; and second to contribute to the fundamental understanding on the influence of organic additives on the hydration of OPC, in particular on its retardation.

Cement has already been used by the Romans and, when combined with aggregates, has gradually replaced ashlar as the material of choice for construction, due to its simplicity of use and its wide availability. Behind this apparent simplicity, the physical and chemical processes involved in its hydration and setting are still the subject of ongoing research. From an academic point of view, this is explained by the complexity of the system and processes involved. Indeed, cement is polyphasic and can be described as a granular system that gradually transforms into a colloidal system (attractive colloidal glass) during hydration. Moreover, hydration involves two of the most complex physico-chemical processes, namely dissolution (of the cement grains) and nucleation/growth (of the hydrates), two processes occurring simultaneously. From a societal point of view, production of cement clinker is estimated to contribute 8 to 10% to the anthropogenic CO_2 emissions. Finding solutions to this problem can only benefit a better understanding of the mechanisms underlying hydration.

Organic admixtures with specific functions are used to control the workability of the fresh paste and the kinetic of the hardening reaction. This is the case, for example, of high performance concrete where superplasticizers are used as water reducers to increase the mechanical strength of the finished material. It is also the case of low clinker cements (low carbon emitters), where there is a need to find specific additives to improve the fluidity/workability of the fresh paste. However, most of these organic admixtures have the side effect of retarding the hydration (and setting) of the cement, which is particularly a problem for the development of greener cements, which typically have a lower clinker content and thus a lower reactivity.

The research carried out on this issue remains fragmentary and the mechanisms involved poorly understood. Indeed, if the effect of many admixtures on the hydration of cement has been observed and characterized, only a very few studies have investigated in depth their effects on the dissolution and precipitation processes separately. This is particularly true for the precipitation of hydrates. This limited knowledge is not very surprising since the elucidation of the reaction pathways of the dissolution of the silicate phases of cement, tricalcium silicate, and of the nucleation of the main cement hydrate, calcium silicate hydrate (C-S-H), is only very recent. For the record, the process limiting the hydration of cement without admixture is still under debate! Another reason is the difficulty to determine the driving force of dissolution and precipitation in the presence of admixture, without which any quantification is impossible. This is explained by the strong complexation power of the admixtures with ions, the complexity of admixture composition and the difficulty to characterize and model it. The effective development of new organic admixtures with controlled effects seems difficult as long as the mechanisms at their origin have not been quantified, fully understood and linked to the particularity of the organic compounds used.

As such, the present study aims at determining and modelling the complex formation of small organic molecules with Ca and other ions, and at investigating its influence on the homogeneous nucleation and pre-nucleation processes of C-S-H. Small organic molecules were used as model for cement admixtures. In particular, we focused on sodium gluconate, which shares the same charge functionality as poly carboxylate ether (PCE) based superplasticizers and three neutral sugar molecules (hexitols) which only differ from their stereochemistry. As the hydration of the main cement clinker, C_3S, involves its dissolution and the precipitation not only of C-S-H but also of portlandite, the study also focused on the nucleation of portlandite and the comparison of the influence of organics on the precipitation and dissolution kinetics. We were also interested in linking the nucleation kinetics to the adsorption of the organic molecules.

To achieve these objectives, the first chapter first recalls the basic concepts and information from the literature necessary for the study. The second chapter describes the strategy followed regarding the choice of materials and methods used to carry out this work. Then, a third chapter presents the different results obtained through three consecutive papers, which are further discussed in the fourth chapter. Finally, conclusions and perspectives to this thesis are presented.

CHAPTER I. GENERAL PRESENTATION

1. Basic concepts of thermodynamics and kinetics

The precipitations and dissolution of mineral phases are dependent on thermodynamics of the aqueous and solid phases. In this chapter, we introduce the fundamental thermodynamic concepts and review the key principles of precipitation, which are pivotal to the understanding of cement hydration described in Chapter II.

1.1 Solubility

By definition the solubility of a mineral is the number of moles of pure solid that will dissolve in a liter of solvent at a given temperature. In other words solubility is a measure of the analytical composition of a saturated solution expressed as a proportion of a designated solute in a designated solvent (1). For the general case let us consider the following solubility equilibrium of a solid containing chemical species A, B, ..., X:

$$A_{\nu_A}B_{\nu_B}\ldots X_{\nu_X} \leftrightarrow \nu_A A + \nu_B B + \ldots + \nu_X X \quad [1]$$

At equilibrium, the solubility *s* is then defined as

$$s = \frac{c_X}{\nu_X} \quad [2]$$

Where c_X is the concentration of chemical species X. Equilibrium further imposes the following equality for the chemical potential:

$$\Delta\mu_s = \mu_{solid} - (\nu_A\mu_A + \nu_B\mu_B + \ldots + \nu_X\mu_X) = 0 \quad [3]$$

where the chemical potential is a function of the standard chemical potential, $\mu^0(T)$, and activity, *a*, of the species i

$$\mu_i(T) = \mu_i^0 + RT\ln a_i \quad [4]$$

By convention the activity of pure solid is set to 1. *R* and *T* are respectively the gas constant and the temperature. Eqs. [3] and [4] leads to the definition of the solubility product, $K_s(T)$ and standard Gibbs free energy change of the reaction of a solid, $\Delta_r G_s^0$, which at equilibrium reads

$$a_A^{\nu_A} a_B^{\nu_B} \ldots a_X^{\nu_X} = exp(\Delta_r G_s^0/RT) = K_s(T) \quad [5]$$

with

$$\Delta_r G_s^0(T) = \mu_s^0(T) - \nu_A\mu_A^0(T) - \nu_B\mu_B^0(T) - \ldots - \nu_X\mu_X^0(T) \quad [6]$$

Note that $\Delta_r G_s^0$ and K_s as well as μ^0 are *only dependent on the temperature*. It is also good to notice from the definition of $\Delta_r G^0_s$, Eqs [5-6], that $\Delta\mu_s$ defined in equation [3] is nothing but a measure of the departure from equilibrium. As it will be further illustrated later, $\Delta\mu_s$ is the *driving force* for the precipitation and dissolution. This is thus an essential quantity to determine when one is interested to compare the effect of various organic molecules on the precipitation and dissolution of solid phases. However, it is a task, which turns out to be complicate and tedious when complexation occurs.

1.2 Complexation

In the particular case of an ideal solution, where the activities and concentration of species are equal, i.e. their activity coefficent (γ_i) ($a_i = \gamma_i c_i$) is unity, the solubility product could be directly obtained by measuring the ion concentrations or solubility because

$K_s = (\nu_A s)^{\nu_A}(\nu_B s)^{\nu_B}\ldots(\nu_X s)^{\nu_X}$ for ideal solutions [7]

but in water , it is not as simple as the activity coefficient does not equal to 1 and

$K_s = \prod(\frac{\nu_i s}{\gamma_i})^{\nu_i}$ in the general case. [8]

As it can be seen from the previous equation, one further needs to determine the activity coefficient, γ_i which is, not entering the details, a normalized measure of the mean interactions felt by the species in solutions (γ_i > 1 for repulsive interactions, γ_i < 1 for attractive interactions). The latter is solved using a speciation model and is straightforwardly obtained with simple and common salt solutions for which parameterized models are available. As an illustration Figure 1 gives the variation of the solubility of portlandite in aqueous solution with addition of NaCl.

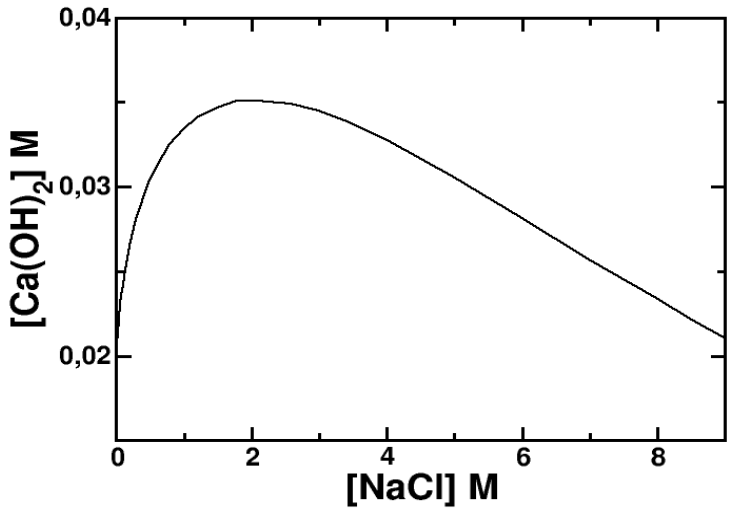

Figure 1 Calculated portlandite solubility in the $Ca(OH)_2$ -NaCl system at 25°C

When complexation of ions with organic molecules occurs, things become more complicate as the total concentration of e.g. calcium is not only influenced by the concentration of free Ca^{2+} ion but also by the concentration of complexed calcium. As an example if one considers the solubility of portlandite

$Ca(OH)_2(s) \leftrightarrow Ca^{2+} + 2OH^-$ [9]

in presence of an organic molecule, Org, that forms complexes with Ca and OH such as

$OrgCaOH^+ \leftrightarrow Org + Ca^{2+} + OH^-$ [10]

with the associated equilibrium constant defined as

$$K_{OrgCaOH^+} = \frac{a_{Org} \cdot a_{Ca^{2+}} \cdot a_{OH^-}}{a_{OrgCaOH^+}}, \quad [11]$$

the concentration of calcium in equilibrium with portlandite depends on the quantity of the complex as well

$$c_{Ca}^{tot} = c_{Ca^{2+}}^{free} + c_{OrgCaOH^+} \quad [12]$$

However, this property can be used to our advantage to determine the complexation constants and the speciation of ions in presence of organic molecules by measuring the solubility of solid minerals, where the solubility product is known. This is one of the strategy used in my work to determine the ion speciation in presence of small organic molecules.

1.3 Supersaturation

The transition from liquid to solid happens because the free energy of the initial solutions phase is higher than the sum of the final solution phase plus the crystalline phase (2). In the same manner, the logic can be pursued in term of chemical activities, where the activity product of the reactants goes beyond the equilibrium activity product of the reactants, the latter being the ionic compounds of C-S-H in this present study.

To identify specifically the driving force of nucleation/growth of C-S-H, the reasoning focuses on the change of chemical potential Δμ of the components that crystallize into the new phase (2)(16), this new phase being nuclei/small particles of C-S-H.

Thus, Δμ is related to the activity product of the reactants in the solution, AP, and to the solubility product of the solid (K_s). Combining Equations [3] and [4] leads to:

$$\Delta\mu = K_B T \cdot \ln\left(\frac{AP}{K_{sp}}\right) \quad [13]$$

where AP is defined as the product of the actual activities of species *i* taking part in the reaction

$$AP = \prod_{i=0}^{N} a_i \quad [14]$$

However, the saturation index (SI) is more used than Δμ when it comes to the study of crystal growth. Thus, the following equation is more pertinent to use :

$$SI = \log\left(\frac{AP}{K_s}\right) \quad [15]$$

If SI is positive, the solution is supersaturated, if SI is negative it is undersaturated, and 0 indicates equilibrium with respect to the solid.

The saturation index is thus as measure to what extent a solution is out of equilibrium and represents the thermodynamic driving force for precipitation.

1.4 Nucleation

Nucleation is defined as a localized emergence of a distinct thermodynamic phase, a nuclei that can be described as a seed substance for crystallization, at nanometric scale, which macroscopically grows with the attachment of growth particles. (3)

Nucleation is, thus, a reaction that marks the passage from an old phase to a new phase, e.g. from a liquid to a solid. We distinguish homogeneous from heterogeneous nucleation.

Homogenous nucleation indicates precipitates that form randomly in a perfect medium (4) (5): it is observed in supersonic nozzles for example (6), but also in explosion where spontaneous and homogeneous nucleation occurs in the cold liquid with the formation of vapor in a very short period of time (7).

Heterogeneous nucleation involves the formation of nuclei on the surface of a foreign substrate (8).

As we have just seen a necessary condition for which nucleation and then growth of the formed nuclei occur is a saturation index larger than zero, SI>0. In other words, nucleation can only happen when the free energy of the old phase become higher than the free energy of the new one. Although necessary, this condition is in fact not sufficient, because nucleation is an activated process and, for the same reason, is a *rare* event. We shall illustrate this in the context of homogeneous nucleation with, to date, the most used theory, namely the classical nucleation theory (CNT).

1.4.1 Thermodynamics

Thermodynamic aspects of CNT are described by the fundamental approach to the description of heterogeneous systems, already developed a century ago by J. W. Gibbs, initially in application to condensation and boiling (9).

In the CNT, a nuclei is regarded as a sphere of a condensed phase. The Gibbs free energy of formation of a nucleus is decomposed in the CNT as the sum of two Gibbs free energy of formation, that of the surface and of the volume, which for a sphere of radius r can be written as (10) (11) :

$$\Delta G(r) = 4\pi r^2\gamma + \frac{4}{3}\pi r^3 . \Delta G(v) \qquad [16]$$

Where γ is the surface free energy per unit area and $\Delta G(v)$ the free energy per unit volume of a crystal. The latter is expressed as the difference between the free energy of the monomer in the crystal and in solution :

$$\Delta G(v) = \frac{-RT\ln S}{V_m} \qquad [17]$$

with V_m the molar volume of the crystal and S the supersaturation ($S=AP/K_{sp}$).

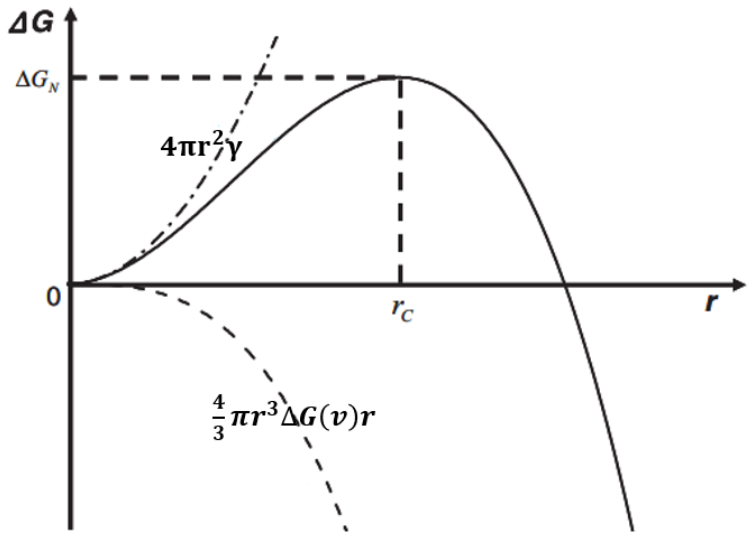

Figure 2 : Plot for crystallization free energy vs. particle radius (solid line). The cross-over of the bulk with the volume term $\frac{4}{3}\pi r^3 \Delta G(v)$ and surface terms $4\pi r^2 \gamma$ (in dashed lines) combined with their opposing signs leads to a free energy barrier. r_c and ΔG_N are the critical radius of the nucleus and the corresponding free energy.

As illustrated in Fig. 2, the volume term, $4/3\pi r^3 \Delta G(v)$, is negative (when $SI>0$) and decreases as r^3, whereas the surface term, $4\pi r^2 \gamma$ is always positive and varies as r^2.

As a consequence, $\Delta G(r)$, which is the sum of these two terms, goes through a free energy maximum, ΔG_N, at a critical cluster size, r_c, as illustrated in Fig.2

This corresponds to the *activation energy* for homogeneous nucleation, which is expressed in the CNT as

$$\Delta G_N = \frac{16\pi\gamma^3 {v_m}^2}{3(kT\ln S)^2} \qquad [18]$$

where v_m is the molecular volume, $v_m = V_m/Na$ with Na the Avogadro number. The critical radius, r_c, can be expressed as

$$r_c = \frac{2\gamma V_m}{RT\ln S} \qquad [19]$$

The rate of homogeneous nucleation takes the form of an Arrhenius law, and is defined as

$$J_N = A\mathrm{e}^{\left(\frac{-\Delta G_N}{k_B T}\right)} \qquad [20]$$

where A is the kinetic prefactor and k_B, the Boltzmann constant.

The presence of the energy barrier ΔG_N (that can be also written as $\Delta G(r_c)$, see figure above) induces a supersaturation level for homogeneous nucleation that is much higher than that for the growth of the formed particles.

Based on equations [18] and [20], it is clear that the temperature, but also the surface energy γ and the saturation index SI greatly affect the rate of nucleation. In particular, it can be seen from equation [18] that the Gibbs free energy barrier to the nucleation varies as the square of *SI* and the cube of the surface tension. As an example, Figure 3 illustrates how strongly the induction time until nucleation, being the reciprocal to J_N, varies with the saturation index.

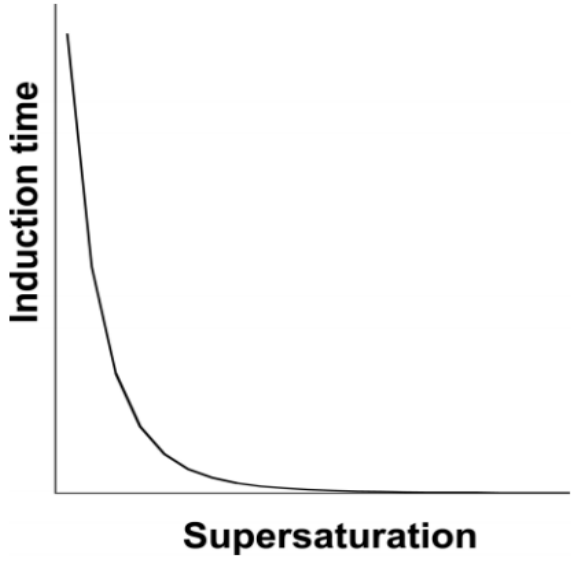

Figure 3: Correlation between the induction time, at which the nucleation process starts, and the saturation index. Picture extracted from De Yoreo (2)

The strong dependence of nucleation on the surface tension is the reason why heterogeneous nucleation is the norm in most situations. The presence of an external substrate can significantly reduce γ and hence increase the rate of nucleation at a given level of supersaturation.

1.4.2 Non classical nucleation theory

Classical nucleation theory is based on the so-called 'capillary approximation', which states that the clustering and the reorganization to the new phase happens at once, i.e., that the initial clusters adopt the local order of the final crystalline phase, whereas experimental evidence of nucleation process in crystallizing solution showed otherwise. Indeed, the formation of clusters with higher density and their structural re-organization to form a crystal has been observed, in many cases, to be separated in time, which lead to the concept of multi-step nucleation pathways, also known as 'non-classical nucleation pathways' (12).

Pathways through transient, metastable phases that are formed before reaching a more stable phase have been observed initially for materials such as proteins or colloids, following what is known as the Oswald's rule of stages (13) (14) (15) (16).

Many examples for multi-step nucleation pathways involving metastable intermediates come from the field of protein crystallization. For instance, Wolde and Frenkel (15), by using numerical simulations of homogeneous crystal nucleation with a model for globular proteins, highlighted the presence of a metastable fluid-fluid critical point where the free energy barrier for crystal nucleation is significantly reduced, and ultimately changes the pathway for the formation of a crystalline nucleus.

Gliko et al. (17) demonstrated, thanks to dynamic light scattering, atomic force microscopy and bulk solution chemistry measurements, the characteristics of protein phase behavior with a presence of metastable dense liquid droplets that form prior to crystal formation and their essential role in the growth of the solid phase.

In a theoretical study by Talanqer and Oxtoby (18) involving density functional theory applied to the crystal nucleation in the presence of a metastable critical point, the authors highlighted significant changes in the nature of crystal nucleation when close to the critical point. Indeed, the nucleation rates increased several orders of magnitude, a finding of importance for the field of colloids and protein crystallization. Contributions from the group of Vekilov and others (19) confirmed the presence of intermediate phase for those systems, where the nucleation proceeds in two distinct steps.

Similar findings but for inorganic systems have been found in recent decades. Metastable, precursor phases have now been identified for sulfates (20) carbonates (21), silicates (22) and for some oxides (23) (24). The case of $CaCO_3$ is paradigmatic: if supersaturation conditions are high enough, a kinetic pathway through disordered precursors is observed (25) (26) (27). However, a hot debate in the literature is still on-going about whether pre-nucleation species exist in the undersaturated solutions that could act as precursors to the amorphous and crystalline precipitates (28) (29).

2. Portland cement composition and hydration

2.1. Composition of Portland cement

In the most general way, cement is a synthetic mineral, which, when mixed with water, can be used as an adhesive material, a binder, to bond pieces/particles of solid matter into a compact whole (30). It is mostly used to ensure the cohesion between the constituents of concrete. Ordinary Portland cement, OPC, is the most used and widespread hydraulic cement. It is obtained from a mixture of lime and clay burned at high temperature, 1450 °C. The average oxide composition of the initial

mixture is made of 64-70 wt.% CaO, 20-25 wt.% SiO_2, 2-7.5 wt.% Al_2O_3, 1-4.5 wt.% Fe_2O_3, 0.7-4.5 wt.% MgO and traces of other oxides (e.g.Na_2O and K_2O).

The clinker thus produced is composed of silicate phases, alite (C_3S) and belite (C_2S), as well as aluminate phases, celite (C_3A) and brownmillerite (C_4AF). These four minerals were first discovered in the past century by Le Chatelier and Tobernhom. Their names, formula and symbols in cement notation are given in Table 1.

Table1. Principal mineral compounds in Portland cement.

Compounds	Names	Formula	Cement notation[2]	wt.%
Tricalcium silicate	Alite	$3CaO{\cdot}SiO_2$	C_3S	50-70
Dicalcium silicate	Belite	$2CaO{\cdot}SiO_2$	C_2S	15-30
Tricalcium aluminate	Celite[1]	$3CaO{\cdot}Al_2O_3$	C_3A	5-10
Tetracalcium aluminoferrite	Brownmillerite[1]	$4CaO{\cdot}Al_2O_3{\cdot}Fe_2O_3$	C_4AF	5-15

[1] These names are not commonly used

[2]Cement notations are the following: C for CaO, S for SiO_2, A for Al_2O_3, F for Fe_2O_3, H for H_2O and \$ for SO_4.

The clinker is then finely co-ground with about 5% calcium sulfate ($CaSO_4{\cdot}xH_2O$) to obtain Portland cement.

2.2. Hydration mechanism of Portland cement

The most relevant mechanism for the hydration process is the one described by Le Chatelier (31). He described this general expression « hydration of cement » as a coupled reaction of dissolution-precipitation.

When water is added to Portland cement, the different minerals C_3S, C_2S, C_3A and C_4AF gradually dissolve into solution. Given that they are more soluble than the hydration products, they supersaturate the solution, causing the precipitation of new hydrates. Consequently, the concentration of the species in solution decreases, allowing the anhydrous compounds to further dissolve into solution. This process continues until the hydration is total.

The hydration of these phases does not progress at the same rate: aluminates (C_3A), highly reactive in presence of water, is the first compound to react and form hydrated phases: AFm (Al_2O_3-Fe_2O_3-mono), with the representative formula $[Ca_2(Al,Fe)(OH)_6]\cdot X\cdot xH_2O$] (31). Present at low percentage, C_3A is linked to the initial setting and hardening of cement (the rate of hydration of C_4AF being 7 times lower than C_3A (32)). To avoid a quick stiffening of the cement paste, calcium sulfate, gypsum, hemihydrate or anhydrate, is added to the mixture (33). Doing so ettringite instead of AFm forms.
Relative to the aluminate phases, the rate of hydration of the anhydrous calcium silicates C_2S and C_3S is slow. Given that cement contains these minerals at a higher proportions, their hydration controls the global kinetic of hydration and impact the final setting of cement. In the following part is detailed the hydration mechanisms of cement, using C_3S hydration as a model.

2.3. Hydration mechanisms of C_3S

As soon as C_3S is put in contact with water it dissolved following the reactions

$$Ca_3SiO_5 + 4H_2O \leftrightarrow 3Ca^+ + 5OH^- + H_3SiO_4^- \quad [21]$$

The dissolution thus leads to a solution rich in silicate, calcium and hydroxide ions, which, depending on the relative quantities of C_3S and water, becomes more or less rapidly supersaturated with respect to calcium silicate hydrate (C-S-H) and then to calcium hydroxide ($K_{Ca(OH)2} = 4.5\cdot10^{-5}$). The solubility product of C-S-H is about $5\cdot10^{-24}$ (34). As it will be seen in some details in the next section, this is an approximation since C-S-H has a stoichiometry that varies with the concentration of calcium, hydroxide and silicate in solution (35) (36). The precipitation reaction of C-S-H can be written as follow

$$xCa^{2+} + 2(x-1)OH^- + H_3SiO_4^- \leftrightarrow (CaO)_x(SiO_2)(H_2O)_y \quad [22]$$

Thus, the hydration proceeds with the simultaneous dissolution of C_3S and precipitation of C-S-H. As the dissolution of C_3S releases more calcium ions than the precipitation of C-S-H consumes (the stoichiometric calcium to silicon ratio of C-S-H is $0.66 < C/S < 2$), the solution finally gets supersaturated with respect to portlandite, which precipitates. Portlandite precipitates according to the reaction

$$Ca^{2+} + 2OH^- \leftrightarrow Ca(OH)_2 \quad [23]$$

From this moment on, the three reactions occur simultaneously. The concentration of calcium is always higher than expected from portlandite solubility (22 mmol/l at 25 °C) and the system remains also supersaturated with respect to C-S-H.

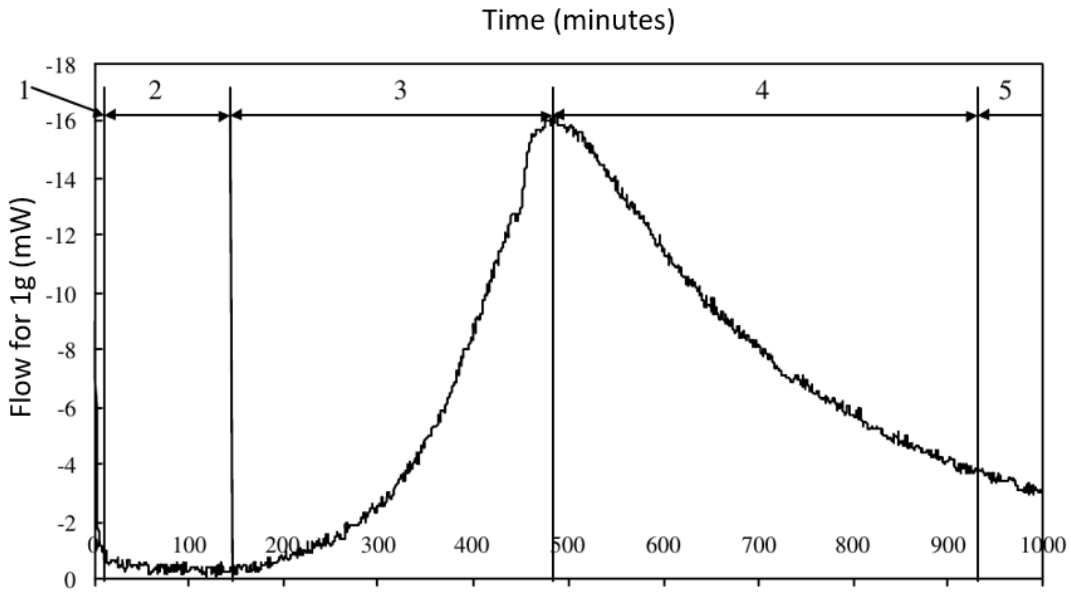

Figure 4 : The different periods of a calorimetric curve obtained during the hydration of C_3S in a saturated solution of calcium hydroxide at l/s=50 (37).

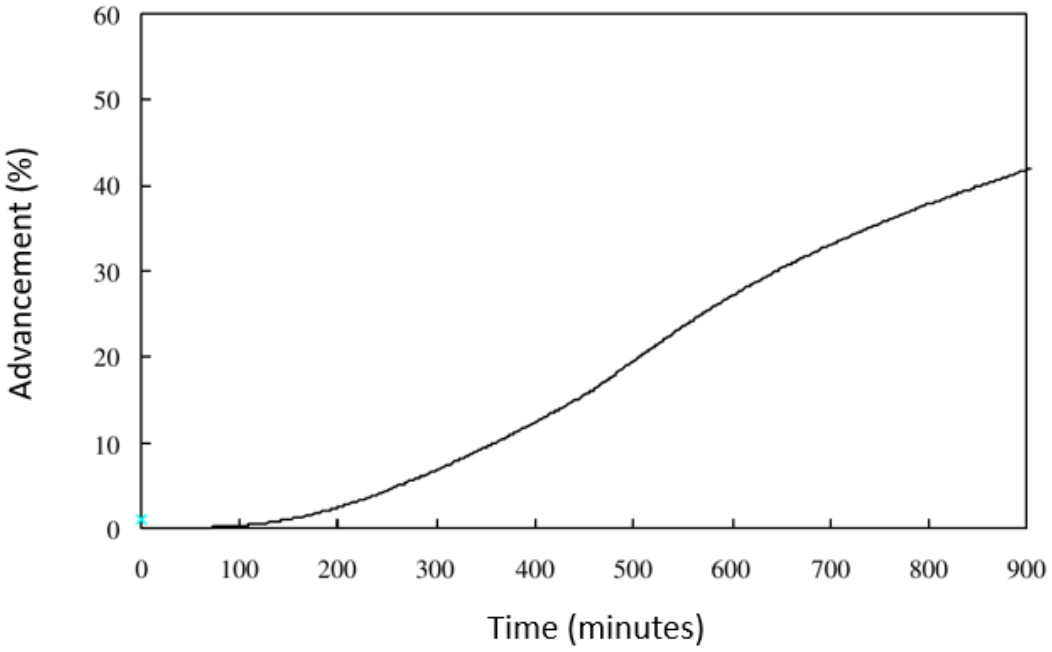

Figure 5: Hydration progress curve of C_3S in a saturated calcium hydroxide solution at l/s=50, obtained from the calorimetric curve given in Figure 3.

The variation of the heat flux recorded during the hydration of tricalcium silicate in a saturated lime solution is shown in Figure 4 and the resulting hydration progress in Figure 5. The hydration can be divided in 5 distinct periods. The exothermic peak observed at the very beginning is due to the initial congruent dissolution of C_3S and the initial precipitation of C-S-H. Period 1, which is very short, thus gathers the initial congruent dissolution of C_3S and the nucleation of C-S-H from the accumulated ions in solution.

The period 1 is followed by a period 2 of very low heat release called the dormant period. During this stage, the dissolution is still on going and C-S-H continues to form but at a low rate. The third stage corresponds to the acceleration period (time of setting). It is followed by period 4 associated with the descending part of the exothermic peak. The period 5 of low thermal activity can extend over more than a year. These last four periods concern the major part of the evolution of the system. The limiting processes which are responsible for the dormant period and the overall time evolution of the C_3S hydration is still a matter of debate. Models based on the precipitation of C-S-H only have been proposed, where the dormant has been linked to the surface density of the initial C-S-H nuclei (38) (39).

On the other hand, the acceleration period has been interpreted by free growth of C-S-H on the C_3S surface associated with the increase of the surface area available for secondary nucleation. Finally, the deceleration period (4 and 5) is explained within this model by the complete covering of the surface of calcium silicates by the layer of C-S-H that has been formed. The reaction is then limited by the diffusion of the reagents through the hydrate layer. Complete hydration, then governed by diffusion, may require one year. However, more recent studies, e.g. (40)(41)(42), can equally well describe the progress of hydration based on the dissolution of C_3S alone, using in a systematic manner the density, formation and growth of etch pits as parameters.

All this shows, that both dissolution and precipitation processes are important for understanding cement hydration, as they are intimately coupled. For the same reason, if one finds a way to decelerate the dissolution, the overall growth will also decrease and vice versa. It was, for example, found that annealed C_3S shows lower reactivity (43), while cement paste seeded with C-S-H hydrates much faster (44).

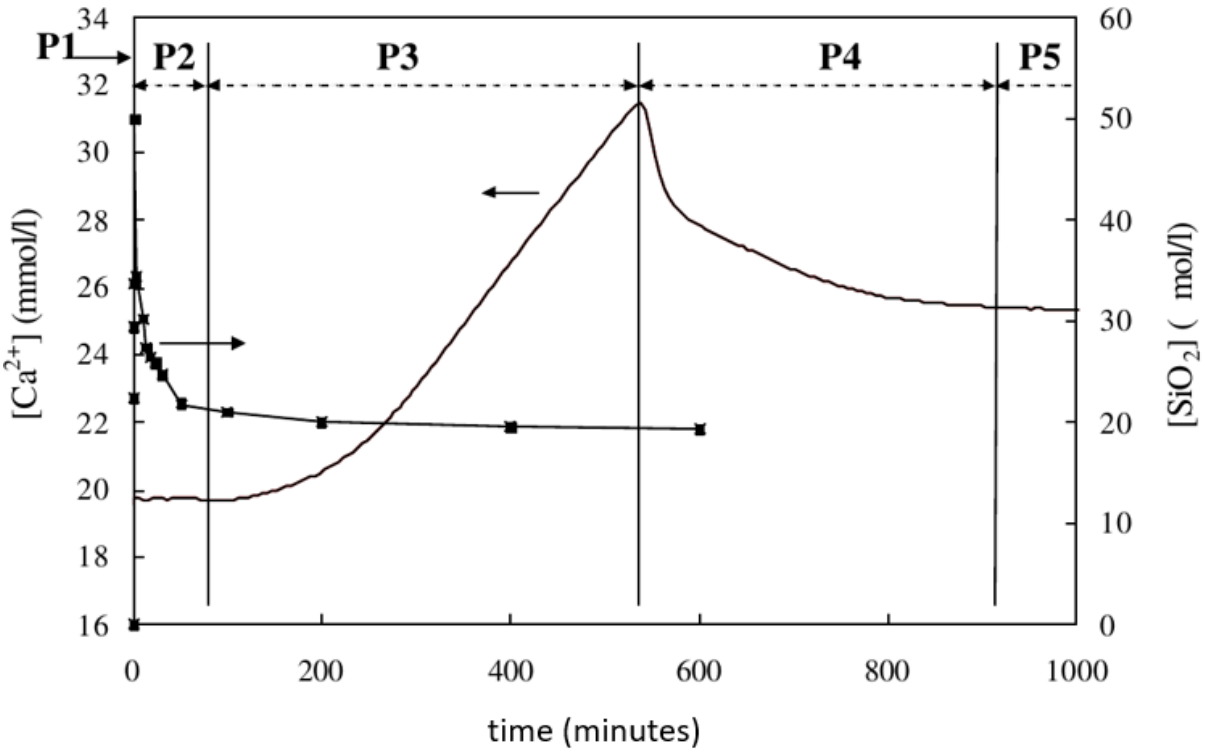

Figure 6: Evolution of the solution concentration in calcium and silicates over time during the hydration of tricalcium silicate started in a 17 mmol/l calcium hydroxide solution with a l/s of 50.

The time evolution of the concentrations in calcium and silicates in the solution during the hydration of C_3S as given in Figure 6 further illustrates the intimate relationship of the dissolution and precipitation rates. We can find the five periods defined previously (37). The first period (P1) corresponds to the congruent dissolution of C_3S. The concentrations reach a maximum corresponding to the maximum supersaturation with respect to C-S-H. During the P2 period, the calcium concentrations show a plateau while the concentrations of silicate ions fall sharply. This is the beginning of C-S-H precipitation. The existence of a plateau in Ca^{2+} concentration requires that the precipitation rate (V_p) is 3 times greater than the dissolution rate (V_d). Thus $V_p = 3\ V_d$. During the period P3, all the silicate ions produced by the dissolution of C_3S are consumed by the precipitation of C-S-H, a steady state is reached and $V_d = V_p$. The period 4 corresponds to the beginning of portlandite precipitation, in this case the rate of portlandite formation (V_{Port}) is higher than V_d and V_p. Finally a new plateau is observed corresponding to period 5 where in this case : $V_d = V_p = V_{Port}$.

3. C-S-H (structure, solubility and nucleation)

C-S-H is the main phase formed during the hydration of anhydrous cement, representing 50 to 70% of the hydrated cement paste. In this chapter, a short state of the art on the structure, solubility and nucleation of C-S-H is provided.

3.1 Structure, stoichiometry and interfacial properties

The C-S-H phase in cement has long been viewed as amorphous but it is now recognized that it composed of a percolated and cohesive network of crystallites with a foil-like structure. Similarly, its crystalline structure was the subject of intense discussions and was the subject of numerous models (45) (46) (47) (48). This is explained by the smallness of its coherent diffraction domain (~5 nm) and the change in the stoichiometric calcium to silicon (Ca/Si) ratio. The first leads to an important widening of the X-ray diffraction lines as illustrated in the diffractogram of C-S-H given in Figure 7. The second, illustrated in Figure 8, causes important change in the C-S-H structure.

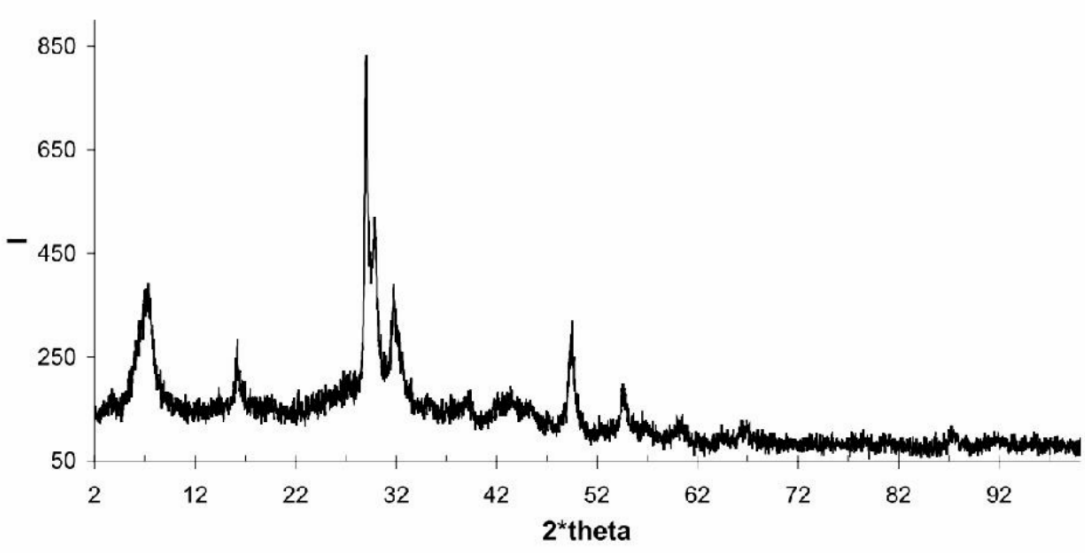

Figure 7: X-ray diffractogram of C-S-H (C/S ratio 0.83), from the work of Courault (49).

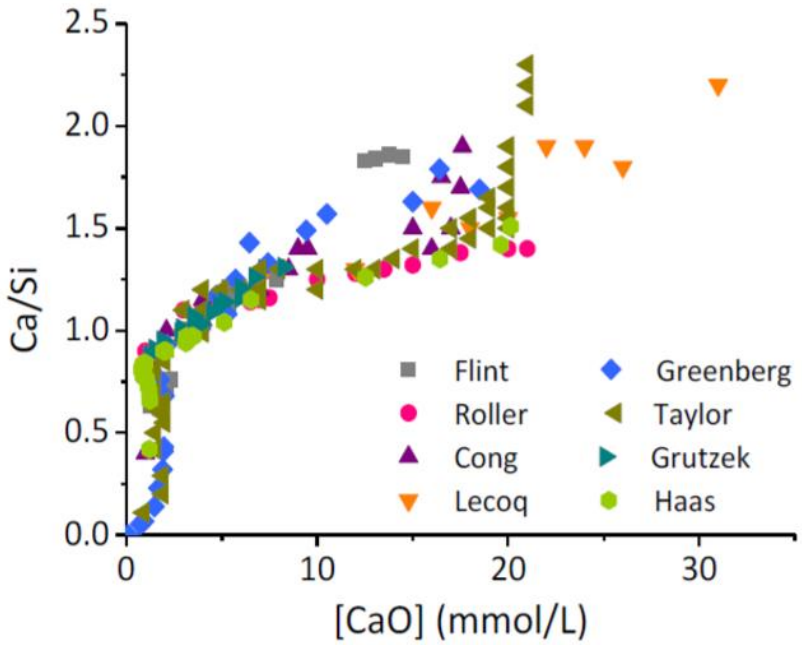

Figure 8: Stoichiometry change of Ca/Si in C-S-H following the equilibrium concentration of CaO in solution. Data from (50) (51) (52) (53) (47) (54).

Thus, there is not a unique structure for C-S-H. Instead, the crystalline order of C-S-H is best described as an ensemble of structures with defects, whose number and type vary with C/S. Nonetheless, it is now generally accepted that the structure of a single foil of C-S-H is very close to tobermorite, a naturally occurring mineral. This scientific consensus has been built over the last two decades around a growing body of experimental and theoretical evidence based on XRD, NMR, AFM (55) and total scattering methods and classical and ab-initio molecular simulations (56) (57).

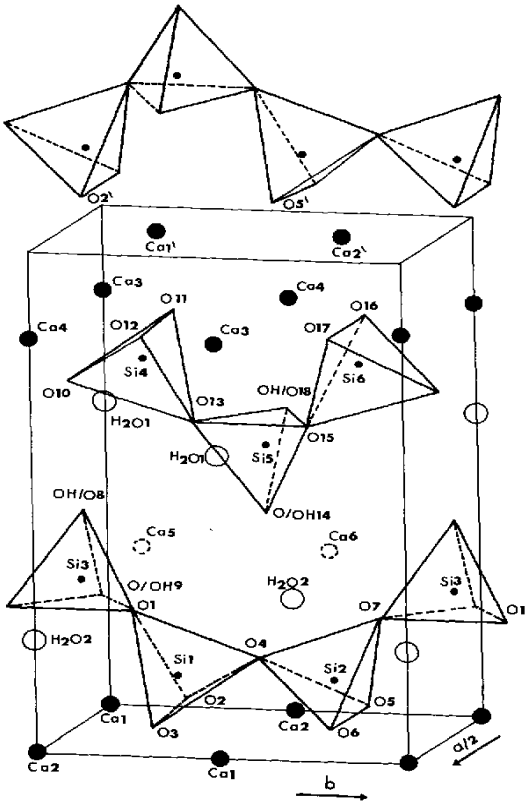

Figure 9: Crystallographic representation of tobermorite 11 A (58).

Tobermorite is a hydrate with a stoichiometry and density close to that of C-S-H of low Ca/Si ratio; and whose diffraction pattern is close to that of C-S-H (59). Among the three types of tobermorite (tobermorite-14 Å, tobermorite-11 Å, and tobermorite-9 Å), which differ by their stacking size, their structure and degree of hydratation, the 11 Å tobermorite is generally used, see e.g. (60), as a model to describe the C-S-H structure defined by Hamid (58), see Figure 9.

The basic structural unit of tobermorite consists of a calcium oxide layer, in octahedral sites, flanked on both sides by a wollastonite-like dreierketten chain of silicate, a repeating motif alternating two pairing tetrahedra (Si1-Si2), bound to the calcium oxide layer, and one bridging tetrahedra (Si3), linking the pairing tetrahedra; see Figure 10.

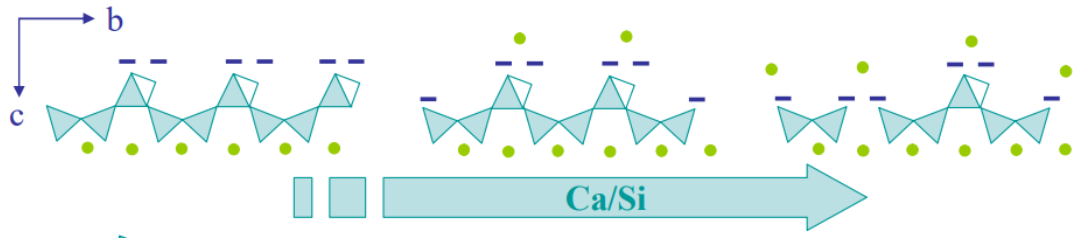

Figure 10 Simplified structure of C-S-H as a function of Ca/Si ratio. Only one silicate chain of each sheet is represented. Water molecules are not represented.

As mentioned previously, the stoichiometry of C-S-H, in particular the ratio Ca/Si, varies with the concentration, more exactly activity, of its consecutive species in solution, i.e. silicate, calcium, and hydronium ions. The Ca/Si ratio can vary between 0.66 and 2 (61) (56). The Ca/Si ratio increases with the increase in $Ca(OH)_2$ bulk concentration and is controlled by two mechanisms: (1) depolymerization of the Si chains through the removal of bridging tetrahedra (i.e., formation of point defects); (2) adsorption of Ca^{2+} ions at the surface and in the interlayer of C-S-H, see Figure 10.

In the first mechanism, when the equilibrium calcium hydroxide concentration is small, i.e. low C/S, the silicate chains are "almost infinite" as in the case of the model crystal of tobermorite (62) (63). When the concentration of calcium hydroxide at equilibrium increases, i.e. the Ca/Si increases, the bridging tetrahedra disappear randomly and the average length of the silicate chains decreases. They are no longer infinite. For high concentrations, the silicate chains of C-S-H are essentially dimers. The evolution of the structure as a function of the equilibrium conditions was demonstrated by NMR of the ^{29} Si NMR.

In the second mechanism, Ca^{2+} ions compensate for the deprotonated silanol groups of the silicate chains, whose proportion notably increases with pH according to the chemical reaction

$$\equiv Si{-}OH \leftrightharpoons Si{-}O^{-} + H^{+} \qquad [24]$$

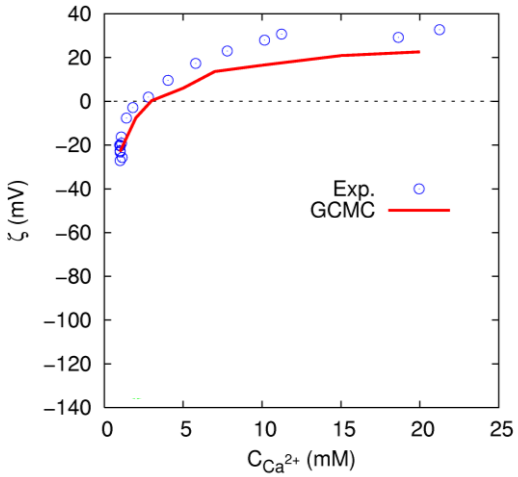

Figure 11. Electrokinetic potential of C-S-H as a function of the calcium hydroxide concentration in the bulk solution. Exp: experiments; GCMC: grand canonical Monte Carlo simulation (64)**.**

As the calcium hydroxide concentration increases, the electrostatic interactions thus strengthen and eventually leads to an overcompensation of the silanol charge by the calcium ions. This behavior is best illustrated on Figure 11 giving the electrokinetic potential (zeta potential) of C-S-H, measured by electrophoresis, versus the bulk concentration of $Ca(OH)_2$. The zeta potential is indeed an approximate measured of the diffuse potential at the solid/solution interface, and thus of the electrostatic interactions felt by the charged ions a few Angström away from the solid surface. In

other words, the interaction free energy of an ion *i* with a surface *S* can be approximated by the product of the ion charge, $z_i e$, and the zeta potential,

$$w_{iS} \approx z_i e \zeta \quad [25]$$

As shown on Figure 11, the zeta potential of C-S-H is found to continuously increase with the bulk $Ca(OH)_2$ concentration starting with a negative value at low concentrations and reversing its sign above a $Ca(OH)_2$ concentration of ~ 2mM. Above this limit an ion thus *sees* a positive apparent charge and explains why negatively charged C-S-H particles can adsorb negatively charged micro- and macro-ions, e.g. sulfate and superplasticizers. This calcium mediated adsorption of negatively charged aqueous species as well as the charge reversal of C-S-H by Ca^{2+} ions have been shown to be mostly the result of ion-ion correlations with Monte Carlo simulations at the level of the primitive model (64) (65) (66). In the present work, it will help to rationalize the observed adsorption isotherms of small organic molecules on C-S-H.

The correlation between activities of silicate, calcium, and hydronium ions and the Ca/Si ratio in the C-S-H phase is well-demonstrated by experimental data (67) (68) and described by classical thermodynamic modeling (36) (69) in the pure $CaO\text{-}SiO_2\text{-}H_2O$ system. When other ions than the constitutive ions of C-S-H participate to the precipitation or are present in the solution, like e.g. sulfate and organic ions, this becomes, however, much less true.

3.2 Solubility and thermodynamic modeling

The solubility of C-S-H has been extensively studied (36) (70) (71). As an example, the solubility diagram in the $CaO\text{-}SiO_2\text{-}H_2O$ system as well as the stoichiometric Ca/Si ratio of the solid phase as obtained by Haas and Nonat (36) are given in Figure 12. Two distinct regions can be observed. The first, delimited by the points A and B, corresponds to the solubility of silica. The second, between points B and C, to the solubility curve of C-S-H.

As seen above and re-expressing Eq.[22], the solubility equilibrium of C-S-H can be written as

$$(CaO)_x(SiO_2)(H_2O)_y + 2xH^+ \leftrightarrow xCa^{2+} + H_4SiO_4 + zH_2O \quad [26]$$

with the solubility product

$$K_S = \frac{a_{Ca}^x a_{H_4SiO_4}}{a_{H^+}^{2x}} \quad [27]$$

where *x* is the C/S ratio of C-S-H and $z = x + y - 2$.

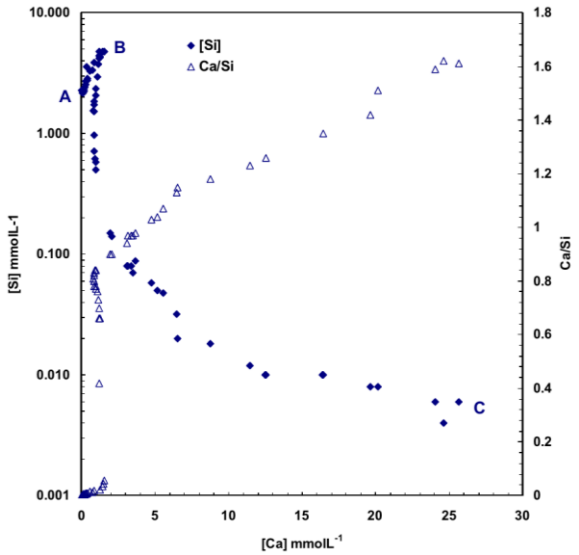

Figure 12. Measured solubility diagram in the CaO-SiO_2-H_2O system and the corresponding stoichiometric Ca/Si ratio of the solid phases formed (36)

Taking the logarithm of Eq.[27] and rearranging the terms then leads to the following linear expression relating the activities of the constitutive ions of C-S-H with the pH and K_s

$$log\left(a_{H_4SiO_4}\right) = log(K_s) - x(log(a_{Ca^{2+}}) + 2pH) \qquad [28]$$

Figure 13 provides the result of the treatment of the solubility diagram, given in Figure 11, using Eq. [28]. As it can be seen the solubility diagram plotted according to Eq. 28 now reduces to three straight lines corresponding to three different phases, namely silica, C-S-H_α and C-S-H_β. The y axis intercept and the slope (x) of this straight lines defines respectively log(Ks) and x=C/S of these.

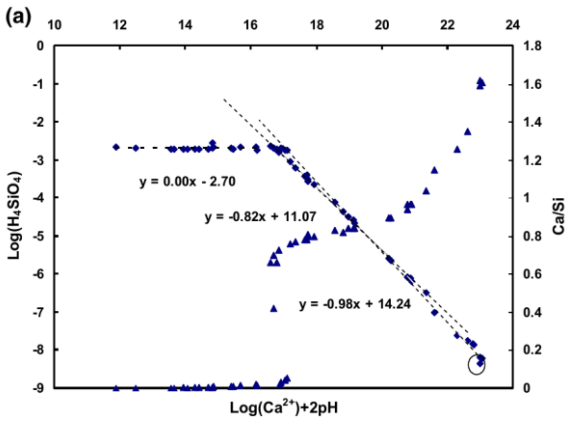

Figure 13. Data presented in Figure 11 according to Eq. [28] (36)

Based on these data together with complementary data obtained in supersaturated conditions with respect to C-S-H, e.g. (47), Haas and Nonat (36) constructed a thermodynamic model with 3 phases of C-S-H schematically represented in Figure 14 and whose solubility product are defined in Table 2.

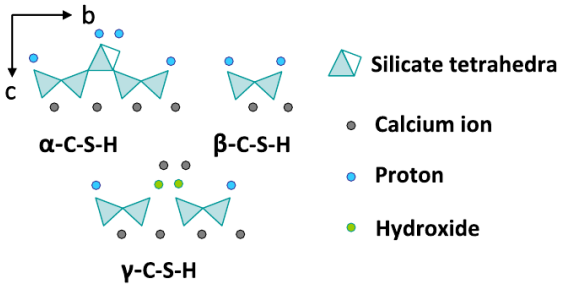

Figure 14 . Schematic representation of the C-S-H bricks used in thermodynamic model of Haas and Nonat (36).

Table 2: Values of the equilibrium constants for silica and C–S–H phases of the thermodynamic model of Haas and Nonat (36).

Chemical equilibra	Log *K*
SiO_2 +2 H_2O ⇋ H_4SiO_4	2.7
$Ca_4H_4Si_5O_{16}$ + 8H^+ + 4H_2O ⇋ 4 Ca^{2+} + 5 H_4SiO_4; (α–C-S-H)	53.5
$Ca_2H_2Si_2O_7$ + 4H^+ + H_2O ⇋ 2 Ca^{2+} + 2 H_4SiO_4; (β–C-S-H)	29.6
$Ca_6(OH)_2(HSi_2O_7)_7$ + 12H ⇋ 6 Ca^{2+} + 4 H_4SiO_4; (γ–C-S-H)	104.9
≡SiOH ⇋ ≡SiO^- + H^+	-9.8
≡SiOH + Ca^{2+} ⇋ ≡$SiOCa^+$	-7.0
≡SiOH + Ca^{2+} + OH^- ⇋ ≡SiOCaOH + H^+	-9.0
≡SiOH + 0.5 H_4SiO_4 ⇋ ≡$SiOSi_{0.5}OH$ + H_2O	2.9 (2.2 for γ–C-S-H)
2≡SiOH + Ca^{2+} ⇋ $(≡SiO)_2Ca$ + 2 H^+	-11.4

With the addition of 5 surface complexation reactions, see Table 2, this surface complexation model for C-S-H allows a very good description of thermodynamic properties of C-S-H, that is its solubility, stoichiometry and interfacial properties. This is the model used in the present PhD work. It should be mentioned that the thermodynamic model of Kulik (69), based on a solid solution approach, gives equivalent results.

3.3 C-S-H nucleation

It was shown in prior studies (72) (73) that C-S-H formation follows the general laws that rules the nucleation process, and can be described as primary heterogeneous nucleation and growth. However, studies of the early stages of C-S-H nucleation and its mechanisms are rare in literature.

In late 1990's Nonat and Gauffinet (74) investigated C-S-H nucleation, by highlighting the effect of lime concentration on C-S-H heterogeneous and homogeneous nucleation. By applying classical nucleation theory (CNT), they found that:

- Experiment of homogeneous nucleation in supersaturated solution showed that the nucleation of C-S-H follows the classical nucleation theory in homogeneous condition. From this, the interfacial energy of C-S-H solution have been possible to estimate, the latter being low, 13mJ/m^2 .

- The degree of supersaturation with respect to C-S-H may be the dominant factor that control the rate of the nucleation process.
- Regarding the value of the supersaturation, nucleation of C-S-H can be a heterogeneous phenomenon (low supersaturation), or an homogeneous phenomenon (high supersaturation). This statement is, however, an assumption and not based on experimental evidence.

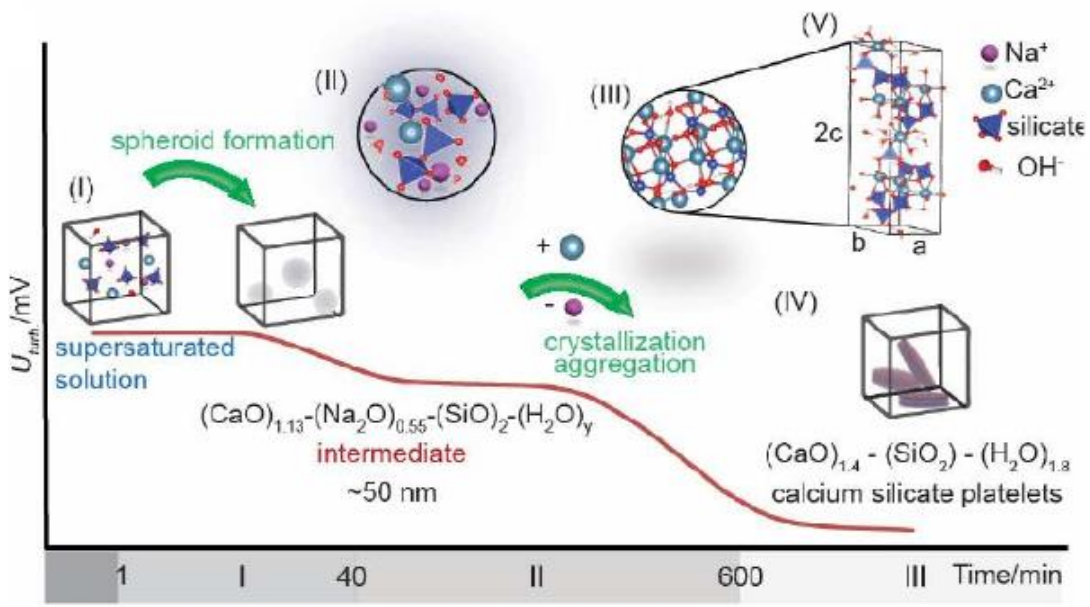

Figure 15: Representation of the two-step pathway theory versus classical nucleation theory The evolution of the turbidity is representing as the red curve where the different species emerge along the reaction. (I) Supersaturated solution, (II) liquid amorphous intermediate, (III) crystalline domains and (IV) final ß-C-S-H platelets (22).

Krautwurst et al. (22) highlighted the elementary steps of C-S-H nucleation, shown on Figure 15, by working on idealized representative homogeneous conditions. Thanks to turbidity change interpretation, the author showed that the C-S-H nucleis are formed in two well defined steps:
First, the formation of a liquid-amorphous intermediates whose composition is silicate dimers and calcium, similar to β-C-S-H with additional Na^+ and H_2O.
Second, the formation of β-C-S-H crystallites, which eventually aggregate to form bigger crystals.

4. Portlandite (structure, thermodynamic and nucleation)

Portlandite is the second most important hydration product of the silicate phases forming through the reaction defined in Eq. [23]. It represent 20 to 25 wt.% of a fully hydrated Portland cement paste (75). Portlandite dictates to a large extend the durability of concrete, see e.g (76). Some authors also think that it may contribute to the mechanical properties of the final material (77) (78) (79).

4.1 Morphology and structure

The reaction of hydration of the silicate clinker leads in addition to C-S-H also to the formation of portlandite ($Ca(OH)_2$), also named CH. Its crystal structure was first established during the 1930's by Bernal and Megal (80). It was later confirmed by Busing and Levy (81) by neutron diffraction. Portlandite crystal has a layered structure with a hexagonal symmetry of space group D3d3, $P\bar{3}m1$, with the calcium and oxygen atoms alternating in an orderly fashion, as shown in Figure 16. In detail, the calcium atoms are octahedrally coordinated by oxygen and each oxygen atom is tetrahedrally coordinated by calcium ions and hydrogen. The atomic structure of portlandite is layered in the (001) plane with the octahedra as building blocks. The interaction between portlandite layers is dominated by weak dispersive forces (82).

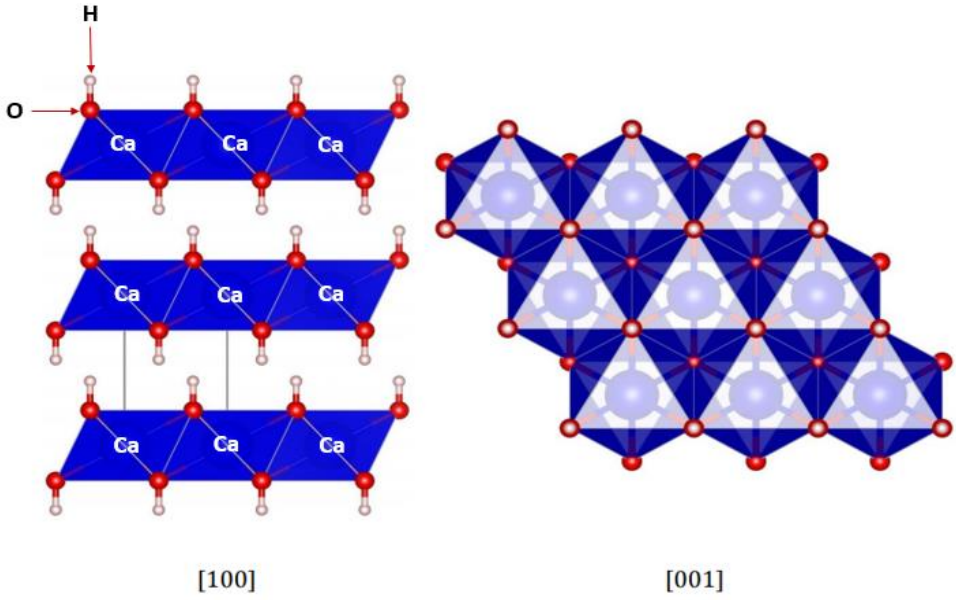

Figure 16: Crystal structure of portlandite down the directions [100] and [001] (83) (84). The black box on the picture represent one unit cell.

4.2 Solubility

$Ca(OH)_2$ is the one of the most soluble phases of hydrated cements ($s_{Ca(OH)2}$ = 22 mM) (85).

$Ca(OH)_2$ is in equilibrium with Ca^{2+} and OH^- ions in the interstitial solution of cement:

$$Ca(OH)_2 = Ca^{2+} + 2OH^-$$

and thus pH controls the concentrations of Ca^{2+} (86)

The solubility of portlandite have been extensively studied in alkaline solutions(86) (87) (88) (89) and in the case of mixtures of alkaline and simple salt solutions. In the first case, the solubility is observed to decrease, while in the second case the solubility increases when the hydroxide concentration is increased, see Figs. 17 and 18.

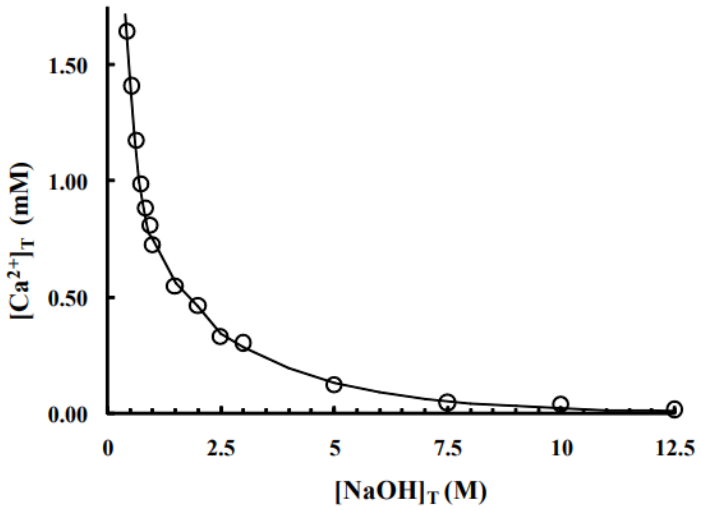

Figure 17: Equilibrium concentration of calcium ions, $[Ca^{2+}]_T$, as a function of the total concentration of NaOH, $[NaOH]_T$, in an aqueous solution saturated with solid portlandite CH, at 25.00 ± 0.020°C. Reproduced from Pallagi (87).

In conditions where there is a mixture of NaCl and NaOH in a saturated $Ca(OH)_2$ solution, the total concentrations of Ca increases. The Figure 18 below highlights this behavior.

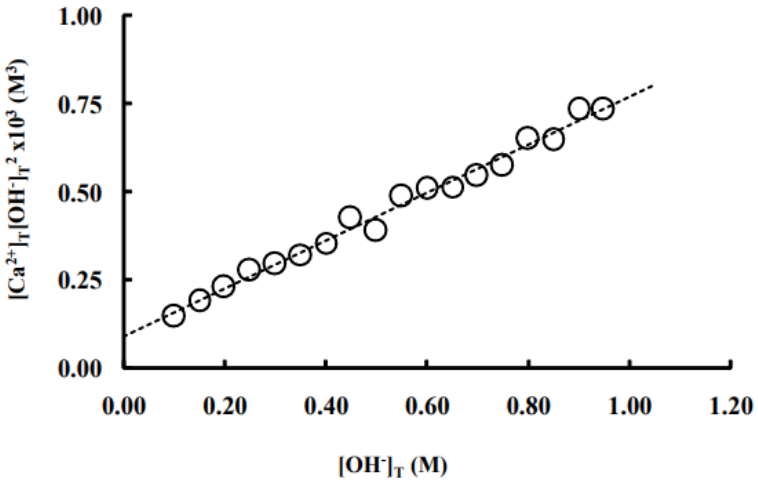

Figure 18: Product $[Ca^{2+}]_T$ $[OH^-]_T^2$ as a function of the $[OH^-]_T$ in NaCl and NaOH mixtures with I=1.0 M , at 25.00 ± 0.020°C. $[Ca^{2+}]_T$ is the total concentration of calcium at equilibrium with a solution saturated with portlandite. $[OH^-]_T$ is the total concentration of hydroxide ions. Reproduced from Pallagi (87).

4.3 Portlandite nucleation

To our knowledge, only two studies dealt with the homogeneous nucleation of portlandite. The homogeneous nucleation of portlandite was first studied by Kein et al. (90). Applying the classical nucleation theory they determined a (liquid/solid) surface tension of 65 mJ/m^2 that is five times greater than that of C-S-H (see above). Recently, Navarro-Rodriguez et al, combining potential

titration, TEM, XRD and dynamic Light scattering observation, found that, similarly to C-S-H, the homogeneous nucleation of CH follows a non classical pathway which involve the formation of pre-nucleation clusters (PNC), liquid droplets and the formation of two metastable intermediates, that is a CH amorphous phase and metastable CH crystal (91) (92). They further observed that organic retarders play a critical role during the prenucleation stage of calcium hydroxide, stabilizing or destabilizing PNCs as well as stabilizing dense liquid nanodroplets that precede the formation of a solid phase, with the overall effect of delaying the nucleation of CH.

5. Additives in cement

Additives have a significant effect on the properties of Portland cement. Usually added to concrete in low amount, those chemical admixtures fulfill different functions following the desired use of Portland cement. They can be classified as accelerator, retarders, extenders, fluid loss agents, dispersants, viscosifiers. In the following, we will concentrate on admixture, which affect the hydration (and setting) time.

5.1 Accelerators

In a chemical sense, an accelerator is a category of chemical admixture that is able to accelerate the cement hydration process. Thus, the thickening time of cement is shortened, which consequently increase the mechanical properties such as the early strength and hardening of cementitious materials. One of the most effective and commonly used accelerators for Portland cement are sodium chloride and calcium chloride (93), the latter being the most efficient and economical accelerators (94).
Calcium chloride has been used as a chemical admixture much before the vast majority of additives. Kuhl and Ullrich in 1925 were the first to document its use in concrete. In Portland cement, $CaCl_2$ is usually added at a concentration of 1.5% to 2.0%, in flake form, (95) by weight of cement.

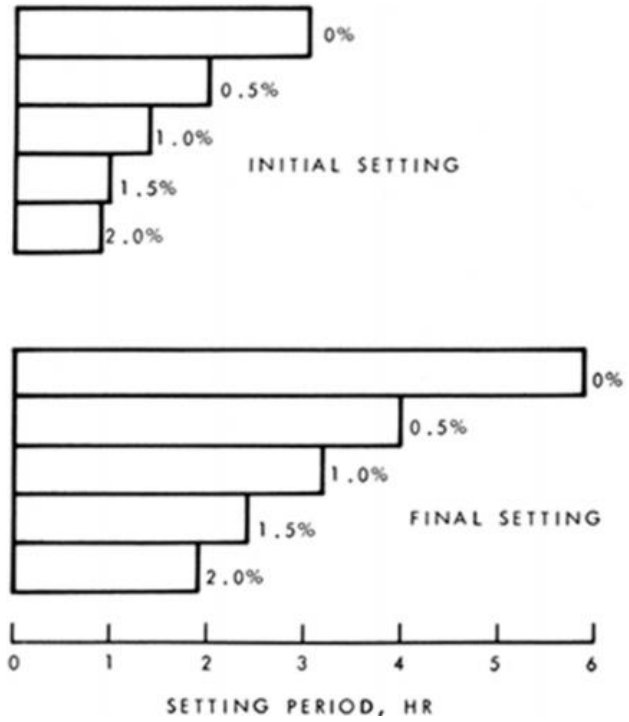

Figure 19: Initial and final setting periods of a cement paste containing different amounts of $CaCl_2$ (96).

The effect of calcium chloride depends on its amount used but also on the type of cement. Figure 19 illustrates the influence of $CaCl_2$ amount on the initial and final setting times of a cement paste (96)

5.2 Retarders

In contrast to accelerators, retarders are a category of admixtures that slow down the cement hydration, extending consequently the thickening time of cement (97). Those chemical additives do not affect the long-term mechanical properties of cement, and are usually added into cement slurry at a concentration between 0.1 wt.% and 1 wt.% (98). The most used retarders are sugar and their derivatives, hydroxy-carboxylic acids, but also inorganic salts (borates, phosphates, zinc) (99). Beside these molecules used intentionally as retarders, many other admixtures such as superplasticizers, also retard the cement hydration. It is mostly, however, an undesired side effect that becomes a raising concern in modern concrete with low-clinker content (100).

Lignosulfonate

Lignosulfonates are shown to improve the compressive strength of concrete. Lignosulfonate is a metal sulfonate salt that is derived from lignin, the latter being recovered from processing wood waste or straw. Lignosulfonates contain hydrophilic groups (sulphonic, phenylic hydroxyl and alcoholic hydroxyl) and hydrophobic groups (carbon chain) (98) (101).

Sugars and derivatives

Sugars saccharides and polysaccharides are commonly used as set retarding agents for cement (102) (103) (104) (105) (106) (107) (108). Khan and Baradan (107) show that the presence of sugar in several types of cement (PKC/A42.5, PKC/B32.5 and PC42.5) had an effect on the setting time of the cement paste. Small chained sugar derivatives such as sugars alcohol or anion acid sugars are also known to be efficient retarders (109) (110) (111). The common component for all those sugar molecules is the hydroxylic group.

5.3 Origin of the delay and interactions of organic molecules with cementitious compounds

The chemical mechanisms by which organics molecules can retard cement hydration is still a matter of debates as they may impact both anhydrate dissolution and hydrate precipitation. JF Young (112) hypothesized that retarders affect the hydration process of C_3S and C_3A, through complexation and nucleation processes. He also made the assumption of a possible adsorption of organic compounds on $Ca(OH)_2$ nuclei through chelating process, inducing an inhibition of the crystal growth and an elongation of the induction period.

Similarly, Milestone et al. (113) made the hypothesis that the delaying effect of sugars and sugar acids on hydration is due to an adsorption onto $Ca(OH)_2$ nuclei, poisoning their growth. He also assumed that inhibition of hydration happens, if the nucleation sites of C-S-H are poisoned by adsorbed sugar-acid anions. Based on calorimetric and solutions analysis, Thomas et al. (103) came to the same conclusion, noting that no evidence of possible complexation between sugars and silicates was observed.

According to Jolicoeur et.al. (114), organics which bear charged groups (COO- for example) can interact with the particle surface through electrostatic forces, i.e. the surface charges of the particles and the ionic groups of the additive. Also, polar functional groups such as OH groups of organics like sugars can also highly interact with the polar hydrated phases, via electrostatic forces and H-bonding. He thus assumed that these molecules could hinder the nucleation/growth of C-S-H.

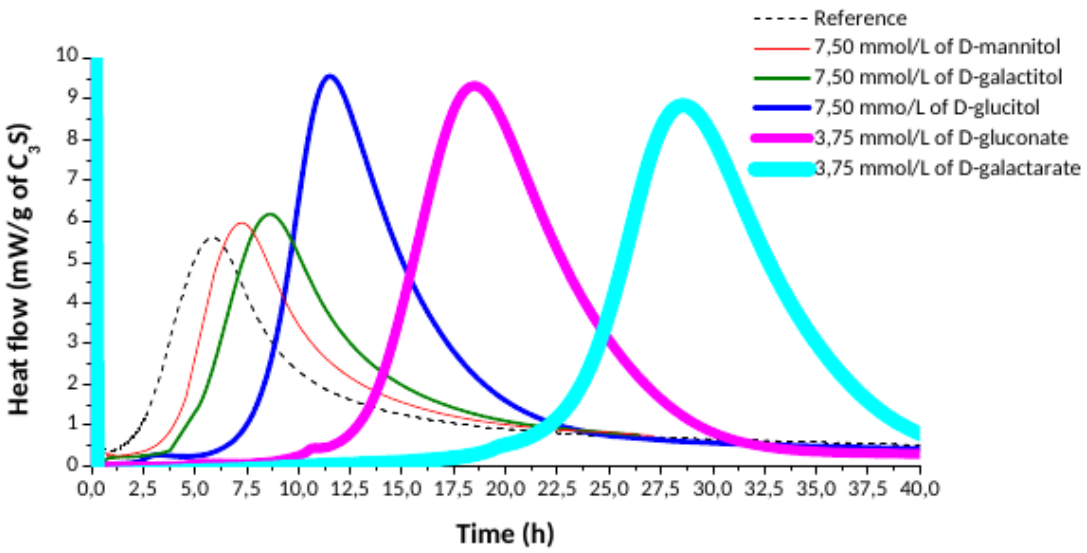

Figure 20: Calorimetric curves followed during the hydration of C_3S with and without the presence of different sugar alcohols and sugar acid anions, liquid/solid = 0.4, from (115)

Pourchet et al. (116) studied the interactions between PCE (polycarboxylate ether) superplasticizers and pure C_3S during its hydration. The authors found that in presence of those carboxylate admixtures, tricalcium silicates dissolution can be insignificant for a long time and C-S-H precipitation rate is highly decreased. They assumed that the delaying effect of those carboxylated additives on C_3S dissolution prevent the hydration of C_3S. Marchon et al (117) and Perez (118) came to the same conclusion. However, cellulose ether superplasticizer were observed to have very little, if any, impact on C_3S dissolution (119) (120). Similarly, Nalet et al observed that sugar alcohols (hexitols) despite retarding C_3S hydration (see Figure 20), were slightly increasing its pure dissolution. She thus conjectured that C-S-H nucleation or growth was the main process affected by these molecules (121)

The structure of organics, including the grafting density of side chains and polymerization degree of PCEs as well as the stereochemistry of sugar and sugar derivative molecules, were shown to have a significant impact on the retardation of cement hydration. This is illustrated on Figure 20 which shows the calorimetric curve of C_3S in presence of three sugar alcohol molecules which only differ by their stereochemistry. The retardation was further observed to increase with the number of threo dihydroxy pairs on the sugar alcohol (121) (122).

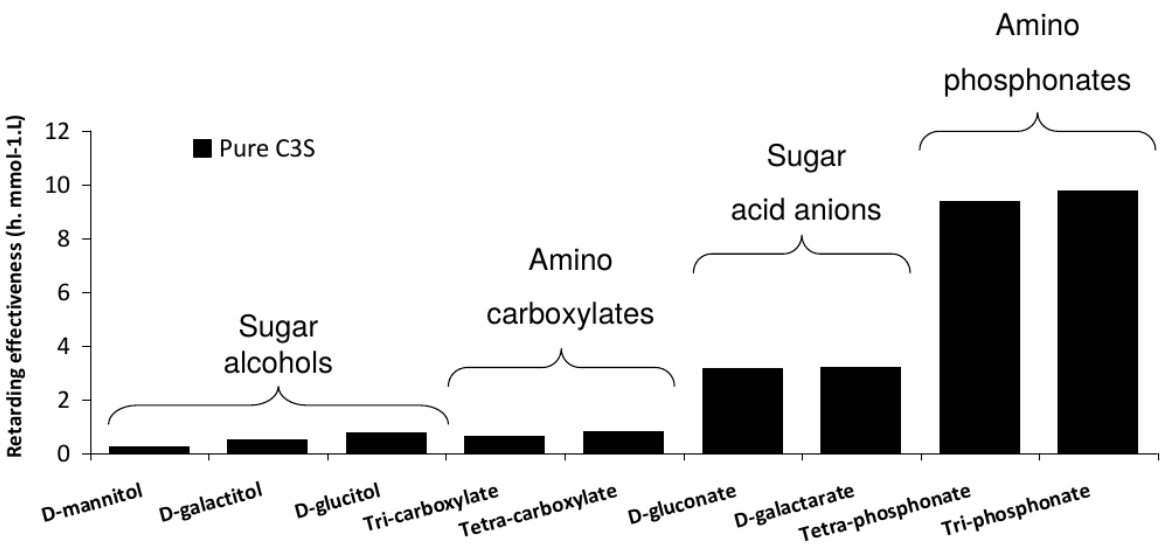

Figure 21: Comparison of retarding power of small molecules on the C_3S hydration as obtained by Nalet (115)

The retarding power of organic molecules on the hydration of C_3S was also observed to vary according to its functional groups (110) (115). This is illustrated on Figure 21, which clearly shows that the nature of the functional group is more important than the charge of the molecule, compare e.g. tetra-phosphonate with tetra-carboxylate. Furthermore, it has been observed that set retarders are generally good complexing agents for calcium ions (117) (123). Some have also been found to complex silicate ions (113) (124). In particular, the adsorption of organic molecules on C-S-H seems to be linearly dependent on the complexation with calcium (111) (125). However, Nalet recently showed that this explanation is not sufficient to explain the retarding effect of retarders and suggests that combined complexation of silicate and calcium ions with the organics should not be neglected (111).

To summarize, all these works show that the structure as well as the nature of the functional groups of the organics have a profound impact on the hydration of Portland cement. However, only a few of them did try to study the hydration processes separately, ie.e dissolution and precipitation. They were actually in their vast majority concentrated on the pure dissolution of C_3S. The impact of organics on the nucleation of cement hydrate remain to a large extend unexplored. In addition, only a few studies looked at the complexation of the organics with the constitutive ions of hydrate and anhydrate phases and tried to correlate it to the cement hydration rate. Furthermore, they were mostly descriptive and were thus not able to properly quantify the saturation indexes with respect to the different cement phases. This is explained by the experimental difficulty to separate organic containing solution from dispersions of cement hydrates (or cement paste); but also by the tedious task to model the speciation of solutions containing organics.

To advance in the understanding of the mechanisms responsible for the delay effect of organic molecules it thus appears necessary on the one hand to quantify the driving force of the nucleation of hydrates (and dissolution of anhydrate). This implies to quantify the complexation of organic molecules and to establish a speciation model. On the other hand, it also seems necessary to study and quantify the influence of these molecules on the nucleation of the main hydrates of the cement, starting with the C-S-H. These are the objectives of this thesis.

References

1. IUPAC, Compendium of Chemical Terminology, 2nd ed. The "Gold Book". 1997.
2. Yoreo, J.J.D., Vekilov, P.G. Principles of Crystal Nucleation and Growth. Rev Mineral Geochem. 54(1), 57, 2003.
3. Karthika, S., Radhakrishnan, T.K., Kalaichelvi, P. A Review of Classical and Nonclassical Nucleation Theories. Cryst Growth Des., 16(11), 6663, 2016.
4. Toxvaerd, S. Dynamics of homogeneous nucleation. J Chem Phys. 143(15), 154705, 2015.
5. Katz, J.L. Homogeneous nucleation theory and experiment: A survey. Pure Appl Chem. 164(11), 1661, 1992.
6. Wegener, P.P. Nonequilibrium flow with condensation. Acta Mech. 21(1), 65, 1975.
7. Reid, R.C. Possible Mechanism for Pressurized-Liquid Tank Explosions or BLEVE's. Science. 203(4386), 1263, 1979.
8. Mukai, K. Interfacial phenomena, metals processing and properties. Woodhead Publishing Series in Metals and Surface Engineering, Fundamentals of Metallurgy, 237-269, 2005.
9. Gibbs, J.W. On the equilibrium of heterogeneous substances. Am J Sci. s3-16(96), 441, 1878.
10. Mullin, J.W. Crystallisation, 4th Edition, Butterworth Heinemann, Oxford, UK. 6(2), 201, 2001
11. Strey, R., Wagner, P.E., Viisanen, Y. The Problem of Measuring Homogeneous Nucleation Rates and the Molecular Contents of Nuclei: Progress in the Form of Nucleation Pulse Measurements. J Phys Chem. 98(32), 7748, 1994.
12. Shanmugam, K., Radhakrishnan,T.K., Kalaichelvi, P. A review on classical and non classical nucleation theories. Crystal Growth & Design, 2016.
13. Soga, K.G., Melrose, J.R., Robin, C.B. Metastable states and the kinetics of colloid phase separation. The Journal of chemical physics. 110(4), 2280-2288, 1999.
14. Anderson, V., Lekkerkerker, H. Insights into phase transition kinetics from colloid science. Nature. 416, 811-815, 2002.
15. Wolde, T., Frenkel, D. Enhancement of protein crystal nucleation by critical density fluctuations. Science. 277(5334), 1975-8, 1997.
16. Ostwald, W.Z.Z. Phys. Chem. 22, 289-330, 1897.
17. Gliko, O., Neumaier, N., Pan, W., Haase, I., Fischer, M., Bacher, A., Weinkauf, S., Vekilov, P.G. A metastable prerequisite for the growth of lumazine synthase crystals. Journal of the American Chemical Society. 127(10), 3433-3438, 2005.
18. Oxtoby, D.W., Talanquer, V. Crystal nucleation in the presence of a metastable critical point. 109(1), 223-0, 1998.
19. Vekilov, P.G. Dense liquid precursor for the nucleation of ordered solid phases from solution. Crystal Growth & Design. 4(4), 671-685, 2004.
20. Van Driessche, A., Stawski, T., Benning, L., Kellermeier, M. Calcium Sulfate Precipitation Throughout Its Phase Diagram. New Perspectives on Mineral Nucleation and Growth. 227-256, 2017.
21. Bots, P., Benning, L.G., Rodriguez-Blanco, J.D., Roncal-Herrero, T., Shaw, S. Mechanistic Insights into the Crystallization of Amorphous Calcium Carbonate (ACC). Crystal Growth & Design.12 (7), 3806-3814, 2012.

22.Krautwurst, N., Nicoleau, L., Dietzsch, M., Lieberwirth, I.,Labbez, C., Fernandez-Martinez, A., Van Driessche, A. Two-step nucleation process of calcium silicate hydrate, the nano-brick of cement. Chemistry of Materials. 30(9), 2018.
23.Baumgartner, J., Kumar Ramamoorthy, R., Freitas, A.P., Neouze, M.A., Bennet, M., Faivre, D., Carriere, D. Self-Confined Nucleation of Iron Oxide Nanoparticles in a Nanostructured Amorphous Precursor. Nano Letters. 20 (7), 500, 2020.
24. Fleury, B., Neouze, M.A., Guigner, J.M., Menguy, N., Spalla, O., Gacoin, T., Carriere, D. Amorphous to Crystal Conversion as a Mechanism Governing the Structure of Luminescent YVO4:Eu Nanoparticles. ACS Nano. 8(3), 2602-2608, 2014.
25. Gebauerantje, D., Volkel, A., Colfen, H. Stable Prenucleation Calcium Carbonate Clusters. Science. 322(5909). 1819-1822, 2008.
26. Wallace, A.F., Hedges, L.O., Fernandez-Martinez, A., Raiteri, P., Gale, J.D., Waychunass, G.A., Whitelam, S., Banfield, J.F., De Yoreo, J.J. Microscopic Evidence for Liquid-Liquid Separation in Supersaturated $CaCO_3$ Solutions.Science. 341(6148), 885-889, 2013.
27. Bewernitz, M., Gebauer, D., Long, J., Cölfen, H., Gower, L. A metastable liquid precursor phase of calcium carbonate and its interactions with polyaspartate. Faraday Discussions. 159, 291-312, 2012.
28. Gebauer, D., Raiteri, P., Gale, J.D., Cölfen, H. On classical and non-classical views on nucleation. American Journal of Science. 318(9), 969-988, 2018.
29.Henzler, K.,Fetisov, E.O.,Galib, M.,Baer, M.D.,Legg, B.A., Borca, C., Xto, J.M., Pin, S., Fulton, J.L., Schenter, G.K., Govind, N., Siepmann, J.I., Mundy, C.J., Huthwelker, T., De Yoreo, J.J. Supersaturated calcium carbonate solutions are classical.Science Advances.4(1), 2018.
30. Soroka, I. Portland Cement Paste and Concrete. Palgrave Macmillan. 1979
31. Matschei, T., Lothenbach, B., Glasser, F.P. The AFm phase in Portland cement. Cement and Concrete Research. 37(2), 118-130, 2007.
32. Plowman, C., Cabrera, J.G. Mechanism and kinetics of hydration of C3A and C4AF, extracted from cement. University of Leeds, England. Cement and concrete research. 14, 238-248, 1983.
33. Tang, F.J., Gartner, E.M. Influence of sulphate source on Portland cement hydratation. Advances in Cement Research. 1(2), 67-74, 1988.
34. Barret, P. Fundamental hydration kinetic features of the major cement constituants : Ca_3SiO_5 and Ca_2SiO_4 . Jour. Chimie Physique. 765-775, 1986
35. Lecoq, X. Etude de l'hydratation à concentration controlée du silicate tricalcique Ca_3SiO_5 et des caracteristiques de ses produits de reaction. Universite de Bourgogne, Dijon, 1993.
36. Haas, J., Nonat, A. From C–S–H to C–A–S–H: Experimental study and thermodynamic modelling. Cement Concrete Research. 68, 124-138, 2015.
37.Damidot, D. Etude de l'hydratation du silicate tricalcique en suspension diluée par microcalorimétrie isotherme. Thèse de doctorat, Université de Bourgogne, 1990.
38. Garrault, S., Nonat, A. Hydrated Layer Formation on Tricalcium and Dicalcium Silicate Surfaces: Experimental Study and Numerical Simulations. Langmuir, 17(26), 8131–8138, 2001.
39. Garrault-Gauffinet, S. Etude expérimentale et par simulation numérique de la cinétique de croissance et de la structure des hydrosilicates de calcium, produits d'hydratation des silicates tricalcique et dicalcique. Thèse de doctorat, université de Bourgogne, 1998.
40. Nicoleau, L., Nonat, A. A new view on the kinetics of tricalcium silicate hydration. Cem Concr Res. 86(1), 2016
41. Juilland, P., Gallucci,.E.et.al. Dissolution theory applied to the induction period in alite hydration, Cement and Concrete Research. 40(6), 831-844, 2010.
42. Juilland, P., Nicoleau, L.et.al. Advances in dissolution understanding and their implications for cement hydration. RILEM Technical Letters. 2, 90-98, 2017.
43. Bazzoni, A.et.al. Impact of Annealing on the Early Hydration of Tricalcium Silicate. Journal of the American Ceramic Society. 97(2), 584-591, 2014.
44. Nicoleau, L. New Calcium Silicate Hydrate Network. Transportation Research Record. 2142(1), 42-51, 2010.
45. Klur, I. Etude par RMN de la structure des silicates de calcium hydratés, en relation avec leurs propriétés d'adhération. in Chimie-Physique/ESPCI (Zanni). Université Paris VI, 158, 1996.

46. Taylor, H.F. Proposed structure for calcium silicate hydrate gel. Journal of the American Ceramic Society. 69, 464-467, 1986.
47. Nonat, A., Lecoq, X. The Structure, stoichiometry and properties of C-S-H prepared by C_3S hydration under Controlled Condition. Nuclear Magnetic Resonance Spectroscopy of Cement-Based Materials. 197-207, 1998.
48. Yu, P., Kirkpatrick, R.J., Poe, B., McMillan, P.F. Cong X. Structure of Calcium Silicate Hydrate (C-S-H): Near-, Mid-, and Far-Infrared Spectroscopy. J Am Ceram Soc. 82(3),742,8,
49. Courault, A.C. Simulation expérimentale des C-S-H dans les bétons modernes : étude de la composition et des propriétés a l'équilibre dans les milieux complexes. Université de Bourgogne, Dijon,2000.
50. Flint, E.P., Wells, L.S. Bur Stand J Res 12, 751, 1934.
51. Taylor, H.F.W. J Chern Soc 72, 3682, 1950.
52. Greenberg, S.A., Chang, T.N., Andreson, E. J Am Ceram Soc. 72(4), 665, 1960.
53. Greenberg, S.A., Chang, T.N. J Phys Chern 69(1), 182, 1965.
54. Plusquellec, G. Analyse in situ de suspensions de silicate de calcium hydraté : application aux interactions ioniques à la surface des particules. Université de Bourgogne. 2014
55. Grangeon, S.et.al. Quantitative X-Ray Pair Distribution Function Analysis of Nanocrystalline Calcium Silicate Hydrates: A Contribution to Understanding of Cement Chemistry. J Appl Cryst, 50 (1), 14–21, 2017.
56. Kumar, A. et.al. The Atomic-Level Structure of Cementitious Calcium Silicate Hydrate. J. Phys. Chem. C. 121 (32), 17188–17196, 2017.
57. Kovačević, G.et.al. Atomistic Modeling of Crystal Structure of Ca1.67SiHx. Cement and Concrete Research. 67, 197–203, 2015
58. Hamid, S.A. The crystal structure of the 11 Ä natural tobermorite $Ca_2.25[Si_3O_7.5(OH)1.5]\cdot 1H_2O$. 1981.
59. Grangeon, S., Claret, F., Linard, Y., Chiaberge, C. X-ray diffraction: a powerful tool to probe and understand the structure of nanocrystalline calcium silicate hydrates. Acta Crystallogr Sect B Struct Sci Cryst Eng Mater. 69(5), 465, 2013
60. Renaudin, G. et al. Structural characterization of C-S-H and C-A-S-H samples-Part I: Long-range order investigated by Rietveld analyses. Journal of Solid State Chemistry. 182(12), 3312-3319. 2009
61. Nonat, A., X, Lecoq. The structure, stoichiometry and properties of C-S-H prepared by C_3S hydration under controlled solution. in Nuclear Magnetic Resonance Spectroscopy of cement based materials. Bergamo, Italie, Spinger, 1996.
62. Cong, X. and R.J, Kirkpatrick. 29Si MAS NMR study of the structure of calcium silicate hydrate. Advanced Cement Based Materials. 3(3-4), 144-156, 1996.
63. Lognot, I. NMR and infrared spectroscopies of C-S-H and Al-substituted C-S-H synthesised in alkaline solutions. in 2nd international conference on NMR-spectroscopy of cement-based materials. Bergamo: Springer, 1996.
64. Labbez, C.et.al. Surface Charge Density and Electrokinetic Potential of Highly Charged Minerals: Experiments and Monte Carlo Simulations on Calcium Silicate Hydrate. J. Phys. Chem. B, 110 (18), 2006.
65. Labbez, C.et.al. C-S-H/Solution Interface: Experimental and Monte Carlo Studies. Cement and Concrete Research. 41, 161-168, 2011
66. Turesson, M.et.al. A. Calcium Mediated Polyelectrolyte Adsorption on Like-Charged Surfaces. Langmuir. 27(22), 13572-13581, 2011.
67. Nonat, A. The structure and stoichiometry of C-S-H. Cem Concr Res. 34(9), 1521, 2004.
68. Bullard, J.et.al. Mechanisms of Cement Hydration. Cem. Concr. Res. 41, 1208-1223, 2011.
69. Kulik, D.A. Improving the Structural Consistency of C-S-H Solid Solution Thermodynamic Models. Cem. Concr. Res. 41, 477-495, 2011.
70. Chen, J.J.et.al. Solubility and structure of calcium silicate hydrate. Cement and concrete research. 34(9), 1499-1519, 2004.
71. Gisby, J.A.et.al. CSH solubility modeling at different temperatures. In 12th International Congress on the Chemistry of Cement, Cement Association of Canada, Montreal, 128, 2007.
72. Gauffinet, S., Finot, E., Nonat, A. Proc. Int. RILEM Workshop. Dijon, in press, june, 1997.

73. Nonat, A., Lecoq, X., Gauffinet, S. Proc. X Int. Congress on Chemistry of Cement, Goteborg, Suède, 1997.
74. Garrault-Gauffinet, S., Nonat, A. Experimental investigation of calcium silicate hydrate (C-S-H) nucleation, Journal of Crystal Growth, 200(3-4), 565-574, 1999.
75. Taylor, H.F.W. Cement Chemistry. T. Telford, 1997.
76. Kobayashi, K.et.al. Carbonation of concrete structures and decomposition of C-S-H. Cem. Concr. Res, 24, 55, 1994.
77. Zheng, Q.et.al. New Insights into the Role of Portlandite in the Cement System: Elastic Anisotropy, Thermal Stability, and Structural Compatibility with C-S-H. Crystal Growth & Design, 20 (4), 2477–2488, 2020.
78. Berger, R.L. Calcium Hydroxide: Its Role in the Fracture of Tricalcium Silicate Paste. Science, 175 (4022), 626-629, 1972.
79. Concrete, Baudoin, J.J. Calcium Hydroxide in Cement Matrices: Physico- Mechanical and Physico-Chemical Contributions. In Materials Science of Concrete: Calcium Hydroxide in, Wiley, Special volume, (64), 131-142, 2000.
80. Bernal, J.D., Megaw, H.D. The Function of Hydrogen in Intermolecular Forces. Proceedings of the Royal Society A: Mathematical, Physical and Engineering Sciences, 151(873), 384–420, 1935.
81. Busing, W.R., Levy, H.A. Neutron Diffraction Study of Calcium Hydroxide. The Journal of Chemical Physics, 26(3), 563, 1957.
82. Aïtcin, P.C., Flatt, R.J. Science and Technology of Concrete Admixtures, 2016.
83. Jewell, S., Kimball, S.M. U.S. Geological Survey: Mineral commodity summaries, 2015.
84. Newman, A.C.D. Chemistry of clays and clay mineral. Mineralogical Society monograph, Wiley, Harlow, UK, 1987.
85. Dinh, T.T.X. Etude expérimentale et numérique de l'approche physico-chimique pour le matériau hétérogène: Application au matériau cimentaire soumis au dioxyde de carbone (CO_2). Thèse de doctorat, Université d'Evry Val d'Essonne, 2012.
86. Duchesne, J., Reardon, E.J. Measurement and prediction of portlandite solubility in alkali solutions, Cement and Concrete Research, 25(5), 1043-1053, 1995.
87. Pallagi, A. The solubility of $Ca(OH)_2$ in extremely concentrated NaOH solutions at 25°C. Central European Journal of Chemistry, 10(2), 332-337, 2011.
88. Yuan, T., Wang, J., Li, Z. Measurement and modelling of solubility for calcium sulfate dihydrate and calcium hydroxide in NaOH/KOH solutions. Fluid phase equilibria. 297(1), 129-137, 2010.
89. Konno, H., Nanri, Y., Kitamura, M. Crystallization of aragonite in the causticizing reaction. Powder Technology. 123(1), 33-39, 2002.
90. Klein et D.H., Smith, M.D. Homogeneous Nucleation of Calcium Hydroxide. Talanta, 15 (2), 229-231, 1968.
91. Rodriguez-Navarro, C.et.al. Nonclassical Crystallization of Calcium Hydroxide via Amorphous Precursors and the Role of Additives. Crystal Growth & Design, 20 (7), 4418-4432, 2020.
92. Rodriguez-Navarro et.al. Crystallization and Colloidal Stabilization of $Ca(OH)_2$ in the Presence of Nopal Juice (Opuntia Ficus Indica): Implications in Architectural Heritage Conservation. Langmuir, 33(41), 10936-10950, 2017.
93. Broni-Bediako, E., Ogbonna-Friday, J., Ofori-Sarpong, G. Oil well cement additives: a review of the common types, 2, 2016.
94. Salain, I.M.A. Using calcium chloride as an accelerator for Portland pozzolan cement concrete compressive strength development, IOP Conference Series: Materials Science and Engineering, 2019.
95. Ramachadran, V.S. Calcium chloride in concrete: applications and ambiguities. Canadian Journal of Civil Engineering. 5, 213-221, 1978.
96. Ramachandran, V.S. Calcium Chloride in Concrete, 1974.
97. Satiyawira, B., Fathaddin, M.T., Setiawan, R. Effects of lignosulfonate and temperature on compressive strength of cement. Proceedings World Geothermal Congress, 2010.
98. Kamsuwan, T., Srikhirin, T. Effect of lignosulfonate on mechanical and setting time properties of geopolymer paste, 2010.
99. Ogbonna, J. The secondary effects of ligno sulfonate cement retarder on cement slurry properties. Journal of Engineering and Applied Science, 4(9), 2009.

100. Marchon, D.et.al. Impact of chemical admixtures on cement hydration. Science and technology of concrete admixtures, 2016.
101. Ramachandran, V.S. Interaction of calcium lignosulfonate with tricalcium silicate, hydrated tricalcium silicate, and calcium hydroxide. Cement and Concrete Research, 2(2), 179-194, 1972.
102. Previte, R.W., Grace, W.R. Some insights on the mechanism of saccharide set retardation of portland cement. Cement and Concrete Research, 1(3), 301-316, 1971.
103. Thomas, N.L., Birchall, J.D. The retarding action of sugars on cement hydration. Cement and Concrete Research, 13, 830-842, 1983.
104. Luke, K., Luke, G. Effect of sucrose on retardation of Portland cement. Advances in Cement Research, 12(1), 9-18, 2000.
105. Mazumder, A.F. Effect of sugar on setting time of portland cement. 3rd International Conference on Advances in Civil Engineering, 21-23, 2016.
106. Otunyo, A.W., Koate, I. Sugar cane juice as a retarding admixture in concrete production. Global Journal Of Engineering Research, 14, 17-23, 2015.
107. Khan, B., Baradan, B. The effect of sugar in setting-time of various types of cements. Materials Science, 2002.
108. Peschard, A., Govin, A., Grosseau, P., Guilhot, B., Guyonnet, R. Effect of Polysaccharides on the Hydration of Cement Paste at Early Ages. Cement and Concrete Research, 34, 2153-2158, 2004.
109. Akstinat, M.H. Interaction of saccharides and sugar alcohols with well cement. Advances in Cement Research, 28(8), 503-517, 2016.
110. Nalet, C., Nonat, A. Effects of functionality and stereochemistry of small organic molecules on the hydration of tricalcium silicate. Cement and Concrete Research, 87, 97-104, 2016.
111. Nalet, C., Nonat, A. Ionic complexation and adsorption of small organic molecules on calcium silicate hydrate: Relation with their retarding effect on the hydration of C3S. Cement and Concrete Research, 89, 96-108, 2016.
112. Young, J.F. A review of the mechanisms of set-retardation in portland cement pastes containing organic admixtures, Cement and Concrete Research, 2(4), 415-433, 1972.
113. Milestone, N.B. Hydration of tricalcium silicate in the presence of lignosulfonates, Glucose, and Sodium Gluconate. Journal of the American Society of Ceramic, 62(7-8), 321-324, 1979.
114. Jolicoeur, C., Simard, M.A. Chemical admixture-cement interactions: phenomenology and physico-chemical concepts. Cement and Concrete Composites, 20(2-3), 87-101, 1998.
115. Nalet, C. Influence de la stéréochimie et de la fonctionnalité de molécules organiques sur l'hydratation de composés cimentaires. Thèse, université de Bourgogne, 2015.
116. Pourchet, S.et.al. Influence of PC Superplasticizers on Tricalcium Silicate Hydration. Proceedings of the 12th International Congress on the Chemistry of Cement, Montréal, Canada, 2007.
117. Marchon, D.et.al. Molecular and Submolecular Scale Effects of Comb-Copolymers on Tri-Calcium Silicate Reactivity: Toward Molecular Design. Journal of the American Ceramic Society, 100 (3), 817-841, 2017.
118. Perez, J.P. The mechanism of action of sodium gluconate on the fluidity and set of Portland cement, Proceedings of the 12th International Congress on the Chemistry of Cement, Montreal, 2007.
119. Pourchez, J.et.al. Current understanding of cellulose ethers impact on the hydration of C_3A and C_3A-sulphate systems, Cem. Concr. Res. 39, 664-669, 2009.
120. Pourchez, J.et.al. Changes in C_3S hydration in the presence of cellulose ethers, Cem. Concr. Res. 40, 179-188, 2010.
121. Nalet, C., Nonat, A. Effects of hexitols on the hydration of tricalcium silicate. Cement and Concrete Research, 91, 87-96, 2017.
122. Zhang, L.et.al. Effects of Saccharide Set Retarders on the Hydration of Ordinary Portland Cement and Pure Tricalcium Silicate. Journal of the American Ceramic Society, 93 (1), 279-287, 2010.
123. Sowoidnich, et.al. Calcium Complexation and Cluster Formation as Principal Modes of Action of Polymers Used as Superplasticizer in Cement Systems. Cement and Concrete Research, 73, 42-50. 2015.
124. Ramachandran, V.S.et.al. The role of phosphonates in the hydration of Portland cement. Mater. Struct., 26, 425-432, 1993.

125. Wilding, C.R.et.al. A classification of inorganic and organic admixtures by conduction calorimetry, Cem. Concr. Res, 14, 185-194, 1984.
126. Plusquellec, G. Analyse in situ de suspensions de silicate de calcium hydraté : application aux interactions ioniques à la surface des particules. Thèse de doctorat, université de Bourgogne, 2014

CHAPTER II. STRATEGY OF THE STUDY

1 General idea and main objectives

As we have just exposed in the introductory chapter, no work has been able to quantify with precision the degree of supersaturation (or undersaturation) with respect to the precipitating hydrates (the dissolving anhydrous phases), i.e. the driving force of precipitation (of dissolution), in the presence of organic additives. Therefore, any quantification of the precipitation or dissolution processes becomes illusory and any observed effects of organic molecules on these processes remain very descriptive and empirical. It is also not surprising that no study has been able to establish with certainty, which process limits the hydration of cement in the presence of organic retarders.

The first objective, which was also the main objective of this study, was the quantification of these processes and first of all of the driving force of the precipitation (and dissolution) of the main hydrates (and anhydrous phases) of Portland cement, which are C-S-H and portlandite (and anhydrous silicate phases) in the presence of different organic retarders. To do so, it was necessary to study the **extent of complex formation between the organic molecules and the constituent ions** of the main hydrates (and anhydrous phases) of Portland cement and to establish a speciation model valid over the whole range of pH and ionic concentrations usual in Portland cement. To reach this first objective, a very pragmatic and efficient approach was chosen, which consisted in measuring with precision the variation of the activity of calcium, silicate and hydroxide ions in the presence of organic molecules in a large range of pH and concentrations and to fit this data set with a speciation model by varying the number, the composition and the stoichiometry of the various complexes which can be formed. The chemical activity of the above cited ions was determined by both a direct and an indirect methods. In the first case, we conducted **potentiometric titration** with proton and calcium specific electrodes to measure the calcium and hydroxide activity of a large set of organic-containing solutions with well defined composition and concentrations. In the second case, we imposed a constant activity product in the solution by adding a **solid in excess (C-S-H or portlandite**), and measured at thermodynamic equilibrium the change in the solution concentration of constitutive ions for increasing amount of organic admixtures. With these data in hand, the game then consisted in finding the set of organic-ions complexes and associated set of equilibrium constants which relate the imposed (potentiometric titration) or measured (solubility) solution concentrations of the species to the measured ion activities (potentiometric titration) or imposed activity product (solubility). These methods are described thereafter and in the next chapter.

The second objective was to compare the influence of organic retarders on the **nucleation of C-S-H,** the main Portland cement hydrate. The literature review in the previous chapter has highlighted the scarcity of work on the influence of organic retarders on the nucleation of cement hydrates. This part

of the work has therefore focused on homogeneous nucleation. In addition, some authors have hypothesized that portlandite precipitation could be responsible for the retarding effects on cement hydration. The influence of organic retarders on the **nucleation of portlandite** has therefore also been studied. For both C-S-H and portlandite, the nucleation rate (J_N) in the presence of several organic retarders was determined from the measurement of the induction time at nucleation, $t_{ind} = 1/J_N$. The kinetic obtained for the different organic molecules could then be quantified and compared by applying the speciation model developed in the first objective. In the case of C-S-H, the idea was also to look at the influence of organic molecules on the non-classical pathway of nucleation. For this, microscopy and X-ray scattering methods were used.

In the next two sections the choice of organic molecules as well as a description of the methods employed are given.

2 Selected molecules

The plethora of molecules having a retarding effect on the hydration of the silicate phases makes the task more difficult when it comes to understanding the processes responsible for in the delay hydration.

The choice of the molecules selected for this study was based on small organic molecules for which we had a large corpus of experimental data on effect on the hydration of Portland cement and its pure phases. These are D-gluconate and three hexitols, D-sorbitol, D-mannitol and D-galactitol, previously studied during Camile Nalet's thesis (115).

They have well defined functional groups and stereochemistry, see Table 3. They also share some functionalities with superplasticizers and are small enough to be modeled by classical speciation models.

Table 3: Cram representation of the selected molecules in the present study.

D-sorbitol

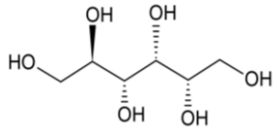

D-mannitol

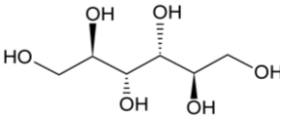

D-galactitol

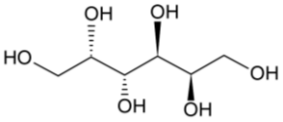

D-gluconate

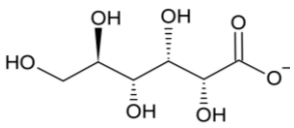

The three hexitols D-sorbitol, D-mannitol and D-galactitol are sugars alcohols that share the same chemical formula but differ by the stereochemistry of their alcohol groups.
D-gluconate is an anionic sugar derivative that share similarities with D-sorbitol, and possesses a carboxylate group in its chain.

3 Materials and methods

The individual methods used will be described in more detail and adapted to the problems addressed in the various articles of Chapter III. In this section, a short overview on the experimental tools and the calculations is presented.

3.1 Potentiometric titration

All the titrations experiments, including the potentiometric titrations and precipitation measurement were performed using a Titrando unit (907 Titrando, Metrohm), controlled by the Tiamo software (Metrohm).
The automatic titrator is composed of dosing systems (800 Dosinos) or glass burettes, that are attached to the reagent bottles. Connected to tips, they allow us to add the titrant solution to the titrated solution at a controlled speed and volume.
Several electrodes are connected to the system:

- A specific electrode of calcium (Ca-ISE), coupled to a reference electrode (Metrohm Ag, AgCl/3 M KCl).
- A combined pH glass electrode (intelligent pH electrode, with Pt 1000, 3 M KCl) with a pH range 0-14.
- An optical electrode (‘optrode’) that measures the turbidity of the sample, monitored with an optical sensor.

A Teflon beaker that contained the titrated solution, was covered with a Teflon lid perforated with several entries for the electrodes, the tips, and the connection to the N_2 stream. In addition, a mechanical overhead stirrer was always used in the titrated solution. For the measurements, the Teflon beaker was placed in a double glass vial thermostated to 23.0°C.

3.2 Solubility measurement

For the solubility measurements, several samples per series were prepared. Each sample consisted of a solid buffer (C-S-H or portlandite) placed in a dialysis membrane immersed in a CO_2 free solution

containing an initial amount of organics. The solution and filled dialysis membrane were hermetically enclosed in 250mL polypropylene bottles.

The samples were prepared in a glove box and finally placed in 16 liter plastic barrel filled with N_2 gas to avoid their carbonation. The barrels were placed on a shaking table during four weeks at 23 °C to reach equilibrium.

Thus, several series were prepared with either C-S-H and/or CH. Each series consist of six samples with increasing concentration of the selected organic molecules and for each sample a blank is prepared with the same solution but without any solid present. The latter was used to control the initial concentration of the molecule of interest. The chemical analysis of the equilibrium solution outside the dialysis bags allowed the determination of the solubility and of the adsorption of the small organic molecules. The chosen set-up has the advantage that no step of separation of the solution from the solid is needed, which is often difficult in case of cement hydrate dispersions (or cement paste) in the presence of organic admixtures. This method also eliminates the artifacts associated with this separation step as the centrifugal force or the hydrostatic pressure necessary to separate the solution from the solid phase can alter the equilibrium conditions (126)

3.3 Chemical analysis

3.3.1. Total organic carbon (TOC)

The total organic carbon (TOC) analysis allows measurement of the total amount of organic carbon present in aqueous samples. Thus, the TOC analyzer oxidizes all the organic molecules to CO_2, and measures the resulting CO_2 concentration. The knowledge of the carbon concentration and the knowledge on the amount of C in the organics used, allows us to measure ultimately the concentration of the organics of interest in the samples prepared.

The determination of the adsorption of the selected molecules on the hydrates C-S-H and portlandite was done by calculating the difference between the initial concentrations of the organics and the concentration measured with TOC at the end of the experiment.

3.3.2. Inductively coupled plasma (ICP)

The determination of ions concentrations in our samples, including calcium, sodium and silicon, was achieved by using Inductively Coupled Plasma coupled with Atomic Emission Spectroscopy (ICP-AES).

3.4 Small angle X-ray scattering (SAXS)

Small angle X-ray scattering (SAXS) experiments were achieved at the NCD beamline of the ALBA synchrotron (Barcelona, Spain) in order to characterize the C-S-H nanoparticles in presence of the selected organic molecules, and its nucleation kinetics.

The set up used is the Metrohm system with in addition, a peristaltic pump to circulate the solution in a closed loop through a 1.5 mm diameter polyimide capillary that was set up at the beam position. The residence time in the tubing and capillary is in the order of approximatively 20 seconds.

A pH electrode and a turbity sensor were immersed in the solution. An X-ray beam of energy E = 12.40 keV, calibrated using a silver behenate standard, was used.

The scattered radiation was collected using a Pilatus 2M two-dimensional detector that was placed at 6.7 m from the sample to yield a q-range $0.03 < q < 2.00$ nm-1. The scattered intensity was acquired every minute in acquisitions of 30 seconds to follow the kinetics of C-S-H nucleation.

3.5 Cryo-transmission electron microscopy (Cryo-TEM)

In order to get an insight on the shape and size of the C-S-H particles in presence of the retardant molecules, 4µl aliquots were retrieved from the solution in the reactor during the C-S-H precipitation experiment, and applied to freshly glow discharged qauntifoil or lacey carbon grid and vitrified using a Thermofisher Vitrobot Mark IV system.

Then, the grids were mounted on a Gatan 626 single-tilt cryo-transfer holder. Imaging and selected area diffraction (SAD) were performed under low-dose conditions on a Tecnai F20 microscope operating at 200 keV. Images were recorded on a Ceta CMOS camera whereas diffraction patterns were recorded on an Amsterdam Scientific Instrument CheeTah hybrid pixel camera.

3.6 Chemical speciation

The measurement of the concentration of the selected organics and calcium, silicon and hydroxide in the solutions in equilibrium with portlandite and C-S-H a well as the potentiometric titration highlighted that several different organic-calcium-silicon-hydroxide complexes could form.

In order to determine the set of organic-ions complexes and associated set of complexation constants needed to describe these systems, various speciation models were constructed, tested and simulated with the chemical speciation software PHREEQC. PHREEQC is an open source code developed by the United State Geological Survey (USGS). The program uses an extended Debye Huckel approach to calculate activity coefficient of simple ions.

The C-S-H model developed by Haas and Nonat (37), presented in the preceding chapter, which takes into account the variation of the solubility and the stoichiometry of the different phases of C-S-H, was used.

4 Structure of the results

The results obtained during this thesis are presented through 3 papers. The first has already been published in the journal Cement and Concrete Research and the two others were recently submitted to the same journal.

Paper 1 presents how the selected molecules affect the calcium activity as well as the portlandite solubility. Different calcium-organic-hydroxide complexes are fitted and compared to the experimental data. The adsorption isotherms of the organic molecules on portlandite are obtained and discussed in relationship with their complexing power with calcium ions.

In paper 2, the solubility of C-S-H in the presence of the selected organics is studied in detail for various stoichiometric C/S ratios. The adsorption isotherms of the organics on C-S-H are determined at two C/S ratios. The calcium-organic-hydroxide complexes from paper 1 are completed with additional Ca-organic-hydroxide-silicon to model the experimental data set.

In paper 3, the influence of the different organic molecules on the induction time of C-S-H nucleation is quantified and compared. The data are further analyzed in terms of thermodynamic and kinetic quantities by applying classical nucleation theory. Finally, the influence of the organics on the nucleation pathway is analyzed with the use of SAXS and Cryo-TEM.

The implications of the results presented in these three papers are discussed in Chapter IV.

CHAPTER III. RESULTS

A. Portlandite solubility and Ca^{2+} activity in presence of gluconate and hexitols

Lina BOUZOUAID[1], Barbara LOTHENBACH[2], Alejandro FERNANDEZ-MARTINEZ[3], Christophe LABBEZ[1]

[1] ICB, UMR 6303 CNRS, Univ. Bourgogne Franche-Comté, FR-21000 Dijon, France

[2] Empa, Concrete & Asphalt Laboratory, Dubendorf, Switzerland

[3] Univ. Grenoble Alpes, Univ. Savoie Mont Blanc, CNRS, IRD, IFSTTAR, ISTerre, 38000 Grenoble, France.

Abstract

The current paper investigates the impact of gluconate, D-sorbitol, D-mannitol and D-galactitol on calcium speciation at high pH values by i) solubility measurements of portlandite ($Ca(OH)_2$) and ii) potentiometric titration measurements of calcium salt solutions. Thermodynamic modeling was used to fit the chemical activities of Ca^{2+} and OH^- ions and thus to determine the strength and kind of the different Ca-organic-hydroxide complexes. The strength of complex formation with Ca decreases in the order gluconate >> sorbitol > mannitol > galactitol, which follows the same order as sorption on portlandite. Heteropolynuclear gluconate complexes with calcium and hydroxide dominate the Ca-speciation in the presence of portlandite, while for sorbitol ternary $CaSorbOH^+$ complexes were dominant under alkaline conditions. We expect that these results will help in better understanding the influence of gluconate and hexitols on the hydration of alite and Portland cement.

1. Introduction

The chemical activity of ions, *a*, and the solubility of minerals are crucial factors in determining the thermodynamic conditions and the driving force of a mineral to dissolve or to precipitate (1). The extent to which a solution is out of equilibrium is given by the deviation from the theoretical solubility and is quantified by the saturation index. For a solid such as portlandite, $Ca(OH)_2$, with the solubility product $K_{sp,}$, the saturation index (SI) is defined as:

$$SI = \frac{a_{Ca2+}.a^2{}_{OH-}}{K_{sp}}$$

The knowledge of the elemental concentrations, the speciation and the ion activities provides a simple measure for the driving force of dissolution or precipitation reactions. However, activity of

ions is sensitive to the presence of other chemical species via the effect of ionic strength. Many ions can also form different soluble complexes such as e.g. calcium gluconate complexes: $Cagluc^{+}$, $Ca(gluc)_2^0$, ... and can in addition promote or inhibit crystal growth/dissolution, which can make the determination of the activity of ions difficult and tedious.

In the case of concrete, organic molecule inhibitors, called retarders, are commonly used in specific applications (2) (3) (4) to delay the cement setting. Superplasticizers, often comb co-polymers, employed in the formulation of ultra high performance concrete, are also known to retard the curing of concrete (5) (6) (7). Although used in low amount, less than 1 wt.% of Portland cement (8), the concentration of organic molecules in the solution present in the interstitial pores formed by cement grains, easily reaches several tens of millimolar concentrations during the first hours after mixing with water and can thus impact the cement reactions involved in the curing. These effects have been illustrated in several studies with various organic molecules (9) (10). Invariably, it was found that the organic molecules acting as cement curing inhibitors can greatly influence the elemental concentrations in the aqueous pore solution and retard the cement hydration. The cement hydration is complex and dependent on two interrelated and concomitant processes, which are the dissolution of the cement grains and the precipitation of the hydrates. However, the physical and chemical mechanisms responsible for this retardation are not fully understood (11) (12) (13) (14) (15). Furthermore, in those organic-cement systems, an accurate quantification of the dissolution rate of cement anhydrates and precipitation rate of cement hydrates at well-defined *SI* is still missing as a result of limited knowledge of complex formation.

For the organics of interest in this paper, the pure dissolution of alite (Ca_3SiO_5) was found to be negligibly affected by gluconate and three different hexitols, namely sorbitol, mannitol and galactitol (15). These organics, however, have a great impact on alite hydration and to a less extend on the hydration of Portland cement (15). These molecules were thus conjectured to mostly act as nucleation-growth inhibitors of calcium silicate hydrate, C-S-H (16) In a recent experimental study, it was suggested that the inhibition of the crystallization of portlandite, $Ca(OH)_2$, could be the main reason of the slowdown of alite hydration (17).

Gluconate, a negatively charged molecule, was found to be a stronger retardant of cement hydration than neutral hexitols (16) (18) (19). For different hexitols also the stereochemical arrangements of the organic molecules, as illustrated in Figure 1, has an influence (16). The retardation was observed to increase from mannitol to galactitol to sorbitol, which have the same chemical composition and functional groups, but a different arrangement. However, the chemical mechanisms, which could explain how these organics retard are poorly understood, e.g. their impact on the anhydrate and hydrate solubility and the eventual formation of aqueous complexes (16) (18). In particular, in the high pH range little is known about possible aqueous complexes with organic molecules or their stability.

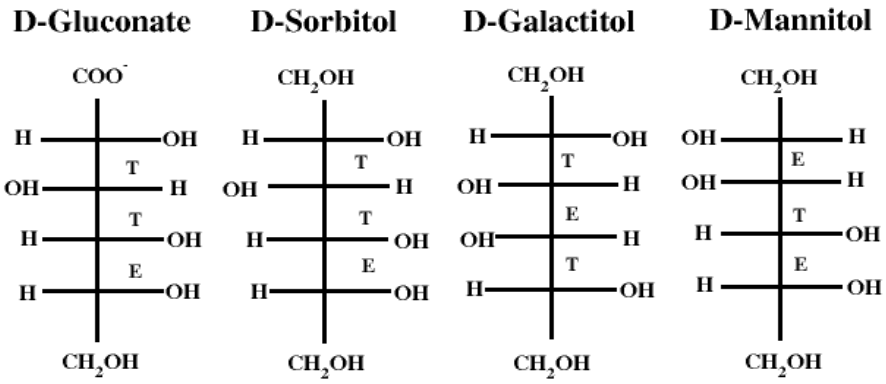

Figure 1: Structure of (from left to right) D-gluconate, D-sorbitol, D-galactitol and D-mannitol. "T" corresponds to the threo diastereoisomer configuration. "E" corresponds to erythro diastereoisomer configuration.

It has been suggested that the ability of the organic molecules to form complexes with Ca^{2+} is directly correlated to their adsorption affinity with calcium rich surfaces of C-S-H and alite (18) (19) which, in turn, may impart the surface tension of the nucleus or the rate of attachment of species to the nucleus and, thus, the nucleation rate. Thus, the understanding and quantification of complex formation between organic molecules and calcium could be fundamental for a better understanding of the observed retardation by organic additives. In addition, only an adequate quantification of the different Ca-complexes formed in the presence of organics makes it possible to determine the ion activities needed to calculate *SI* with respect to Ca_3SiO_5, calcium silicate hydrate and portlandite.

D-gluconate, is a well know retarding additive (20) (21) (22) widely used in the industry. In addition to its role as retarder in cements and concretes, gluconate is also used for water treatment and metal surface treatment due its strong complexation ability with cations. The complex formation between Ca and gluconate has been investigated in several studies (23) (24) (25) (26) (27) (28), but mainly at high ionic strength (1.0 M NaCl) and relatively low pH. On the other hand, the complex formation between hexitols and calcium ions was much less investigated (29) (30) and again at relatively low pH values not relevant for cements.

The present paper thus aims to investigate the speciation of alkaline calcium solutions in the presence of a carboxylate sugar acid: gluconate and several uncharged hexitols: D-sorbitol (D-glucitol), D-mannitol, and D-galactitol, at concentrations and pH values relevant for cementitious systems. A particular emphasis is on the ability of the organics to form complexes with calcium ions. This is assessed experimentally by solubility measurements of portlandite and ion activity measurements of alkaline calcium solutions in presence of increasing amount of organics. The results were then fitted with a speciation model, using the open source software PHREEQC, to determine the strength and the various types of calcium complexes with the organic molecules.

2. Materials and methods

2.1 Materials

The different stock solutions from each compound were prepared by dissolving $Ca(NO_3)_2$ $4H_2O$ (Sigma-Aldrich, ≥99% purity), potassium gluconate ($C_6H_{11}KO_7$, Sigma-Aldrich, ≥99% purity) D-sorbitol ($C_6H_{14}O_6$, Sigma-Aldrich, ≥99% purity), D-mannitol ($C_6H_{14}O_6$, Sigma-Aldrich, ≥99% purity), and D-galactitol ($C_6H_{14}O_6$,, Sigma-Aldrich, ≥99% purity), in boiled and degassed milliQ water. In the potentiometric titration experiments, potassium nitrate (KNO_3, Sigma-Aldrich, ≥99% purity) was used as a background electrolyte (0.1 M) and KOH (>85%, Sigma-Aldrich) to increase the pH values to 11.3, 12.3, 12.7 and 13.0. For the solubility measurement, portlandite, calcium hydroxide ($Ca(OH)_2$, Sigma-Aldrich, ≥ 95%) was used.

It is important to note that the hexitols used in this study are all isomers, sharing the formula, $HOCH_2(CHOH)_4CH_2OH$, but differ in the stereochemical arrangement of the OH groups as illustrated in Figure 1.

2.2 Solubility experiments

For the solubility experiments, various series of samples were prepared in a glove box with 3.92 g of $Ca(OH)_2$, as a solid buffer, enclosed in a dialysis membrane and then placed in a 250 mL polypropylene flask filled with 200 mL of CO_2-free solution with different amounts and type of organic molecule, see Figure 2. Prior to use, the dialysis membranes (Spectra / Por, MWCO 12-14 kD) were dipped in distilled water for 30 minutes to remove any organic residues and dried in a desiccator overnight; the dialysis bags were closed with polyamide clamps (Carl Roth, length 50 mm). Finally, the samples were stored in a 16 L plastic barrel filled with N_2 gas, to guarantee CO_2 free conditions, and placed on a shaking table during four weeks at 23°C to ensure a proper equilibrium.

The pH values were recorded after removing the dialysis bags from the bottles. The pH electrode (Consort C931 electrochemical analyser) was calibrated using Sigma Aldrich buffer (pH 4, 7, 9 and 12). The total concentration of the elements Ca and Si was measured by inductively coupled plasma-optic emission spectroscopy (ICP-OES 5110, Agilent).

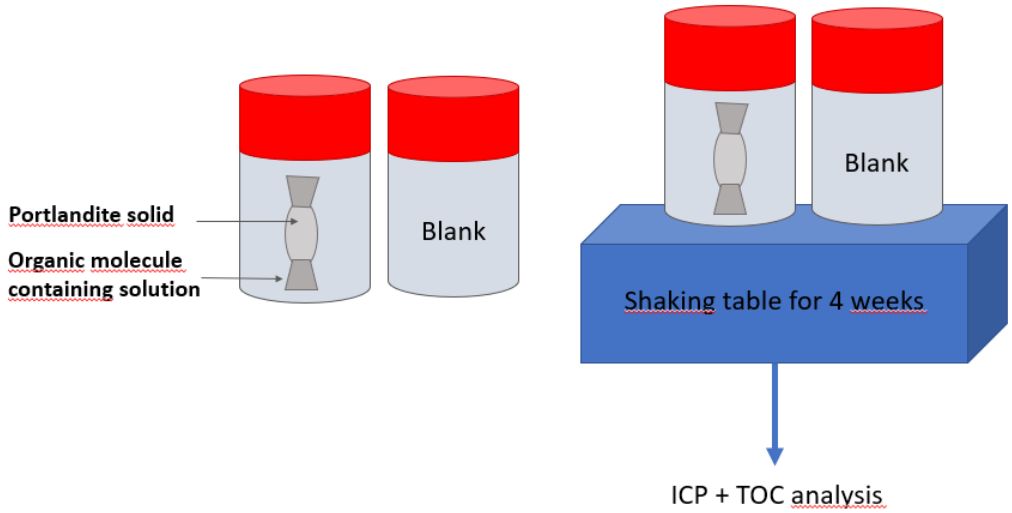

Figure 2: Schematic representation of a pair of samples used for the solubility and adsorption experiments. The flask used for the solubility measurement contains a dialysis bag filled with portlandite powder, immersed in a solution containing the organic molecule. The second flask contains the organic molecule solution only and is used as a blank/reference to verify the organic concentration introduced initially. This allows the determination of the organic adsorption on C-S-H by mass balance based on the measured difference. Note that the same stock solution is used for each sample pair.

The bulk concentration of organics at equilibrium was measured as total organic content with a TOC VCPN instrument (Shimadzu). This method is based on the oxidation of organic molecules contained in solution by gaseous oxygen with a platinum-based catalyst in an oven raised to a temperature of 720°C. The CO_2 formed is detected by Infra-Red Non-Dispersive (NDIR). The detection threshold for this device is very low (4µg/L).

2.3 Titration of Ca^{2+} with the ion selective electrode

The chemical activity of calcium ions was also determined from potentiometric titration measurements using an automatic titrator instrument (Metrohm 905 Titrando); the setup is detailed in Figure 3. All measurements were performed in a titration reactor thermostated to 23.0 ± 0.1°C. The titrated solutions were continuously stirred at a constant rate 430 rpm. A nitrogen flow circulated continuously above the solution to avoid the ingress of CO_2. It was taken care that the gas did not enter the solution to avoid any disturbance of the electrodes. In the reactor, 100 mL of a solution containing 0.1 M KNO_3 background electrolyte and 0.25 mM $Ca(NO_3)_2$ was thermostated for approximately 20 minutes before the start of the titration. After 3 minutes of equilibration time, and only if the change in the electrode signal was < 0.5 mV/min, a titrant solution containing 0.2M of organic molecule was added drop by drop (0.2 ml, 50 times for a total volume added of 10 ml) at the maximal speed registered in the software "Tiamo" (Metrohm).

The Ca^{2+} activity was measured at 23.0 ± 0.1°C with a calcium sensitive electrode (Metrohm Ca ISE, 6.0508.110) coupled to a reference electrode (Metrohm Ag, AgCl/3 M KCl, 6.0750.100). A stable electrode signal could only be obtained with the use of a background electrolyte. The titrations were thus performed in 0.1 M KNO_3 to ensure a stable signal and to limit the influence of the background electrolyte on the complex formation. We have chosen potassium nitrate as K^+ interferes less with the Ca^{2+}- selective electrode than Na^+ (31). The Ca^{2+} electrode was calibrated prior to the measurements by a titration of 100 mM KNO_3 solution with a solution containing 500 mM $Ca(NO_3)_2$ (0.2 ml, 50 times for a total volume added of 10 ml) and by plotting the measured mV against the calculated Ca^{2+} activity calculated with PHREEQC as detailed below. The response of the Ca^{2+} electrode was found to be linear with a slope of 29±1 mV, which corresponds to the expected slope of 29.4 mV at 23°C. The pH was determined with a pH electrode (Metrohm pH Unitrode with Pt 1000, 6.0259.100), which allows reliable measurements up to pH = 14. The pH electrode was calibrated prior to the measurements with standard buffer solutions (pH 9, 10, and 12.45 from Sigma Aldrich).

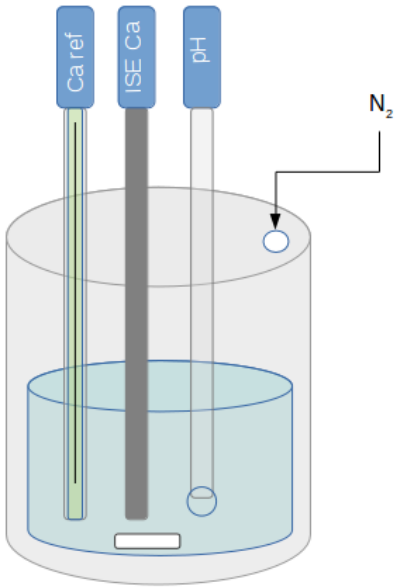

Figure 3: Schematic representation of the experimental titration set up: the reactor contains the titrated solution, the calcium specific electrode, the reference electrode, and the pH electrode.

2.4 Thermodynamic simulation and complexation constants

The solubility of portlandite and the activity of Ca^{2+} were fitted with a speciation model solved by the geochemical software PHREEQC version 3 (3.6.2-15100) (32) and the WATEQ4f database (33). The activity of the Ca^{2+}, a_{Ca2+}, and all other species was calculated according to $a_{Ca2+} = \gamma_{Ca2+} \cdot m_{Ca2+}$, where γ_{Ca2+} is the activity coefficient and m_{Ca2+} the molality in mol/kg H_2O. The activity coefficients were calculated with the WATEQ Debye Hückel equation:

$$\log\gamma_i = \frac{-A_y z_i^2 \sqrt{I}}{1+B_y a_i \sqrt{I}} + b_y I \quad (1)$$

where z_i denotes the charge of species *i*, I is the effective molal ionic strength, while a_i , the ion-size parameter, and b_y are ion specific parameters and A_y and B_y are pressure- and temperature-dependent coefficients (33). This activity correction is applicable up to approximately 1 M of ionic strength (34).

Table 1. Complex formation constants K, expressed in log K, between calcium and gluconate ($Gluc^-$) at standard conditions (1 bar, 25°C) reported in literature and determined in the present study.

	Sayer (28) 0M	Masone (27) *(0.5M)* 0M[1]	Zhang (35) *(0.1M)* 0M	Pallagi (24) *(1M)* 0M	Bretti (36) 0M	Kutus (26) *(1M)* 0M	This study 0 M
Solid							
$Ca^{2+} + 2OH^- = Ca(OH)_2$	-	-	-	-	-	-	**-5.20** [a]
Aqueous complexes							
$Ca^{2+} + OH^- = CaOH^+$	-	-	-	*(0.97)* 1.83	-	-	**1.22** [a]
$GlucH^0 = Gluc^- + H^+$	3.7	-	*(3.30)*3.53	*(3.24)* 3.64 [b]	3.71	-	**3.64**
$Gluc^- + OH^- = GlucOH^{2-}$ [c]	-	-	-	*(0.08)* -0.44	-	-	**-0.44**
$Ca^{2+} + Gluc^- = CaGluc^+$	1.21	*(1.05)* 1.79	-	*(0.37)* 1.23	-	*(0.70)* 1.56	**1.56**
$Ca^{2+} + 2Gluc^- = CaGluc_2^0$	-	*(1.88)* 2.98	-	-	-	*(1.65 [d])* 2.9	**2.85**
$Ca^{2+} + OH^- + Gluc^- = CaGlucOH^0$	-	-	-	*(2.82)* 4.07	-	(*2.86 [d]*)4.11	**3.95** [e]
$2Ca^{2+} + 3\ OH^- + Gluc^- = Ca_2Gluc(OH)_3^0$	-	-	-	*(8.04)* 10.48		-	-
$2Ca^{2+} + 4\ OH^- + 2Gluc^- = Ca_2Gluc_2(OH)_4^{2-}$	-	-	-	-	-	(*9.49 [d]*) 11.34	**11.25** [e]
$3Ca^{2+} + 4\ OH^- + 2Gluc^- = Ca_3Gluc_2(OH)_4^0$	-	-		*(12.44)* 16.07	-	(*12.59 [d]*) 16.22	**16.10** [e]

Values reported for I = 0.1, 0.5 and 1 M extrapolated to 0 M ionic strength in this study using the WATEQ Debye Huckel equation (1); - : not reported; [a] values from Thoenen et al. (37); [b] value from Pallagi et al. (23); [c] notation $GlucOH^{2-}$ represents the two times deprotonated $C_6O_7H_{10}^{-2}$ as suggested in (24) ; [d] recalculated from reaction formulated with H+ (26) using a log K_w of -13.62 at 1 M NaCl; [e] fitted in this study

Table 2. Complex formation constants, expressed in log K, between calcium and sorbitol (Sorb), mannitol (Man) and galactitol (Gal) at standard conditions (1 bar, 25°C) reported in literature and determined in the present study.

	Kieboom (30) *(0.2-0.8M)* 0M	Haas (29) *(0.7M)* 0M	Kutus (25) *(1M)* 0M	This study
$Ca^{2+}+Sorb^{0} = CaSorb^{2+}$	*(0.11)* 0.08	*(-0.52)* -0.54	*(0)* -0.06	**0.10**[a]
$Ca^{2+} + Sorb^{0} + OH^{-} = SorbCaOH^{+}$				**2.85** [a]
$2\ Ca^{2+} + 2Sorb^{0} + 4OH^{-} = Ca_2Sorb_2(OH)_4^{0}$				**9.75** [a]
$Ca^{2+}+ Man^{0} = CaMan^{2+}$	*(-0.05)* -0.08	*(-0.62)* -0.64	*(-0.3)* -0.36	**-0.36**
$Ca^{2+} + Man^{0} + OH^{-} = CaManOH^{+}$				**2.65** [a]
$2\ Ca^{2+} + 2Man^{0} + 4OH^{-} = Ca_2Man_2(OH)_4^{0}$				**9.65** [a]
$Ca^{2+} + Gal^{0} = CaGal^{2+}$		*(-0.51)* -0.53		**-0.53**
$Ca^{2+} + Gal^{0} + OH^{-} = CaGalOH^{+}$				**2.80** [a]
$2\ Ca^{2+} + 2Gal^{0} + 4OH^{-} = Ca_2Gal_2(OH)_4^{0}$				**9.29** [a]

[a] Fitted in this study

The complex formation constants between Ca^{2+} and hydroxide, gluconate, sorbitol, mannitol and galactitol reported in the literature and determined in the present study are detailed in Table 1 and Table 2. For gluconate, sorbitol and mannitol we used as starting values the complexes and associated constants derived from Pallagi and co-workers (23) (24) (25) (26). They were, where necessary, further refined to obtain a good visual fit between the measured and the modeled data. The following procedure to refine the complexation constants was employed. First, the potentiometric data measured at pH 11.3 were used to fit the constants for the $CaGluc^{+}$, $CaSorb^{2+}$, $CaMan^{2+}$, and $CaGal^{2+}$ complexes, which dominate at low pH values. Then, the titration data at higher pH values were used to fit the constants for the $CaGlucOH^{0}$, $CaSorbOH^{+}$, $CaManOH^{+}$, and $CaGalOH^{+}$ complexes. The formation of $CaGluc_2^{0}$, suggested by Pallagi et al. (23) and Kutus et al. (26), and of $Ca_2Gluc_2OH_4^{2-}$ and $Ca_3Gluc_2OH_4^{0}$ complexes suggested by Kutus et al. (26), were also considered. Only traces of the $CaGluc_2^{0}$ complex were calculated to be present in our experiments (less than 1 % of the total Ca in any of the experiments) thus this complex was considered but its constant not further refined. The presence of $Ca_3Gluc_2OH_4^{0}$ and $Ca_2Gluc_2OH_4^{2-}$ complex is not important at low calcium concentrations (i.e. the conditions used in this study for the potentiometric titration) but in the presence of portlandite. Thus their constants were refined using the solubility data of portlandite.

The $CaSorb^{2+}$, $CaMan^{2+}$, and $CaGal^{2+}$ complexes reported in the literature were not found to be in significant quantities in any of our experiments, as they were obtained in near neutral pH conditions. Furthermore, the reported values of the complex formation constants are rather scattered, maybe due to the different methods employed to determine them. We thus introduced in addition $CaHexitolOH^{+}$ complexes, which were found to give a very satisfactory description of our experimental data. As it will be described in the next section, the complexation of calcium by the hexitols is much weaker than by gluconate. The so-obtained complexation constants are compiled together with the literature values in Table 1 and 2.

3. Results and discussion

3.1 Gluconate

3.1.1 Solubility experiment with portlandite

The calcium concentrations in equilibrium with portlandite rise rapidly (Figure 4), when the gluconate concentration is increased. In the absence of gluconate, a calcium concentration of 21 mM was observed, which corresponds well with the expected solubility of portlandite of 21 mM at 23°C. The presence of gluconate increased the total measured calcium concentrations up to 101 mM Ca at a gluconate concentration of 68 mM, due to the formation of different Ca-gluconate complexes as shown in Figure 4. This strong increase of portlandite solubility in the presence of gluconate agrees well with observations reported by Nalet and Nonat (19). The measured increase of the total calcium concentrations ($[Ca]_{total}$ = $[Ca^{2+}]$ +$[CaOH^{+}]$ + [Ca-organic]) is mainly due to the formation of $Ca_3Gluc_2(OH)_4^0$, $CaGlucOH^0$ and $Ca_2Gluc_2(OH)_4^{2-}$ in presence of gluconate, while our calculations indicate that the concentrations of $CaGluc^{+}$, and $CaGluc_2^0$ are negligible. The over-proportional increase of calcium (80 mM more calcium in solution in the presence of 68 mM gluconate) is consistent with the presence of the heteropolynuclear complex $Ca_3Gluc_2(OH)_4^0$, which contains more calcium than gluconate. At gluconate concentrations of above 20 mM the $Ca_3Gluc_2(OH)_4^0$ complex dominates Ca-speciation in the presence of portlandite as shown in Figure 4.

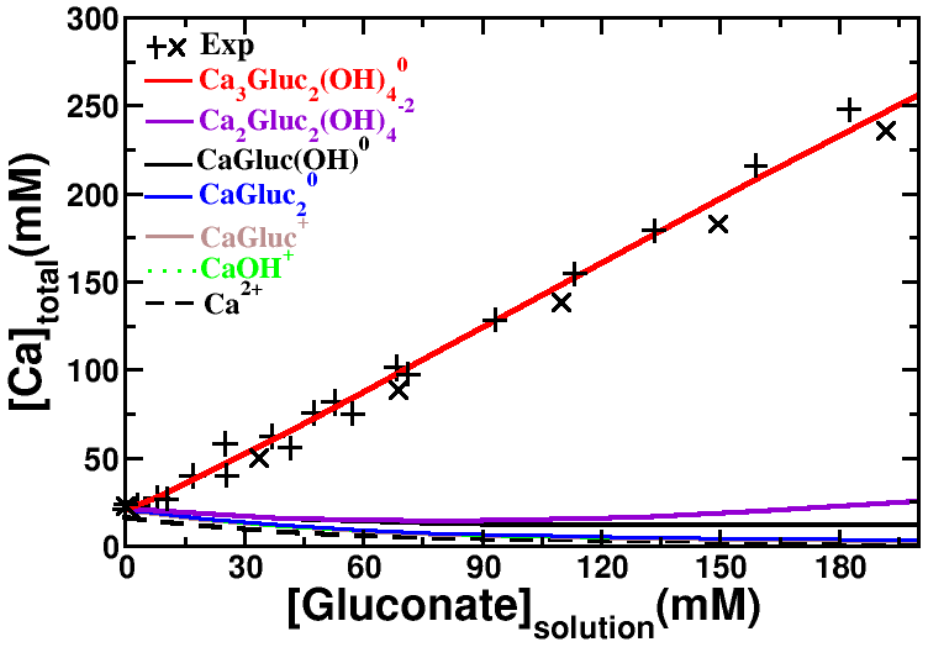

Figure 4: Evolution of total calcium concentrations in equilibrium with portlandite (initial pH 12.6, final pH 12.8) as a function of the gluconate concentration. The crosses represent the total concentrations determined experimentally, while the solid lines represent the cumulative calcium complexes concentrations calculated using the data compiled in Table 1.

3.1.2 Ca-gluconate titration

The measured changes of the Ca^{2+} activity at various alkaline pH values upon the addition of potassium gluconate to a solution containing 0.25 mM calcium nitrate is shown in Figure 5. The drop of the measured Ca^{2+} activity can be attributed i) to a minor extent to the dilution of the solution by the addition of the titrant solution (for the effect of adding solution without organics see SI) and ii) to the complexation of Ca^{2+} with the added gluconate. As it can be seen in Fig. 5 a very good fit of the experimental data with our speciation model is obtained at all pH values.

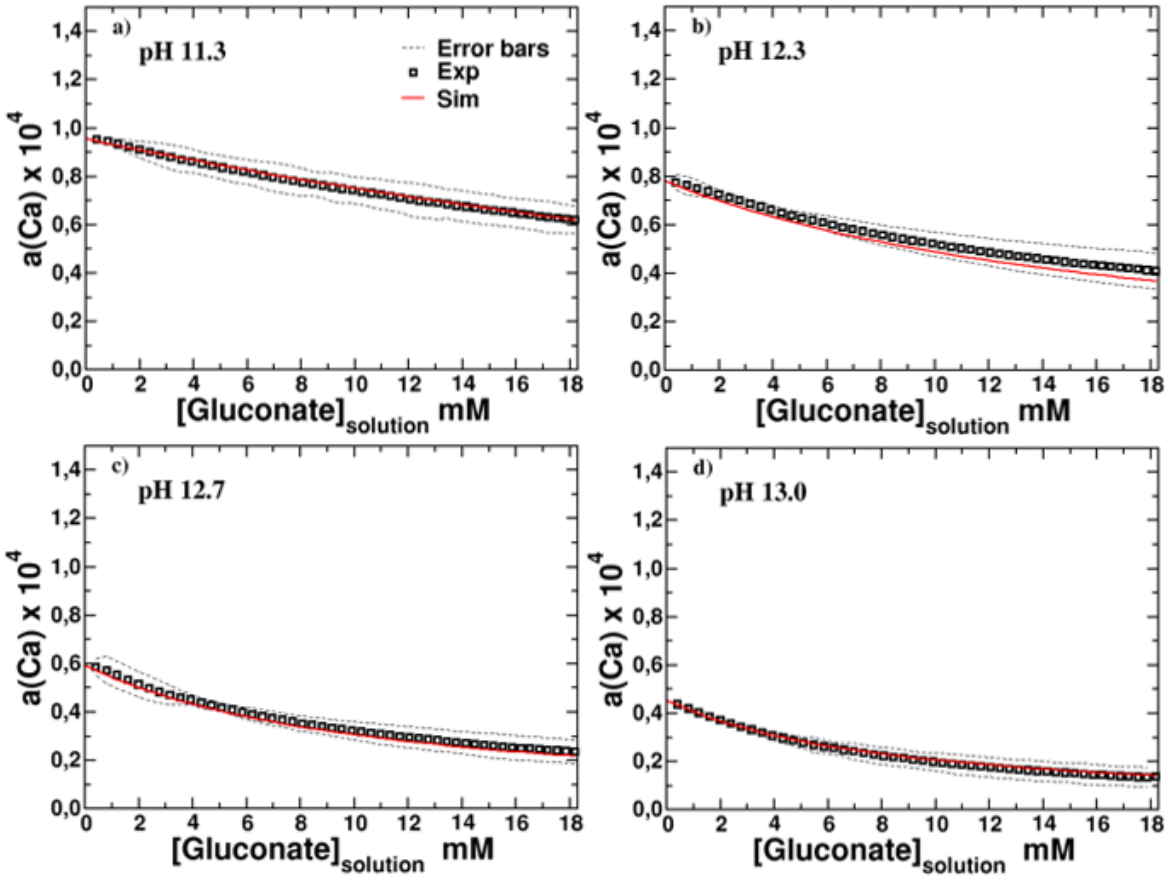

Figure 5: Ca^{2+} activities, a_{Ca}, in a solution containing 0.25 mM $Ca(NO_3)_2$ and increasing amounts of 200 mM K-gluconate solution at pH a) 11.3, b) 12.3, c)12.7 and d) 13.0. The dots indicate the mean of three repetitions of the measurements and the dotted lines the observed standard deviations. The solid red lines show the modeled a_{Ca} based on the data compiled in Table 1.

It can also be observed that the decrease in calcium activity is limited at pH 11.3 but more distinct at higher pH values, which points towards the importance of calcium-gluconate-hydroxide complexes, as further confirmed below.

In Figure 6 the simulated change in the calcium speciation in the same conditions as in Figure 5 is given. In contrast in the solubility experiments, where high calcium concentrations (21 up to 100 mM Ca, see Figure 4) are present and the calcium complexation is dominated by the heteropolynuclear $Ca_3Gluc_2OH_4^0$ complex, $CaGluc^+$ and $CaGlucOH^0$ are the dominant complexes at the low Ca concentrations used in the titration experiments. For the titration at pH 11.3 mainly the formation of some $CaGluc^+$ is predicted, while at pH 13.0 the formation of $CaGlucOH^0$ is principally found, illustrating the strong influence of pH on the calcium speciation. In addition, it can be noted that calcium shows a strong preference for the heterogeneous complex $CaGlucOH^0$, whose concentration is 5 times higher in the presence of 18.8 mM gluconate than that of $CaOH^+$ at pH 13 (~100mM OH^-). Very low concentrations of the heteropolynuclear complexes, $Ca_2Gluc_2(OH)_4^{2-}$and

$Ca_3Gluc_2(OH)_4^0$, were observed due to the relative low Ca (0.25 mM) and gluconate (18.8 mM) concentrations, at high pH (12.7 and 13.0).

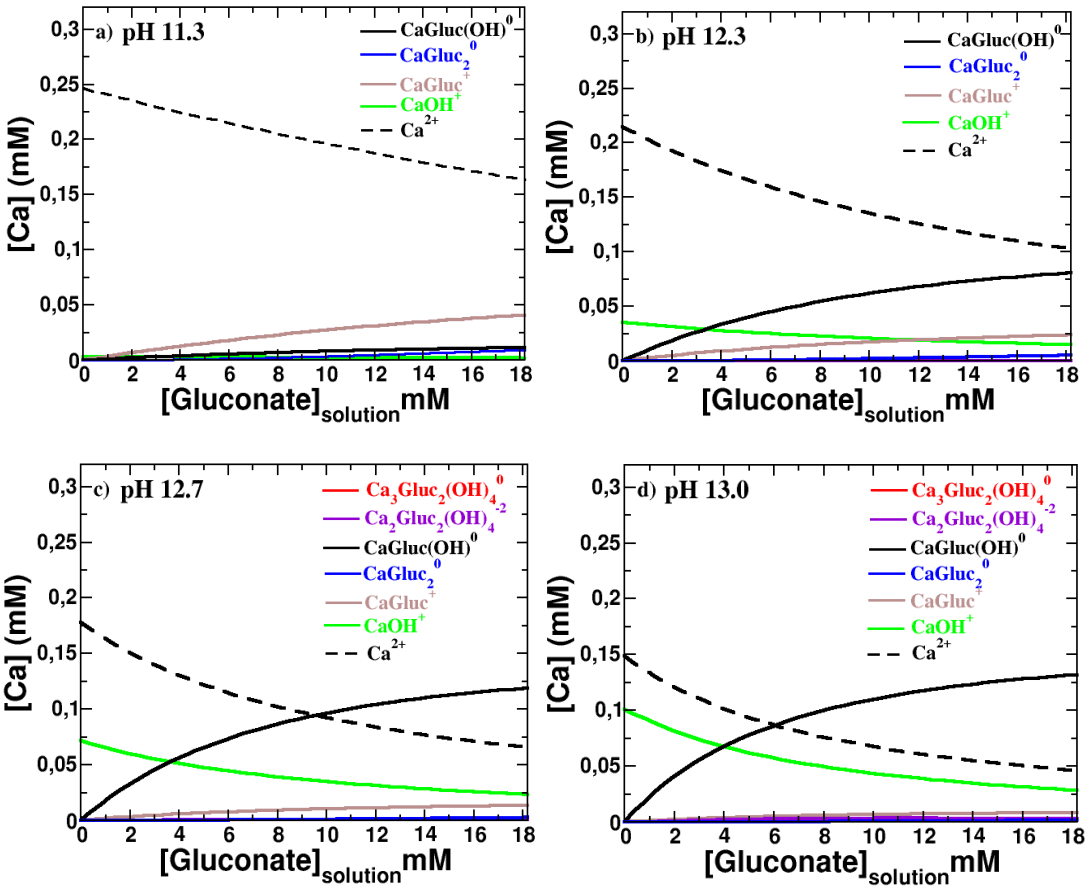

Figure 6: Calculated calcium concentrations (in mM) in a solution of 0.25 mM $Ca(NO_3)_2$ during the titration with 200 mM K-gluconate at pH a) 11.3, b) 12.3, c)12.7 and d) 13.0. The calculations are based on the thermodynamic data compiled in Table 1.

3.2 Sorbitol

3.2.1 Solubility experiments with portlandite

The equilibrium calcium concentration as obtained in the solubility experiments of portlandite in the presence of sorbitol is given in Figure 7. The equilibrium calcium concentration is observed to increase moderately with that of sorbitol, from 21 mM to 55 mM when sorbitol is increased up to 211 mM. The increase is much weaker than the one due to gluconate (Figure 4), indicating a weaker complex formation between Ca^{2+} and sorbitol. The calculations show that the observed increase can be mainly explained by the formation of a $CaSorbOH^+$ complex, while the concentration of $CaSorb^{2+}$ is found to be negligible. No clear indication for the formation of polynuclear complexes is found, although the underestimation of the total calcium concentration at very high sorbitol concentrations

could point towards the formation of such complex. At sorbitol concentrations of 100 mM and above, the $CaSorbOH^+$ complex dominates Ca-speciation (Figure 7).

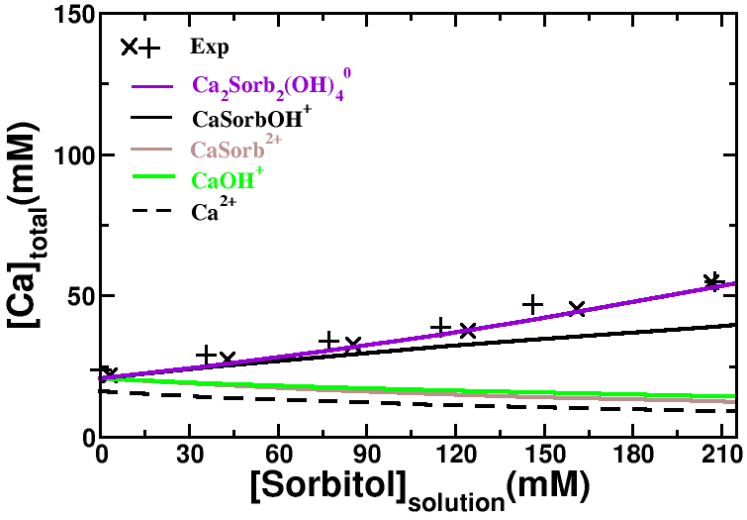

Figure 7: Evolution of the total calcium concentration in equilibrium with portlandite as a function of the sorbitol concentration. The crosses represent the total calcium concentrations determined experimentally, while the lines represent the calcium concentrations calculated using the data compiled in Table 2. The cumulative calcium concentrations due to Ca^{2+} (black, dashed line), $CaOH^+$ (green, solid line), $CaSorb^{2+}$ (grey, solid line), $CaSorbOH^+$ (black, solid line) and $Ca_2Sorb_2(OH)_4^0$ (purple, solid line) are also plotted.

3.2.2 Ca-sorbitol titration

The change in the activity of Ca^{2+} at different pH values upon the addition of sorbitol as measured by potentiometric titration of a diluted calcium nitrate solution (0.25 mM) is shown in Figure 8. In agreement with the solubility experiments (Fig.7), the drop of the Ca^{2+} activity is weaker than the one observed with gluconate and more distinct at high pH values as explained by the formation of $CaSorbOH^+$ complex. This is illustrated in Figure 9, which provides the detailed calculated speciation of calcium. As expected, $CaSorbOH^+$ is prevalent at pH 13 and hardly visible at pH 11.3. In line with the solubility experiments, the $CaSorb^{2+}$ complex is negligible in these alkaline conditions. The overall good agreement obtained between modeled and experimentally observed decrease of the Ca^{2+} activities clearly shows that no or only very little polynuclear Ca-sorbitol complexes are present.

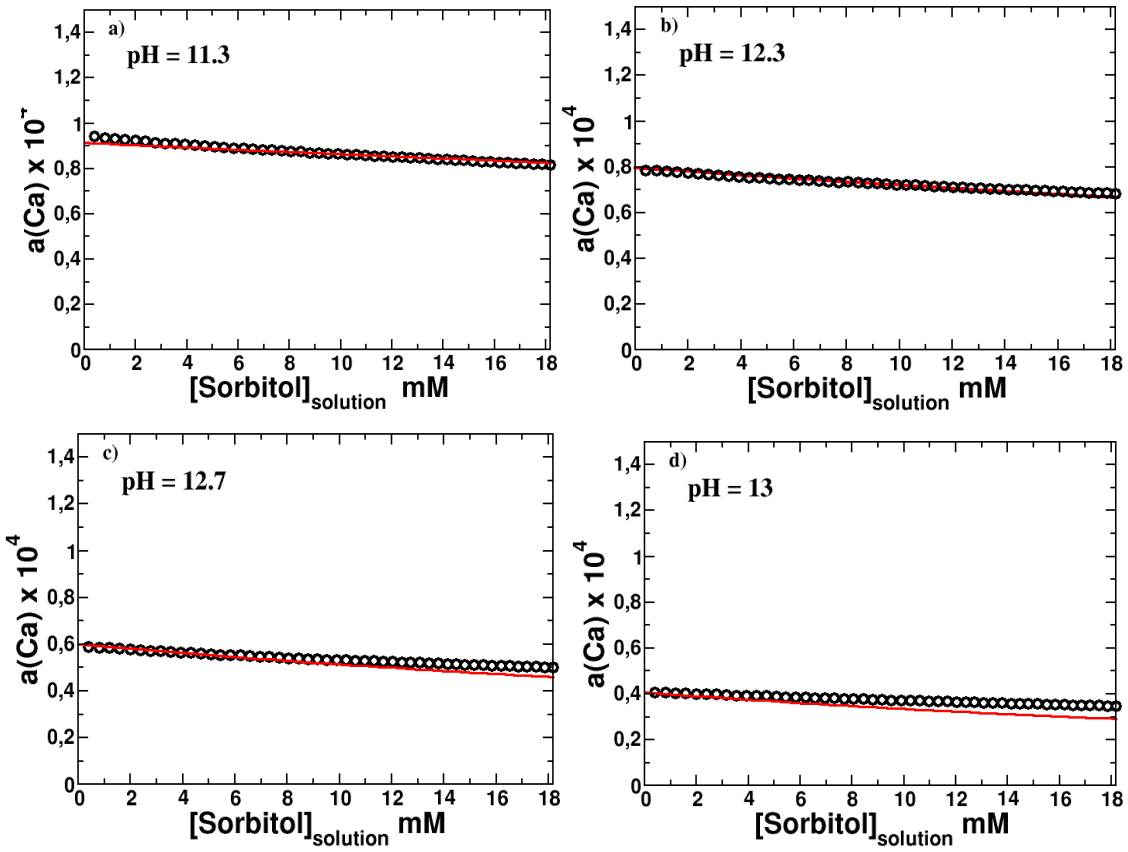

Figure 8: Ca^{2+} activities, a_{Ca2+}, in a solution containing 0.25 mM $Ca(NO_3)_2$ and increasing amounts of 0.2 M sorbitol solution at pH a) 11.3, b) 12.3, c) 12.7 and d) 13.0. The solid red lines show the modeled a_{Ca2+} based on the data compiled in Table 2.

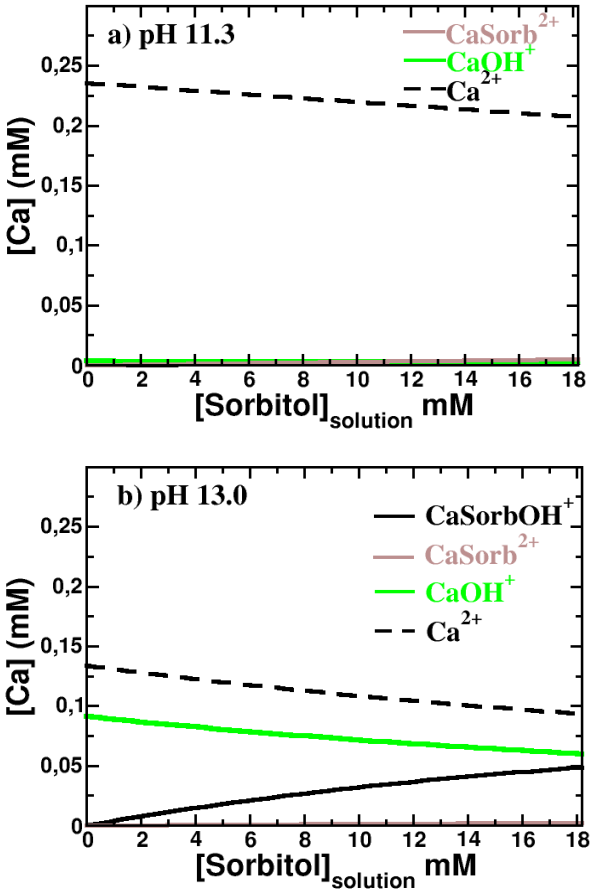

Figure 9: Calcium concentrations (in mM) in a solution of 0.25 mM $Ca(NO_3)_2$ during the titration with sorbitol at a) pH 11.3 and b) pH 13.0 calculated based on the thermodynamic data compiled in Table 2.

3.3 Mannitol and galactitol

3.3.1 Solubility experiments with portlandite

The increase in the equilibrium calcium concentration in the solubility experiments of portlandite in the presence of mannitol and galactitol, given in Figure 10, is comparable to that observed with sorbitol, although somewhat weaker compared with Figure 7. As for sorbitol, the observed increase of the Ca concentration can be principally explained by the formation of $CaManOH^+$ and $CaGalOH^+$ complexes, while the concentrations of $CaMan^{2+}$ and $CaGal^{2+}$ are negligible. Only at mannitol and galactitol concentrations well above 100 mM, $CaManOH^+$ and $CaGalOH^+$ complexes dominate the speciation of calcium (Figure 10).

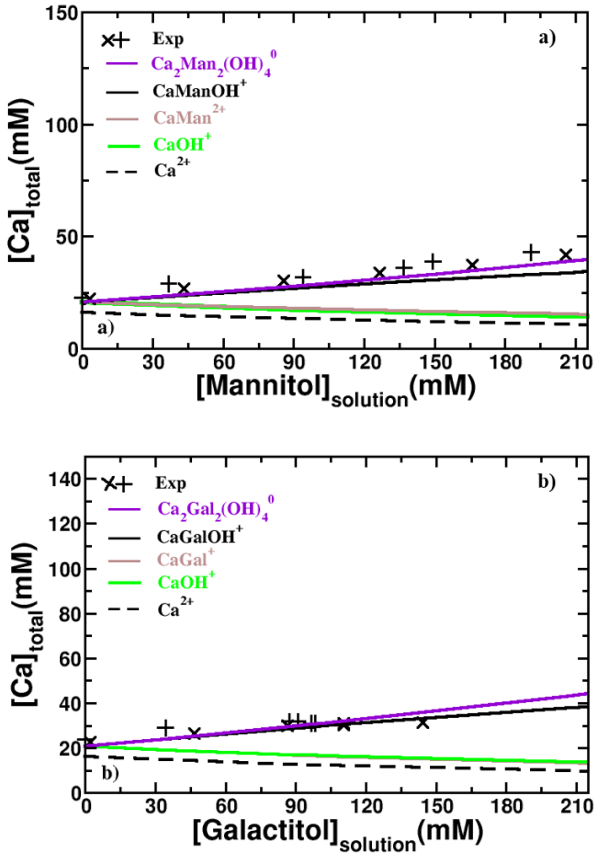

Figure 10: Evolution of calcium concentrations in equilibrium with portlandite at a pH value of 12.6 as a function of a) mannitol and b) galactitol concentration. The crosses represent the total calcium concentrations determined experimentally, while the lines represents the calcium concentrations calculated using the thermodynamic data compiled in Table 2. The cumulative calcium concentrations of Ca^{2+} (black, dashed line), $CaOH^+$(green, solid line), $CaMan^{2+}$ or $CaGal^{2+}$ (grey, solid line), $Ca_2Man_2(OH)_4^0$ or $Ca_2Gal_2(OH)_4^0$ (purple, solid line) and $CaManOH^+$ or $CaGalOH^+$ (black, solid line) are also plotted.

3.3.2 Ca-mannitol and Ca-galactitol titration

The change in the simulated and measured activity of Ca^{2+} and pH upon the addition of 0 to 18 mM mannitol to a 0.25 mM calcium nitrate at pH 11.3, 12.3, 12.7 and 13.0 are shown in Figure 11. The data for galactitol are similar and provided in the supplementary information. In agreement with the solubility experiments of portlandite (Figure 10), the decrease in the measured a_{Ca2+} is less pronounced than in the case of sorbitol and is mainly explained by the formation $CaManOH^+$ and $CaGalOH^+$, at higher pH values.

The strong preference of calcium for the heterogeneous complex with hydroxide ($CaManOH^+$ and $CaGalOH^+$) is further illustrated in Figure 12.

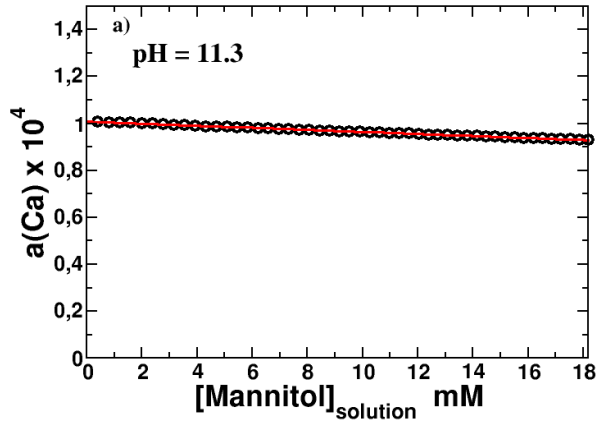
a)
pH = 11.3
a(Ca) x 10^4
[Mannitol]solution mM

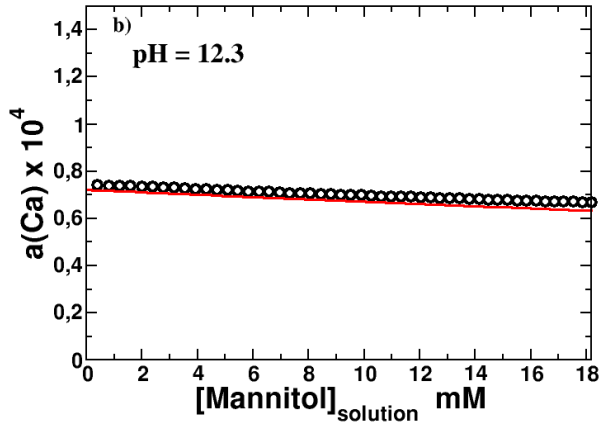
b)
pH = 12.3
a(Ca) x 10^4
[Mannitol]solution mM

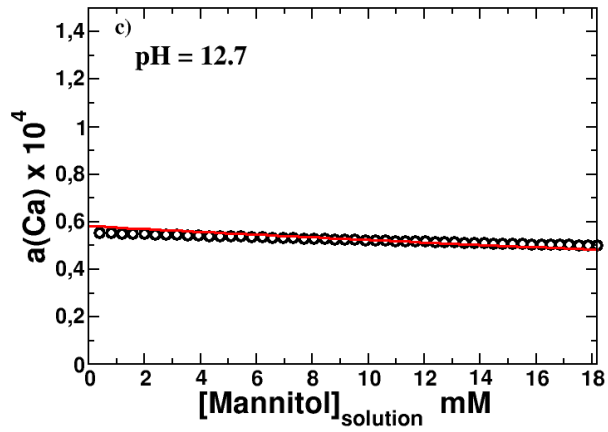
c)
pH = 12.7
a(Ca) x 10^4
[Mannitol]solution mM

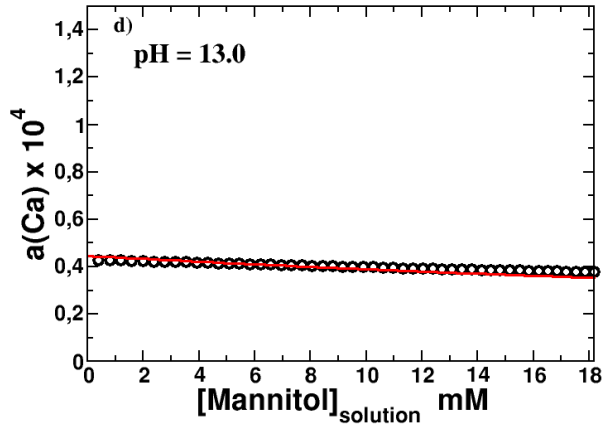
d)
pH = 13.0
a(Ca) x 10^4
[Mannitol]solution mM

Figure 11: Ca^{2+} activities, a_{Ca2+}, in a solution containing 0.25 mM $Ca(NO_3)_2$ and increasing amounts of 0.2 M mannitol solution at pH a) 11.3, b) 12.3, c)12.7 and d) 13.0. The experimental points are shown by the empty circles. The solid red lines give the modeled a_{Ca2+}, based on the data compiled in Table 2, for comparison.

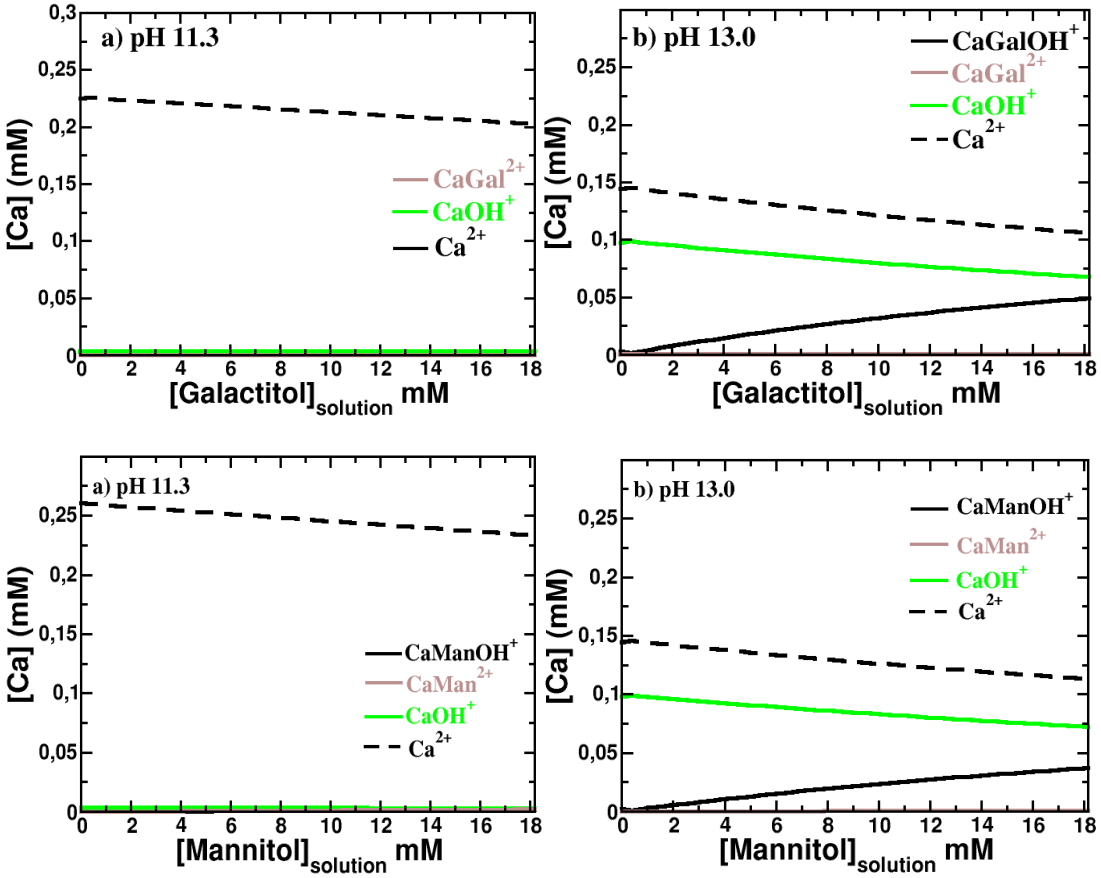

Figure 12: Simulated speciation of calcium in a solution of 0.25 mM $Ca(NO_3)_2$ during the titration with above a) galactitol at pH11.3 and b) galactitol at pH 13.0, and below, a) mannitol at pH 11.3 and b) mannitol at pH 13.0 . The calculations are based on the thermodynamic data compiled in Table 2.

3.4 Effect of complexation on calcium speciation

Calcium has been observed to form a number of different complexes with gluconate and hydroxide. Under conditions relevant for the early-age pore solution of cements (10-40 mM Ca, pH 12.5 -13.5) mainly the $CaGlucOH^0$, $Ca_3Gluc_2(OH)_4^0$ and $Ca_2Gluc_2(OH)_4^{-2}$ complexes are of importance as illustrated in Figure 13b. The importance of $CaGlucOH^0$, $Ca_3Gluc_2(OH)_4^0$ and $Ca_2Gluc_2(OH)_4^{-2}$ complexes at pH values above 12.5 result in much lower concentrations of free Ca^{2+} than in the absence of gluconate. The effect can be expected to be even stronger at later hydration times, where calcium concentrations drop to a few mM, while the concentrations of small organic molecules in the pore solutions tend to remain high. This leads to a stabilization of $CaGlucOH^0$ as shown in Figure 13a and lower Ca^{2+} concentrations.

The strong complexation of calcium can be expected to retard portlandite and C-S-H precipitation during cement hydration. Gluconate sorbs also strongly on calcium at the surface of C_3S, portlandite (see Supplementary Information) and C-S-H (18) (19), which will also strongly influence their dissolution and formation rate.

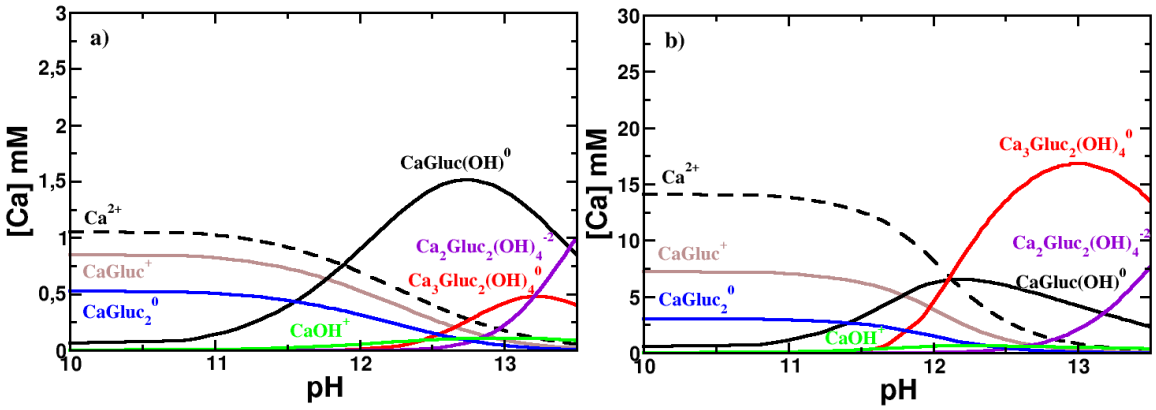

Figure 13: Calcium distribution (expressed as mM Ca) in a solution containing a) 2.5 mM of Ca , b) 25 mM of Ca and 50 mM of gluconate in the pH range 10 to 13.5.

Calcium forms only relatively weak complexes with the three hexitols investigated, in the order sorbitol > mannitol > galactitol. Thermodynamic modelling indicates a non negligeable Ca-complexation in conditions relevant for the pore solution of cements (10-40 mM Ca, pH 12.5 -13.5) as illustrated for sorbitol in Figure 14.

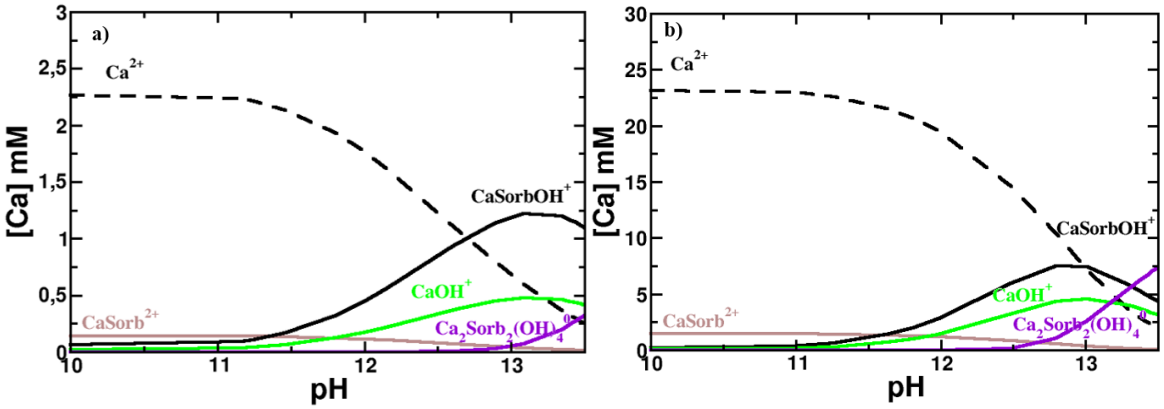

Figure 14: Calcium distribution (expressed as mM Ca) in a solution containing a) 2.5 mM of Ca , b) 25 mM of Ca and50 mM of sorbitol in the pH range 10 to 13.5.

The observed tendency of calcium to form complexes with organics follows the order gluconate >> sorbitol > mannitol > galactitol, which corresponds well with the tendency to sorb on portlandite (see Supplementary informations) and C-S-H (18) (19): gluconate >> sorbitol > mannitol, but only partially with their tendency to retard the C_3S hydration reported in Nalet and Nonat (15): gluconate >> sorbitol > galactitol > mannitol. The reason for the different sequence of galactitol and mannitol on C_3S hydration is presently not clear. The charged gluconate, which complexed strongly with calcium in solution had also the biggest retarding effect on C_3S hydration.

4. Conclusions

The complexation of Ca^{2+} with gluconate, D-sorbitol, D-mannitol and D-galactitol has been studied via portlandite solubility measurement and titration experiments at low ionic strength (0.1 M KNO_3). For gluconate, the multinuclear complexes already described in the literature allowed us to describe the experimental data, after some further refinement of the complexation constants. At a pH of 12.5 and in the presence of portlandite the heteropolynuclear complex $Ca_3Gluc_2(OH)_4^0$ dominates the Ca-speciation, while at lower calcium concentrations $CaGluc^+$ (below pH 12) and $CaGlucOH^0$ (above pH 12) are the main complexes formed. This relative strong complex formation between calcium and gluconate lowers concentrations of free Ca^{2+}, which could contribute to a retardation of portlandite and C-S-H precipitation during cement hydration. The strong tendency of gluconate to form complexes with Ca reported here is consistent with the significant sorption of gluconate on Ca on the surface of C-S-H and portlandite reported (19) .

Sorbitol makes weaker complexes with calcium as observed both from portlandite solubility measurements and titration results. Under all conditions studied, the predominant sorbitol complex is the ternary $CaSorbOH^+$ complex, while the $CaSorb^{2+}$ complex formed in negligible amounts only.

In all cases studied, $CaSorbOH^+$ complex had limited effect on calcium speciation below a pH of 12, but can dominate the calcium speciation at pH 12.5 and above, at higher sorbitol concentrations.
Similar observations have been made for D-mannitol and D-galactitol, which show an even weaker tendency than sorbitol to form calcium complexes. Also for D-mannitol and D-galactitol only the ternary $CaManOH^+$ and $CaGalOH^+$ complexes are relevant and they are expected to form mainly above pH 12.5 and at high mannitol and galactitol concentrations.
The observed tendency of calcium to form complexes follows the order gluconate >> sorbitol > mannitol > galactitol, which corresponds well with the tendency to sorb on portlandite and C-S-H: gluconate >> sorbitol > mannitol (19) but only partially with their tendency to retard the C_3S hydration reported in (15): gluconate >> sorbitol > galactitol > mannitol.

Acknowledgements

The financial support from Nanocem (core project 15) is thankfully acknowledged. We also would like to thank the representatives of the industrial partners: L. Pegado, J.H. Cheung, V. Kocaba, P. Juilland, and M. Mosquet for many helpful discussions and their interest in this project. We sincerely thank L. Brunetti, S. El Housseini and D. Nguyen for their help in the laboratory work. The use of the analytical platform of ISTerre, with the help of D. Tisserand, S. Bureau and S. Campillo, is acknowledged.

References

1. Mann, S. Biomineralization: Principles and Concepts in Bioorganic Materials Chemistry. Oxford University Press, Oxford, New York, 2001.
2. Jolicoeur, C., Simard, M.A. Chemical admixture-cement interactions: phenomenology and physico-chemical concepts. Cement and Concrete Composites, 20(2–3), 87-101, 1998.
3. Young, J.F. A review of the mechanisms of set-retardation in portland cement pastes containing organic admixtures. Cement and Concrete Research, 2(4), 415-433, 1972.
4. Lorprayoon,V., Rossington, D.R. Early hydration of cement constituents with organic admixtures. Cement and Concrete Research, 11(2), 267-277, 1981.
5. Uchikawa, H., Hanehara, S., Shirasaka, T., Sawaki, D. Effect of admixture on hydration of cement, adsorptive behavior of admixture and fluidity and setting of fresh cement paste. Cement and Concrete Research, 22(6), 115-1129, 1992.
6. Jansen, D., Neubauer, J., Goetz-Neunhoeffer, F., Haerzschel, R., Hergeth, W.D. Change in reaction kinetics of a portland cement caused by a superplasticizer — Calculation of heat flow curves from XRD data. Cement and Concrete Research, 42(2), 327-332, 2012.
7. Cheung, J., Jeknavorian, A., Robert, L., Silva, D. Impact of admixtures on the hydration kinetics of Portland cement. Cement and Concrete Research, 41(12), 1289-1309, 2011.

8. Diamond, S. Interactions between cement minerals and hydroxycarboxylic-acid retarders: I, apparent adsorption of salicylic acid on cement and hydrated cement compounds. Journal of the American Ceramic Society, 54(6), 273-276, 1971.
9. Nelson, E.B. Cements additives and mechanisms of action. Well Cementing, 28, 3-1-3-37, 1990.
10. Milestone, N.B. Hydration of tricalcium silicate in the presence of lignosulfonates, glucose, and sodium gluconate. Journal of the American Ceramic Society, 62(8), 321-326, 1979.
11. Singh, N.B., Singh, S.P., Sarvehi, R. Effect of phenols on the hydration of Portland cement. Advances in Cement Research, 2(6), 43-48, 1989.
12. Zhang, L., Catalan, L.J.J., Balec, R.J., Larsen, A.C., Esmaeili, H.H. and Kinrade, S.D. Effect of saccharide set retarders on the hydration of ordinary portland cement and pure tricalcium silicate. Journal of the American Ceramic Society, 93 (1) 279–287, 2010.
13. Thomas, J.J., Jennings, H.M., Chen, J.J. Influence of nucleation seeding on the hydration mechanisms of tricalcium silicate and cement. Journal of Physical Chemistry, 113(11), 4327-4334, 2009.
14. Pourchez, J., Grosseau, P., Ruot, B. Changes in C_3S hydration in the presence of cellulose ethers. Cement and Concrete Research, 40(2), 179–188, 2010.
15. Nalet, C., Nonat, A. Effects of hexitols on the hydration of tricalcium silicate. Cement and Concrete Research, 91, 87-96, 2017.
16. Nalet, C., Nonat, A. Effects of functionality and stereochemistry of small organic molecules on the hydration of tricalcium silicate. Cement and Concrete Research, 87, 97-104, 2016.
17. Juilland, P., Gallucci, E. Hindered calcium hydroxide nucleation and growth as mechanism responsible for tricalcium silicate retardation in presence of sucrose. 329, 143-154, 2018.
18. Hansen, W. Actions of calcium sulfate and admixtures in portland cement pastes in "symposium on effect of water-reducing admixtures and set-retarding admixtures on properties of concrete". American Society for Testing Materials, 3-37, 1960.
19. Nalet, C., Nonat, A. Ionic complexation and adsorption of small organic molecules on calcium silicate hydrate: relation with their retarding effect on the hydration of C_3S. Cement and Concrete Research, 89, 97–108, 2016.
20. Singh, N.B. Influence of calcium gluconate with calcium chloride or glucose on the hydration of cements. Cement and Concrete Research, 5, 545-550, 1975.
21. Singh, N.B. Effect of gluconate on the hydration of cement. Cement and Concrete Research, 6, 455-460, 1976.
22. Ma, S., Li, W., Zhang, S., Ge, D., Yu, J., Shen, X. Influence of sodium gluconate on the performance and hydration of portland cement. Construction and Building Materials, 91, 138-144, 2015.
23. Pallagi, A., Sebők, P., Forgó, P., Jakusch, T., Pálinkó, I., Sipos, P. Multinuclear NMR and molecular modelling investigations on the structure and equilibria of complexes that form in aqueous solutions of Ca^{2+} and gluconate. Carbohydrate Research, 345(13), 1856-1864, 2010.
24. Pallagi, A., Bajnóczi, É.G., Canton, S.E., Bolin, T., Peintler, G., Kutus, B., Sipos, P. Multinuclear complex formation between Ca(II) and gluconate ions in hyperalkaline solutions.Environmental Science & Technology, 48(12), 6604-6611, 2014.
25. Kutus, B., Ozsvár, D., Varga, N., Pálinkó, I., Sipos, P. ML and ML2 complexes forming between Ca(II) and D-glucose derivatives in aqueous solutions. Dalton Transactions, 46, 1065-1074, 2017.
26. Kutus, B., Gaona, X., Pallagi, A., Pálinkó, I., Altmaier, M., Sipos, P., Recent advances in the aqueous chemistry of the calcium(II)-gluconate system - Equilibria, structure and composition of the complexes forming in neutral and in alkaline solutions. Coordination Chemistry Reviews, 417, 213337, 2020.
27. Masone, M., Vicedomini, M. Gluconate and lactate as ligand of calcium ions. 71(9-10), 517-523, 1981.
28. Sawyer, D.T. Metal organic complexes. Chemical Reviews, 64(6), 633-643, 1964.
29. Haas, J.W. Complexation of calcium and copper with carbohydrates. Marine Chemistry, 19(4), 299-304, 1986.
30. Kieboom, A.P.C, Buurmans, H.M.A, Van Leeuwen, L.K., Van Benschop, H.J. Stability constants of (hydroxy)carboxylate and alditol-calcium(II) complexes in aqueous medium as determined by a solubility method. Journal of the Royal Netherlands Chemical Society, 98(6), 393-394, 1979.

31. Barthel, J., Jaenicke, R. Conway: Ionic Hydration in Chemistry and Biophysics: Studies in Physical and Theoretical Chemistry. Elsevier Scientific Publishing Company, 86(3), 264-264, Amsterdam and New York, 1982.
32. Parkhurst, D.L. PHREEQE: a computer program for geochemical calculations. U.S. Geological Survey, Water Resources Division, 80-96, 1981.
33. Ball, J.W., Nordstrom, D.K. User's Manual for WATEQ4F, with Revised Thermodynamic Data Base and Test Cases for Calculating Speciation of Major, Trace, and Redox Elements in Natural Waters. U.S. Geological Survey, 91-183, Washington DC, 1991.
34. Merkel, B., Planer-Friederich, B., Nordstrom, D. Groundwater Geochemistry. A Practical Guide to Modeling of Natural and Contaminated Aquatic Systems. Springer, 2005.
35. Zhang, Z., Gibson, P., Clark, S.B., Tian, G., Zanonato, P.L., Rao, L. Lactonization and protonation of gluconic acid: a thermodynamic and kinetic study by potentiometry, NMR and ESI-MS. Journal of Solution Chemistry, 36(10), 1187-1200, 2007.
36. Bretti, C., Cigala, R.M., De Stefano, C., Lando, G., Sammartano, S. Acid−base and thermodynamic properties of D-gluconic acid and its interaction with Sn^{2+} and Zn^{2+}. Journal of Chemical and Engineering Data, 61(6), 2040–2051, 2016.
37. Thoenen, T., Hummel, W., Berner, U., Curti, E. The PSI/Nagra Chemical Thermodynamic Data Base 12/07, PSI report 14-04, Villigen PSI, Switzerland, 2014

B. Gluconate and hexitols effects on C-S-H solubility

Lina BOUZOUAID[1], Barbara LOTHENBACH[2], Alejandro FERNANDEZ-MARTINEZ[3], Christophe LABBEZ[1]

[1] ICB, UMR 6303 CNRS, Univ. Bourgogne Franche-Comté, FR-21000 Dijon, France

[2] Empa, Concrete & Asphalt Laboratory, Duebendorf, Switzerland

[3] Univ. Grenoble Alpes, Univ. Savoie Mont Blanc, CNRS, IRD, IFSTTAR, ISTerre, 38000 Grenoble, France.

Abstract:

This study investigates the effect of gluconate, a carboxylate ion, and three uncharged hexitols, D-sorbitol, D-mannitol and D-galactitol on the solubility of C-S-H. Thermodynamicmodeling is used to determine the kind and amount of Ca-organic-silicate-OH complexes that potentially form in the conditions studied. All the organics form complexes with calcium and hydroxide, In addition, heteropolynuclear organics complexes with calcium, hydroxide and silicate are observed at high pH values and high calcium concentrations: $Ca_2Hex_2(H_3SiO_4)_2(OH)_2^0$, $Ca_2Hex_2(H_2SiO_4)(OH)_2^{-2}$ and $Ca_3Gluc_2(H_3SiO_4)_2(OH)_2^0$, with the exception of mannitol. The strength of complexation with silicate

decreases in the order gluconate >sorbitol > galactitol. The adsorption of the selected organics on portlandite and C-S-H systems follows the order gluconate >> sorbitol > mannitol ~ galactitol. For C-S-H, a typical Langmuir isotherm is found only when buffered with $Ca(OH)_2$. The adsorption on C-S-H increases with the Ca/Si ratio.

1.Introduction

Hydration of cement, involving mainly the anhydrous phases Ca_3SiO_5 (alite) and Ca_2SiO_4 (belite), is a complex reaction where two main hydrates are formed: calcium silicate hydrates (C-S-H), and portlandite, $Ca(OH)_2$ (1). It involves the concomitant dissolution of the anhydrate phases and precipitation, from the solution, of the hydrate phases. The passage from solution tothese hydrates happens because the ion activity product of the solution (*IAP*) rapidly exceeds the solubility product (*Ksp*) of the newly formed solid phases (2). As the concentration and activity of ions build up, the driving force for the nucleation of hydrates ($\Delta\mu$) increases as does the rate of nucleation, *J*, according to $J = \exp(-\Delta\mu^{-2}/k_BT)$ with k_B being the Boltzmann constant and T the temperature. The driving force is defined by the change in chemical potential ($\Delta\mu$) of the crystallizing ions, and measures the free energy response to transferring the ions from the solution to the solid, $\Delta\mu = K_BT(\ln IAP - \ln K_{sp})$. The same reasoning applies to the dissolution of anhydrous phases in a symmetric way. The activity of the dissolving and crystallizing ions is an essential thermodynamic quantity if one wants to quantify and understand the hydration of cement. However, ion activities are strongly influenced by complex formation, e.g between calcium and organics. In the present study we aim at extending our previous work (3) on the calcium activity in the presence of four cementorganic retarders, namely sodium D-gluconate and three hexitols (D-mannitol, D-sorbitol and D-galactitol), to the speciation and activity of calcium and silicate solution species in the presence of the same organics.

Superplasticizers, in particular, and organic molecules, in general, often behave as retarders when used in concrete (4) (5) (6). At low percentage, less than 1% wt of Portland cement, they retard the initial and final setting times of cement (7) (8). Several studies have been conducted to highlight their influence on the hydration of cements, with the view to obtain a better understanding of the mechanisms of retardation and the setting times, but still the physical and chemical mechanisms responsible for this retardation remains elusive (9) (10)(11)(12)(13). Using small organic molecules as a model for the more complex superplasticizers, previous works have been directed to decipher which step (C_3S dissolution or C-S-H nucleation/growth) of the cement hydration is specifically impacted by organics, including the charged molecule gluconate known to behave as a strong retarder (14) (15) (16) (17) (18). For some hexitols and gluconate, the pure dissolution of Ca_3SiO_5 was observed to be only marginally affected (19) and they were thus conjecture to act as inhibitors of the

nucleation/growth of C-S-H (20) and portlandite (21). (14) (15) (16) (17) (18). The neutral hexitol molecules were observed to retard the hydration of cement much less than the charged gluconate molecule, and their retardation power was found to depend on their stereochemistry (19) (20) (22).

In a recent study, we investigated the effect of gluconate, D-sorbitol, D-galactitol and D- mannitol on calcium speciation at high pH values (3). It was found that the sorption of organics on portlandite as well as the strength of organics complex formation with Ca decreases in the order gluconate >> sorbitol > mannitol ~ galactitol, similar to the organics tendency to retard the C_3S hydration (19): gluconate >> sorbitol > galactitol > mannitol. In the presence of portlandite, hetero-polynuclear complexes with calcium and hydroxide such as $Ca_3Gluc_2(OH)_{40}$ dominate the Ca-speciation with gluconate, while ternary $CaHexOH^+$ and polynuclear $Ca_2Hex_2OH_4^0$ complexes are dominant in the presence of the hexitols (3).

In the present paper, we investigate the combined speciation of calcium, silicate and organics (gluconate, D-sorbitol, D-galactitol or D-mannitol) at concentrations and pH values relevant for cementitious systems. Complex formation is experimentally studied based on solubility measurements of calcium silicate hydrate (C-S-H) at various Ca/Si, ranging from 0.75 to 1.5,in the presence of increasing amount of organics. The strength and the various types of calcium and silicate complexes with the organic molecules is determined with a speciation model.

2. Material and methods

2.1 Material

The sorption and complex formation of organics was studied on pre-synthesized C-S-H. C-S-H was synthesized with a Ca/Si of 0.75 by adding 4.2 g of lime and 5.9 g of silicate. The reactants were mixed with boiled and degassed water, within 250 mL PE containers protectedfrom air, using a liquid to solid ratio (L/S) of 25 to obtain a homogeneous suspension. The containers were placed on a shaking table with a stirring speed of 180 rpm for four weeks at T=23°C. Before filtration, the PE containers were left to stand for 24 hours allowing the solidto settle. The supernatant was filtered through a 40 μm sintered glass filter. The solid phase was dried under suction in a desiccator in presence of silica gel at room temperature for two weeks and then stored in desiccator under vacuum in the presence of silica gel.

The lime powder used is obtained by calcining calcium carbonate $CaCO_3$ (WR Analar Normapur, 98.5-100%) at 1000°C for 24 hours. Aerosil 200 silica (Evonik industries) was used, a hydrophilic fumed silica with a specific surface area of 200 m^2/g and a high reactivity. Different organic

compounds were used for the solubility experiments: potassium gluconate ($C_6H_{11}KO_7$, Sigma-Aldrich, ≥97% purity), D-sorbitol ($C_6H_{14}O_6$, Sigma-Aldrich, ≥99% purity), D-mannitol ($C_6H_{14}O_6$, Sigma-Aldrich, ≥99% purity), and D-galactitol ($C_6H_{14}O_6$,, Sigma-Aldrich, ≥99% purity). Note that the three hexitols have the same structural units but have a different configuration as illustrated in Figure *1*.

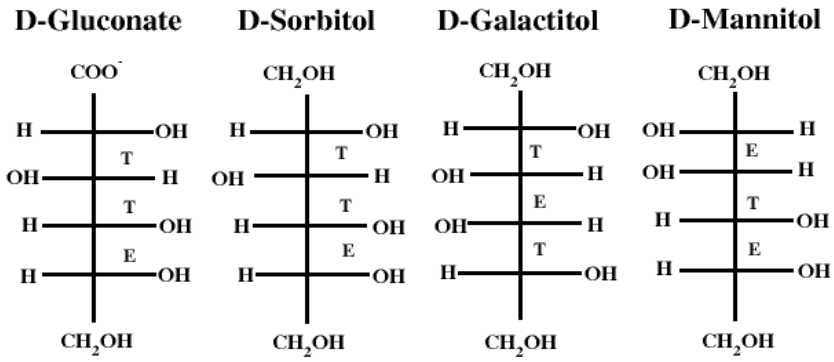

Figure 1: Structure of (from left to right) D-gluconate, D-sorbitol, D-galactitol and D-mannitol. ”T” corresponds to the threo diastereoisomer configuration. “E” corresponds to erythro diastereoisomer configuration.

2.2 Solubility experiments

Four different series of samples were prepared in a glove box for each organic molecules: C-S-H equilibrated with 0 mM, 11 mM and 20 mM calcium as well as a series with saturated lime solution. For each experiment 200 mg of C-S-H (C/S =0.75) were used as a solid buffer, enclosed in a dialysis membrane and placed in a 250 mL polypropylene flask filled with 250 mL of CO_2-free solution with different amounts and type of organic molecule (see Figure 2). Based on mass balance calculations the final Ca/Si in C-S-H corresponded to 0.75 (0 mM Ca), 1.1 (11 mM Ca), 1.3 (20 mM Ca), and to 1.5 (saturated lime solution; initial Ca/Si in solid = 0.75).

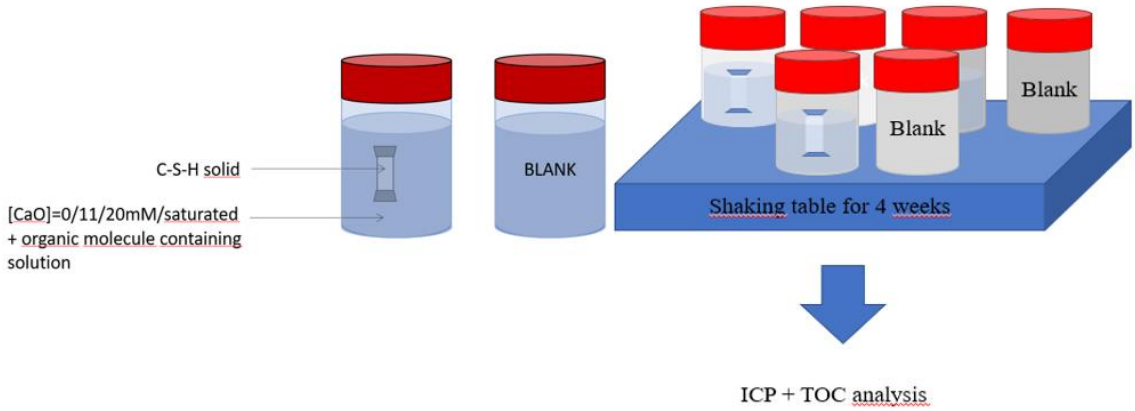

Figure 2: Schematic representation of the different series of C-S-H with 0 mM, 11 mM, 20 mM and saturated with $Ca(OH)_2$, used for the solubility and adsorption experiments. The flask used for the solubility measurement contains a dialysis bag filled with 200mg C-S-H powder, immersed in a solution containing the organic molecule. The second flask containing the organic molecule solution only is used as a blank/reference to verify the organic concentration introduced initially. This allows the determination of the organic adsorption on C-S-H by mass balance based on the measured difference. Note that the same stock solution is used for each sample pair.

The dialysis membranes (Spectra / Por, MWCO 12-14 kD) were dipped before use in distilledwater for 30 minutes to remove any organic residues and dried in a desiccator overnight. The dialysis bags were closed with polyamide clamps (Carl Roth, length 50 mm). Finally, the samples were stored in plastic barrels filled with N_2 gas to guarantee CO_2 free conditions, andplaced on a shaking table during four weeks at 23°C to equilibrate. In each case, in addition tothe samples containing the dialysis bag filled with C-S-H, blank samples containing only the lime and organic molecule solution were prepared and used as reference. The pH values and total elemental concentrations were measured in the solution after removing the dialysis bags. The pH electrode was calibrated using Sigma Aldrich buffer (pH4, 7, 9 and 12). The total concentration of the elements Ca and Si were measured by inductively coupled plasma-optic emission spectroscopy (ICP-OES 5110, Agilent) in dilutedsolution acidified with HNO_3. Five or six different organic concentrations were studied, with a starting concentrations between 0 mM to 200 mM (detailed values are given in the Supplementary Information). The bulk concentration of organics at equilibrium was measured as total organic content witha TOC VCPN instrument (Shimadzu). This tool is based on the oxidation of organic molecules contained in solution by gaseous oxygen with a platinum-based catalyst in an ovenraised to a temperature of 720°C. The CO_2 formed is detected by Infra-Red Non-Dispersive (NDIR). The detection threshold for this device is very low (4µg/L).

2.4 Thermodynamic simulation and complexation constants

The solubility of C-S-H and the activity of calcium, silicate and hydroxide solution species at equilibrium were fitted using a speciation model solved by the geochemical software PHREEQC version 3 (3.6.2-15100) and the WATEQ4f database. The activity of the ion species *i*2+, a_i, was calculated according to $a_i = \gamma_i \cdot m_i$, where γ_i is theactivity coefficient and m_i the molality in mol/kg H_2O. The activity coefficients were calculated in PHREEQC for major species with the WATEQ Debye Hückel equation:

$$log\gamma_i = \frac{-Az_i^2\sqrt{I}}{1+Bd_i\sqrt{I}} + b_i I \quad (1)$$

where z*i* denotes the charge of species *i*, *I* the molal ionic strength, *di* the individual ion-size parameter, and *bi* is an ion specific parameter. *A* and *B* are pressure- and temperature-dependent coefficients. Equation 1 is applicable up to approximately 1 M of ionicstrength. For non tabulated species, the Davies equation is used to calculate the activity coefficients in PHREEQC.

Table 1. Solubility and complex formation constants of calcium, silicate, hydroxide and gluconate ($Gluc^-$) containing species at standard conditions (1 bar, 25°C) reported in literatureand determined in the present study.

	Log K	**References**
Solids		
$Ca(OH)_2 + 2H^+ = Ca^{+2} + 2H_2O$	22.80	-24
$SiO_2(amorphous) + 2H_2O = H_4SiO_4^0$	-2.71	-23
Aqueous species		
$Ca^{+2} + OH^- = CaOH^+$	1.22	-24
$H_4SiO_4^0 = H_3SiO_4^- + H^+$	-9.83	-25
$H_4SiO_4^0 = H_2SiO_4^{-2} + 2H^+$	-23.10	-25
$Gluc^- + H^+ = GlucH^0$	3.64	-26
$Gluc^- + OH^- = GlucOH^{-2}$	-0.44	-27
$Ca^{+2} + Gluc^- = CaGluc^+$	1.56	-28
$Ca^{+2} + 2Gluc^- = CaGluc_2^0$	2.85	-3
$Ca^{+2} + OH^- + Gluc^- = CaGlucOH^0$	3.95	-3
$2Ca^{+2} + 4\ OH^- + 2Gluc^- = Ca_2Gluc_2(OH)_4^{-2}$	11.25	-3
$3Ca^{+2} + 4\ OH^- + 2Gluc^- = Ca_3Gluc_2(OH)_4^0$	16.10	-3
$3Ca^{+2} + 2\ OH^- + 2Gluc^- + 2H_3SiO_4 = Ca_3Gluc_2(H_3SiO_4)_2(OH)_2^0$	20.45	This study

Table 2. Complex formation constants of calcium, silicate, hydroxide and sorbitol (Sorb), mannitol (Man) and galactitol (Gal) containing species at standard conditions (1 bar, 25°C) reported in literature and determined in the present study

	Log K	References
$Ca^{+2} + Sorb^0 = CaSorb^{+2}$	0.10	-3
$Ca^{+2} + Sorb^0 + OH^- = CaSorbOH^+$	2.85	-3
$2Ca^{+2} + 2Sorb^0 + 4OH^- = Ca_2Sorb_2(OH)_4^0$	9.75	-3
$2Ca^{+2} + 2Sorb^0 + 2OH^- + 2H_3SiO_4 = Ca_2Sorb_2(H_3SiO_4)_2(OH)_2^0$	16.00	This study
$2Ca^{+2} + 2Sorb^0 + 4OH^- + H_2SiO_4 = Ca_2Sorb_2(H_2SiO_4)(OH)_4^{-2}$	13.60	This study
$Ca^{+2} + Man^0 = CaMan^{+2}$	-0.36	-3
$Ca^{+2} + Man^0 + OH^- = CaManOH^+$	2.65	-3
$2Ca^{+2} + 2Man^0 + 4OH^- = Ca_2Man_2(OH)_4^0$	9.65	-3
$2Ca^{+2} + 2Man^0 + 2OH^- + 2H_3SiO_4^- = Ca_2Man_2(H_3SiO_4)_2(OH)_2^0$	NA*	This study
$2Ca^{+2} + 2Man^0 + 4OH^- + H_2SiO_4^{-2} = Ca_2Man_2(H_2SiO_4)(OH)_4^{-2}$	NA*	This study
$Ca^{+2} + Gal^0 = CaGal^{+2}$	-0.53	-3
$Ca^{+2} + Gal^0 + OH^- = CaGalOH^+$	2.80	-3
$2Ca^{+2} + 2Gal^0 + 4OH^- = Ca2Gal_2(OH)_4^0$	9.29	-3
$2Ca^{+2} + 2Gal^0 + 2OH^- + 2H_3SiO_4^- = Ca_2Gal_2(H_3SiO_4)_2(OH)_2^0$	14.60	This study
$2Ca^{+2} + 2Gal^0 + 4OH^- + H_2SiO_4^{-2} = Ca_2Gal_2(H_2SiO_4)(OH)_4^{-2}$	13.00	This study

*NA: Not available: no constants could be fitted in this study due to the weak complexation of mannitol with Si.

Table 3. Solubility and surface complexation constants of the C-S-H phases (23)

	Log K
α-C-S-H: $Ca_4Si_5O_{16}H_4^0 + 8H^+ + 4H_2O = 4Ca^{+2} + 5H_4SiO_4^0$	53.5
β-C-S-H: $Ca_2Si_2O_7H_2^0 + 4H^+ + H_2O = 2Ca^{+2} + 2H_4SiO_4^0$	29.6
γ-C-S-H: $Ca_6Si_4O_{15}H_2^0 + 12H^+ + H_2O = 6Ca^{+2} + 4H_4SiO_4^0$	104.5
$\equiv SiOH^0 = \equiv SiO^- + H^+$	-9.8
$\equiv SiOH^0 + Ca^{+2} = \equiv SiOCa^+ + H^+$	-7.0

$\equiv SiOH^0 + Ca^{+2} + OH^- = \equiv SiOCaOH^0$	-9.0
$2\equiv SiOH^0 + H4SiO_4^0 = (\equiv SiO)_2Si(OH)_2^0 + 2H_2O$	5.8*
$2\equiv SiOH^0 + Ca^{+2} = (\equiv SiO)_2Ca^0 + 2H^+$	-11.4

* The indicated value is for b-C-S-H and g-C-S-H; log K = 4.4 for a-C-S-H

The fitted complex formation constants between calcium, silicate, hydroxide and the organicsused in the present study are listed in Tables 1 and 2. The calculations made to identify the ionic composition of the solution at equilibrium with C-S-H in suspensions with and without organic molecules used the surface complexation model of Haas and Nonat, which takes into account the variation of the solubility and stoichiometry of C-S-H phases (23). The values of the solubility constants and surface complexation of the phases a, b and g of C-S-H are listedin Table 3.

3. Results and discussion

3.1 Solubility of C-S-H in presence of the organics

3.1.1. Hexitols

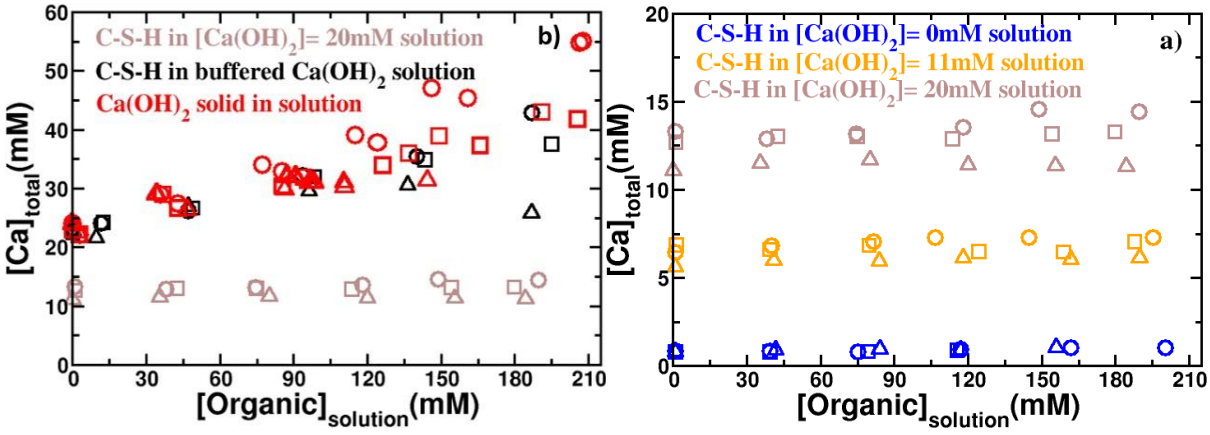

Figure 3: Measured solution concentrations of calcium in equilibrium with C-S-H and portlandite (red symbols, from (3)) as a function of the equilibrium concentration of hexitols. The C-S-H (C/S = 0.75) containing dialysis bags were immersed in 250 mL of ultra-pure and degassed water containing initially 0 mM $Ca(OH)_2$ (blue symbols), 11 mM $Ca(OH)_2$ (orange symbols), and 20 mM $Ca(OH)_2$ (grey symbols). The black symbols provide the results for C-S-H in buffered portlandite conditions. Sorbitol, mannitol and galactitol are represented by circles, squares and triangles, respectively.

The evolution of calcium concentration in solution at equilibrium with C-S-H and portlandite as a function of hexitol concentrations is shown in Figure 3. In the presence of increasing hexitol

concentrations the measured total calcium concentration is observed to raise only moderately independent whether sorbitol, mannitol or galactitol is used. For C-S-H with the lowest C/S studied (0.75), the total equilibrium concentration of calcium remains almost insensitive to the hexitol addition. Only for C-S-H buffered with portlandite (with C/S =1.5 in C-S-H) a significant increase in equilibrium calcium concentrations from 20 mM to approximately 50 mM Ca can be observed, see Figure 3-b, indicating complexation between hexitol and calcium in solution. We can further note from Figure 3-b that the equilibrium calcium concentrations obtained from the solubility experiments with C-S-H in a buffered $Ca(OH)_2$ solution (C/S 1.5) and in experiments where only portlandite was present (for detailssee (3)) show the same trends and concentrations, independent whether sorbitol, mannitol or galactitol has been added. This similarity clearly indicates that the raise in equilibrium calcium concentration is to a great extent due to the formation of the Hex_a-Ca_b-OH_c complexes ($Ca_1Hex_1(OH)_1^+$, $Ca_2Hex_2(OH)_4^0$) already identified in our previous study (3). Wecan expect that the same is true for C-S-H with lower C/S, although the concentration of Hex_a-Ca_b-OH_c complexes is lower. The impact of the various hexitols on the equilibrium calcium concentration follows the strength of the hexitol complex formation with calciumfound with portlandite (3): it increases in the order galactitol ~ mannitol < sorbitol.

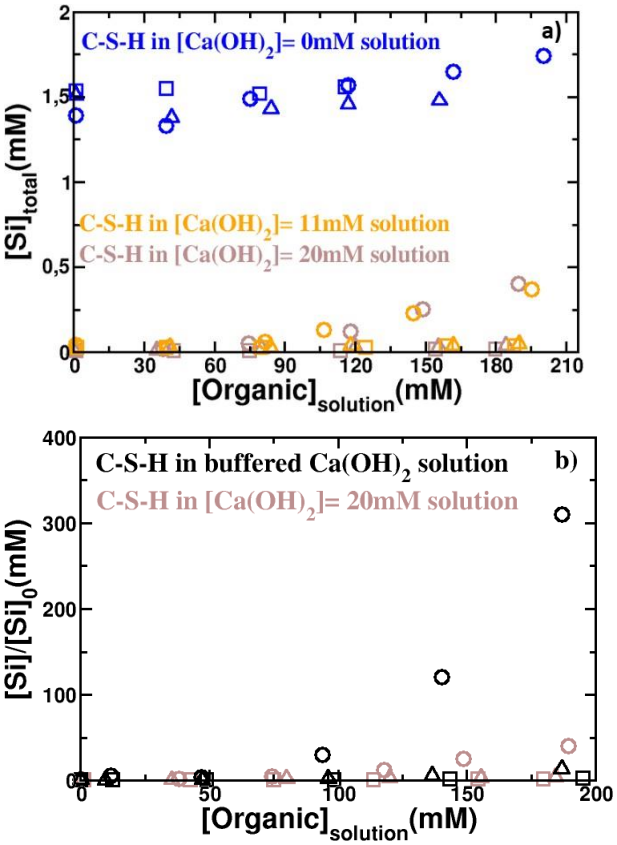

Figure 4: Measured solution concentrations of a) silicate and b) relative increase of the silicate concentration in the solution, in equilibrium with C-S-H (C/S 0.75) prepared in the same conditions

as in Figure 3. The relative increase of silicate is expressed as the ratio of the equilibrium silicate concentration to the equilibrium silicate concentration without hexitols, $[Si]_0$. Circle, square and triangle symbols represent sorbitol, mannitol and galactitol, respectively.

The evolution of silicate concentration in solutions at equilibrium with C-S-H as a function ofthe organic concentrations is shown in Figure 4. Similarly to calcium, the equilibrium silicate concentration rises with the concentration of the hexitols at all C/S studied. At the lowest C/Sratio studied (0.75, blue symbols, see Figure 4), a slight increase of silicate concentration from 1.5 mM in the absence of hexitols to 1.7 mM in the presence of 200 mM hexitol is observed. The increase in the case of sorbitol is slightly more pronounced than for mannitol and galactitol. At C/S =1.1 (11 mM $Ca(OH)_2$), the Si concentration remains below 0.05 mM in the presence of mannitol and galactitol, whereas for sorbitol it increases almost ten times up to 0.37 mM of silicate in the presence of 195 mM sorbitol. At higher C/S (1.3 and 1.5), the increase in silicate concentration remains weak with mannitol and galactitol and strong with sorbitol, as illustrated in Figure 4b.

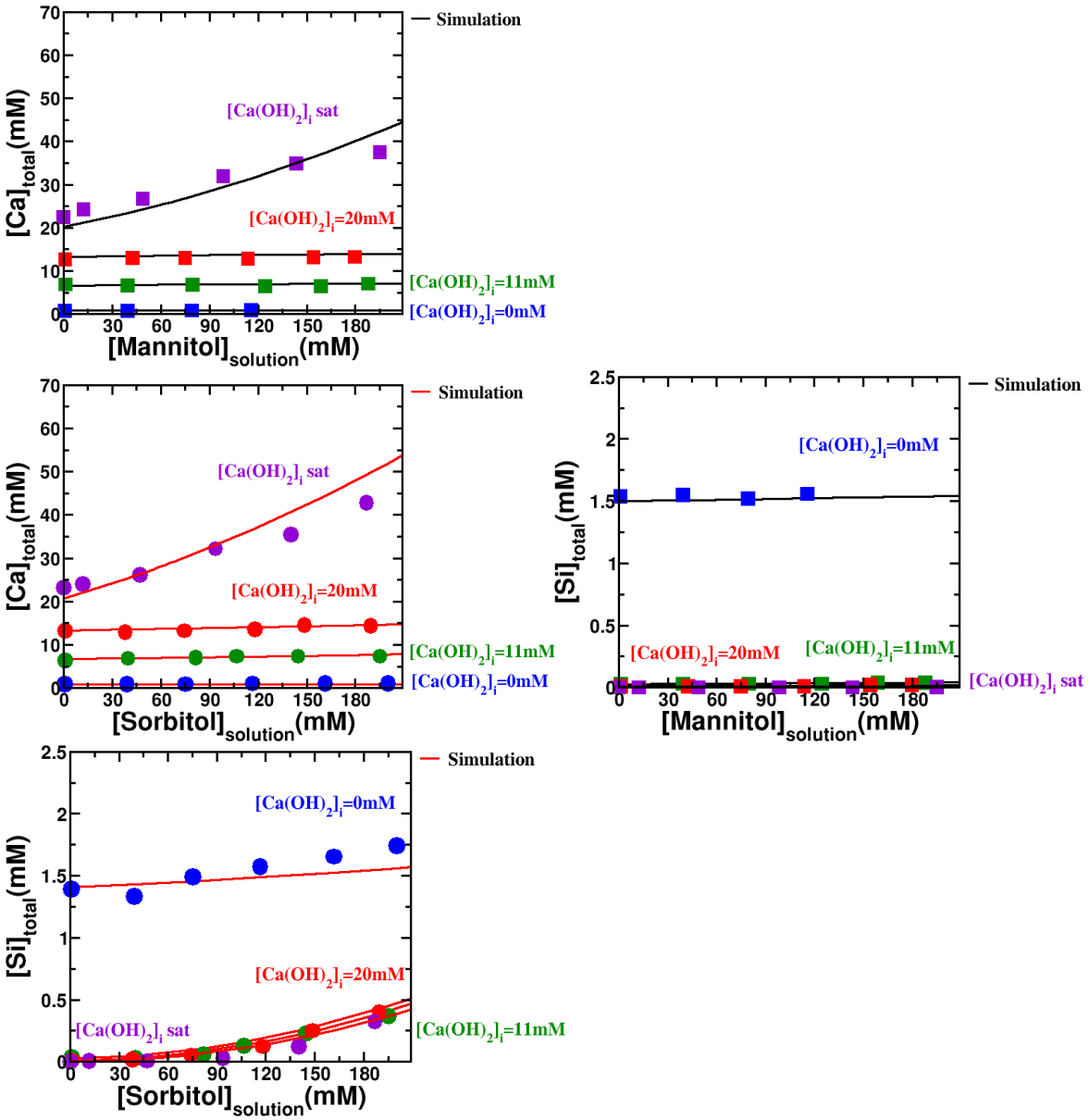

Figure 5: Total experimental (symbols) and simulated (lines) concentrations of aqueous calcium and silicate species at equilibrium with C-S-H (C/S 0.75) immersed in 250 mL ofsolution containing various initial concentrations of $Ca(OH)_2$, $[Ca(OH)_2]_i$, and varying theequilibrium concentration of hexitols.

The raise in silicate and calcium concentration in response to hexitol addition becomes stronger when the C/S of C-S-H is increased, i.e. at high pH and calcium concentrations, while at the lowest C/S studied, C/S = 0.75, the addition of hexitols has no significant impact.At C/S 1.5 ($Ca(OH)_2$ buffered systems) the silicate concentration increases by more than 2 orders of magnitude in presence of ~200 mM of sorbitol, see Figure 4-b. The impact of the different hexitols on the silicate concentration is clearly different and increases in the following order: mannitol < galactitol << sorbitol, i.e. similar to that observed for calcium. These results indicate the formation of quaternary complexes, involving

silicate-calcium- hydroxide and hexitols for galactitol and sorbitol, while none or very weak complexes are formed in the case of mannitol. Below, we shall show that such complexes derived from the ternary complex $Ca_2Hex_2(OH)_4^0$ identified in our previous study can give an accurate description of the solubility data of C-S-H presented above.

The measured and calculated silicate and calcium concentrations are compared in Figure 5. The Ca and Si concentration were calculated using the known Ca-hexitol complexes ($CaHexOH^+$ and $Ca_2Hex_2(OH)_4^0$) as summarized in Table 2 together with two quaternary Si- complexes, $Ca_2Hex_2(H_2SiO_4)(OH)_4^{-2}$ and $Ca_2Hex_2(H_3SiO_4)_2(OH)_2^0$, which were fitted here. The comparison of the calculated with the experimental calcium and silicate concentrations inequilibrium with C-S-H in Figure 5 shows in both cases significant increase of the Ca and silicate concentrations at high C/S and high pH values. The figures forgalactitol are presented in the Supplementary Information.

As the silicate complexes with organics occur mainly at high Ca-concentrations and pH values, we conjuncture polynuclear complexes similar to the main Ca-hexitol complexes present in these conditions, namely $Ca_2Hex_2(OH)_4^0$: a neutral $Ca_2Hex_2(H_3SiO_4)_2(OH)_2^0$ and a negatively charged $Ca_2Hex(H_2SiO_4)(OH)_4^{-2}$ complex. The use of only one of these complexeswas not able to reproduce the experimental data for sorbitol and galactitol adequately as little as the use of simpler complexes, i.e. $CaHexH_2SiO_4^0$ or $CaHex(H_3SiO_4)_2^0$. For mannitol no Si- containing complexes were considered as detailed in Table 2.

It should also be noted that the modeling of the silicate and calcium concentrations using classical speciation modeling (e.g. PHREEQC or GEMS) is strictly equivalent if one uses complexes with different size but same stoichiometry, i.e. $Ca_yHex_y(H_3SiO_4)_y(OH)_y^0$ and $Ca_zHex_{0.5z}(H_2SiO_4)0.5_z(OH)_{2z}^{-z}$ with $y > 2$ and $z > 2$ (provided that the formation constants are modified accordingly) or if one defines a different deprotonation degree (n) for the silicateand hexitols in the complex providing that the overall charge of the complex is maintained constant (i.e. number of OH- groups adapted accordingly). In other words, the use of $Ca_yHex_y(H_{3-n}SiO_4)_y(OH)_{y-n}^0$ and $Ca_y(Hex^{-n})_y(H_3SiO_4)_y(OH)_{y-n}^0$ as well as $Ca_z(Hex^{-n})_{0.5z}(H_2SiO_4)_{0.5z}(OH)_{2(z-n)}^{-z}$ and $Ca_z(Hex)_{0.5z}(H_{2-n}SiO_4)_{0.5z}(OH)_{2(z-n)}^{-z}$ leads exactly to the same modelling results. Again the choice of y=2 and z=2 was guided by previous works by Pallagi et al. (27) (29) and ourselves (3), but is somewhat arbitrary. Indeed, preliminary speciation simulations in the framework of the primitive model indicate that that the complexes tend to form clusters that grow in size (i.e. increase of y and z) with the organic and calcium concentrations. Also, at high calcium and organic concentrations, we experimentally observedthat the solutions were extremely difficult to filtrate, which was one of the motivation to separate the solids from the solution with a dialysis membrane. This is another indication of the formation of large complex clusters and of the variation ofthe size of the complex clusters with the equilibrium conditions.

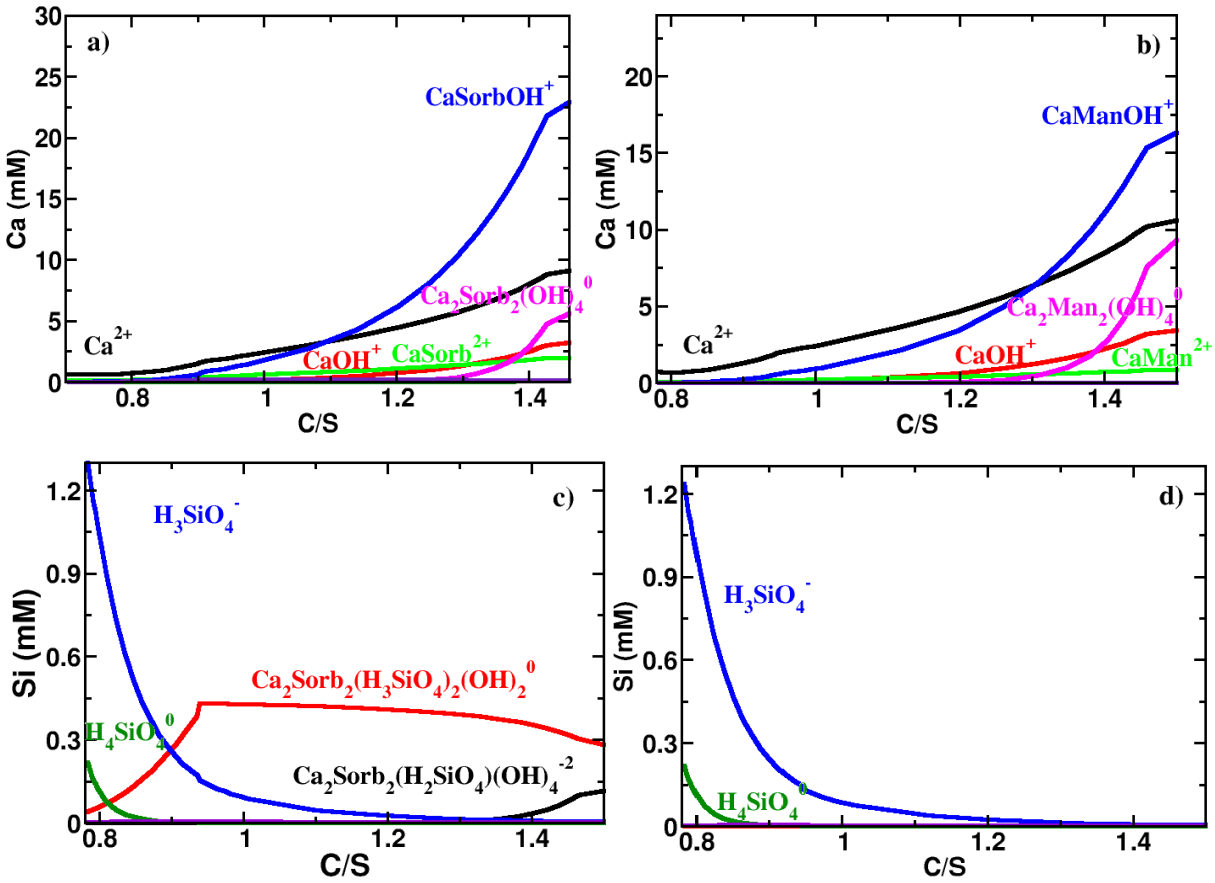

Figure 6: Simulated speciation of calcium and silicate species in a 250 mL solution containing200 mM of hexitols in equilibrium with 200 mg of C-S-H with varying C/S ratio. (a) and (c) provides the results for sorbitol; (b) and (d) those for mannitol.

The use of $CaSorbOH^+$, $Ca_2Sorb(OH)_4^0$ together with $Ca_2Sorb_2(H_3SiO_4)_2(OH)_2^0$ and $Ca_2Sorb_2(H_2SiO_4)(OH)_4^{-2}$ allows to reproduce the increase in Ca concentrations at all Ca/Siratios studied as well as the moderate increase in Si concentrations in the high range of Ca concentrations and pH values. The speciation of Si is dominated by $H_3SiO_4^-$ at low $Ca(OH)_2$ concentration (C/S = 0.75) and by $Ca_2Sorb_2(H_3SiO_4)_2(OH)_2^0$ at C/S of 1 and above, as shown in Figure 6. We can further note that the negatively charged $Ca_2Sorb_2(H_2SiO_4)_2(OH)_4^{-2}$ complex becomes only important at high pH values and Ca concentrations, typically in the buffered portlandite systems, where the concentrations of free silicates ($H_3SiO_4^-$, $H_2SiO_4^{-2}$) arenegligibly small (more than ten times smaller than the quaternary complexes).

In the case of mannitol, a very good fit of the experimental data is also obtained, see Figure 5,without the need of the $Ca_2Man_2(H_3SiO_4)_2(OH)_2^0$ and $Ca_2Man_2(H_2SiO_4)(OH)_4^{-2}$ complexes (see Table 2), as no significant increase of Si-concentration was observed. This is shown by the simulated speciation data plotted in Figure 6 where no polynuclear calcium organic silicate complexes are found, contrary

to the case of sorbitol and galactitol. The $H_4SiO_4^0$, $H_3SiO_4^-$, and $H_2SiO_4^{-2}$ species thus dominate the silicate speciation at all Ca/Si.

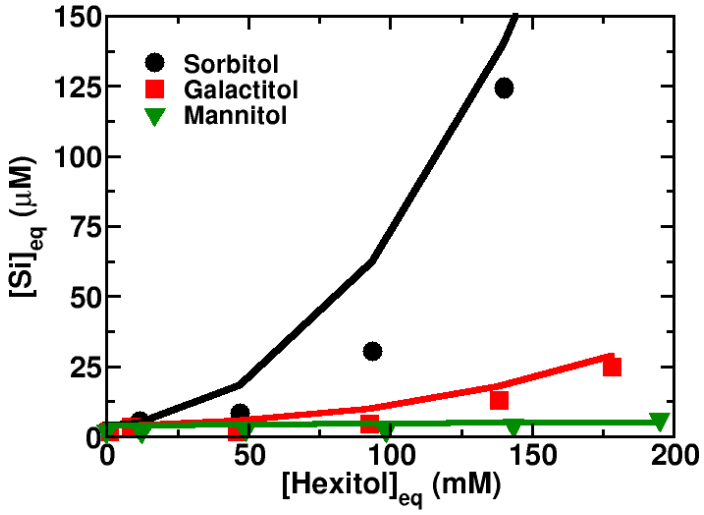

Figure 7: Total experimental (symbols) and simulated (lines) concentrations of silicate speciesin the aqueous phase in equilibrium with C-S-H buffered with portlandite (C/S 1.5) and varying the equilibrium concentration of hexitols.

Similarly to sorbitol, the use of $CaGalOH^+$, $Ca_2Gal(OH)_4^0$, $Ca_2Gal_2(H_3SiO_4)_2(OH)_2^0$ and $Ca_2Gal_2(H_2SiO_4)(OH)_4^{-2}$ complexes allow to fit accurately the measured calcium and silicate concentrations in presence of increasing amount of galactitol. Note that the fitted constants for $Ca_2Gal_2(H_3SiO_4)_2(OH)_2^0$ and $Ca_2Gal_2(H_2SiO_4)(OH)_4^{-2}$ as given in Table 2 are several log units weaker than those obtained for $Ca_2Sorb_2(H_3SiO_4)_2(OH)_2^0$ and $Ca_2Sorb_2(H_2SiO_4)(OH)_4^{-2}$ consistent with the much weaker complexation of galactitol with calcium ions (3). This is alsoillustrated in Figure 7, which compares the solubility of C-S-H buffered with portlandite (C/S 1.5) in the presence of sorbitol, galactitol and mannitol. Compared to sorbitol, a much lower amount of silicate is found in solution for galactitol but clearly more than in the case of mannitol for which no or only very weak polynuclear silicate complexes are formed. $Ca_2Gal_2(H_3SiO_4)_2(OH)_2^0$ and $Ca_2Gal_2(H_2SiO_4)_2(OH)_4^{-2}$ are predicted to dominate the solutionspeciation of silicates only at high C/S ratio, comparable to sorbitol.

3.1.2 Sodium gluconate

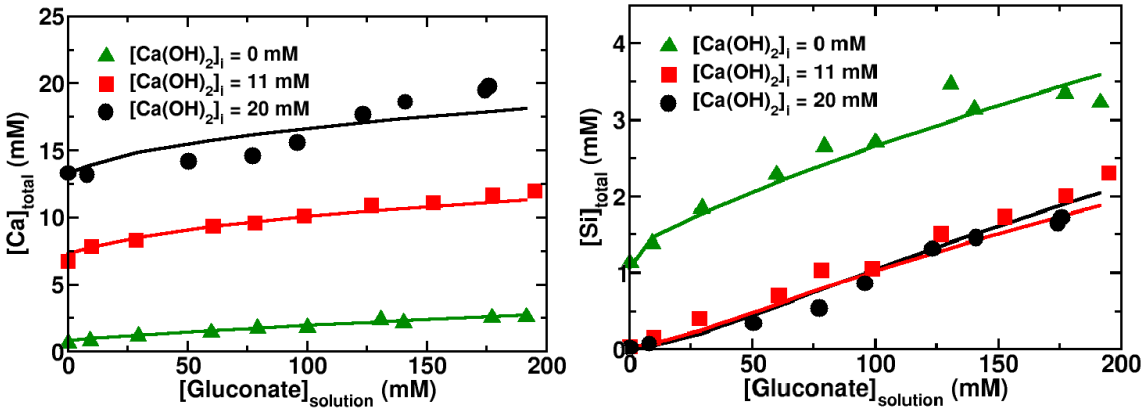

Figure 8: Experimental (symbols) and simulated (lines) concentrations of aqueous calcium and silicate species at equilibrium with C-S-H for various initial concentrations of $Ca(OH)_2$ in the solution, $[Ca(OH)_2]i$, as detailed in materials and methods. The simulations were performed with the complexes listed in Table 1.

The evolution of calcium and silicate concentration in solution at equilibrium with C-S-H as a function of gluconate concentrations is shown in Figure 8. Compared to the hexitols, the measured total calcium concentration is observed to raise more strongly in the presence of gluconate at all C/S studied, indicating a strong complexation between gluconate and calciumin solution. A four times higher calcium concentration is observed in the presence of 192 mMof gluconate for the lowest C/S studied ($[Ca(OH)_2]i$ = 0 mM) than in its absence, while at C/S=1.3 ($[Ca(OH)_2]i$ = 11 mM), the calcium concentration doubled. At the highest C/S, calcium concentration increases from 13 mM to 20 mM at 176 mM of gluconate.

The qualitative evolution of the silicate concentration upon addition of gluconate is similar to that of calcium for all C/S studied. At the lowest C/S ratio (0.75), a moderate increase of silicate concentration from 1.1 mM in the absence of gluconate to 3.2 mM in the presence of 192 mM gluconate is observed. At higher C/S (1.1 and 1.3), the relative increase in silicate concentration in response to gluconate is stronger. The equilibrium silicate concentration with

C-S-H of C/S ratio 1.3 in the presence of ~200 mM of gluconate is observed to be two ordersof magnitude larger than in the absence of gluconate.

In Figure 8, the calculated Ca and Si concentrations using the Ca-gluconate complexes from (3) as summarized in Table 1 together with the polynuclear Si-complex, $Ca_3Gluc_2(H_3SiO_4)_2(OH)_2^0$, were used to describe the increase in the experimental calcium andsilicate concentrations at equilibrium with C-S-H as a function of gluconate concentration. At all C/S studied, the thermodynamic modeling globally describes well the increase in the Si and Ca concentrations.

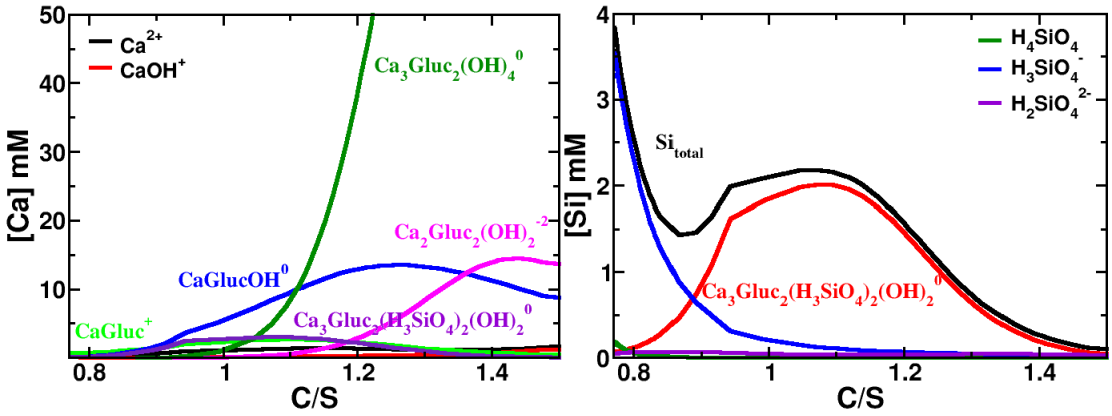

Figure 9: Simulated speciation of calcium and silicate species in a 250 mL solution containing 200 mM of sodium gluconate in equilibrium with 200 mg of C-S-H with varying C/S ratio.

Figure 9 highlights the calculated calcium and silicate speciation as a function of the C/S ratio in C-S-H in solutions in equilibrium with 200 mM of sodium gluconate. The calcium concentration is dominated by Ca-gluconate-hydroxide complexes, while the ternary $Ca_3Gluc_2(H_3SiO_4)_2(OH)_2^0$, complex is present at low concentrations only. In contrast, the experimental and calculated data highlight a visible increase of the silicate complex $Ca_3Gluc_2(H_3SiO_4)_2(OH)_2^0$ in solution, which dominates the silicate speciation at C/S above 0.9, and lower the amount of free silicates species in solution, $H_4SiO_4^0$, $H_3SiO_4^-$, and $H_2SiO_4^-$, in particular at high pH.

3.2. Adsorption of the organics on C-S-H and portlandite.

Based on the comparison of the measured organic concentrations with the initial concentrations, adsorption isotherms of the gluconate, sorbitol, mannitol and galactitol on C-S-H and $Ca(OH)_2$ (portlandite data are reproduced from (3)) could be obtained as summarizedin Figure 10. Gluconate adsorbs strongly on portlandite where an uptake of up 0.3 gluconate per $Ca(OH)_2$ was observed (see Figure 10a), while the sorption of sorbitol, mannitol and galactitol is much weaker. In the case of C-S-H buffered with portlandite (C/S 1.5) an even stronger adsorption of gluconate is observed (up to 0.8 Gluc/Si) and follows a typical Langmuir adsorption. Again the sorption of gluconate was much stronger than the sorption of sorbitol, mannitol and galactitol and reachesup to 0.2 Hex/Si. At low

C/S a weaker adsorption was observed for all organics studied in agreement with the decrease in gluconate adsorption on C-S-H with lower C/S reported in literature. (30) (22) (31)

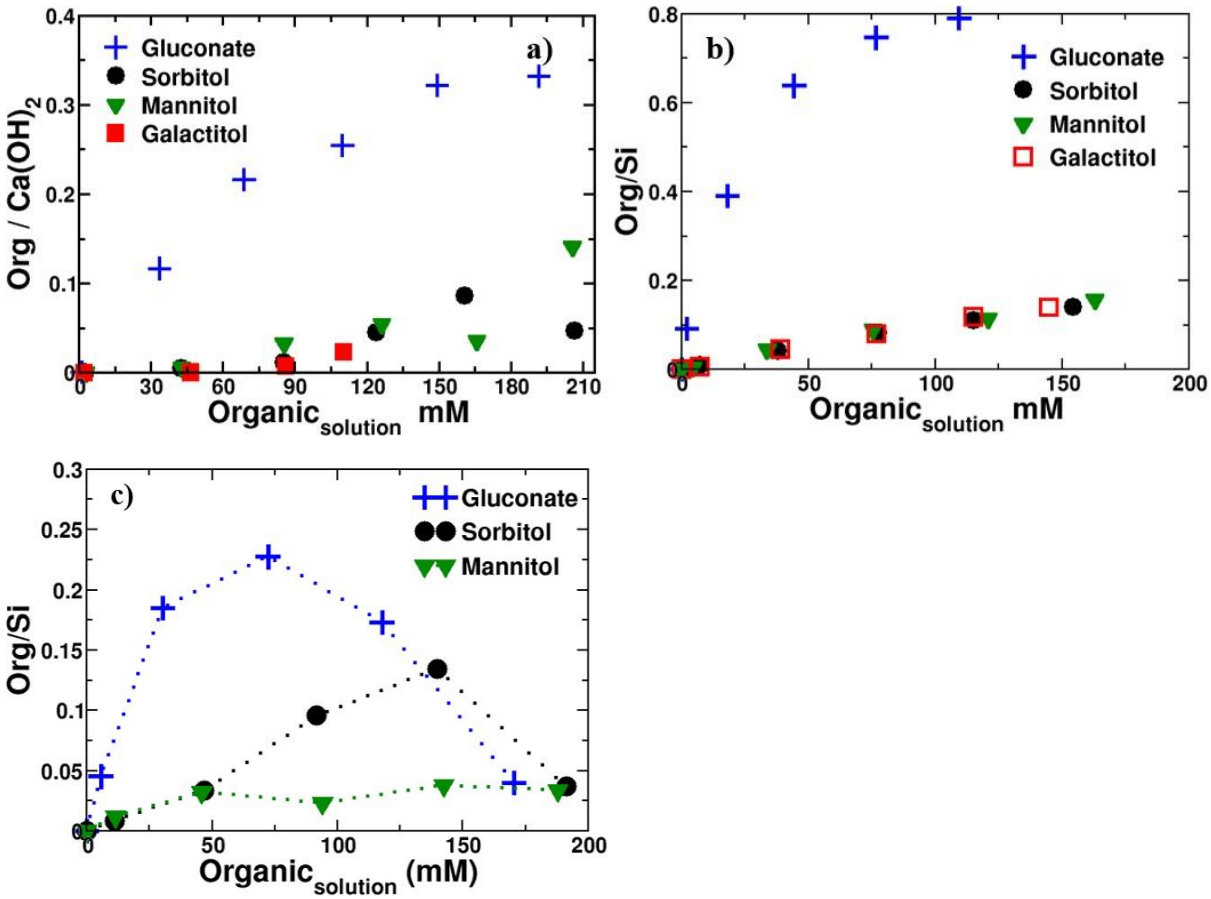

Figure 10: Adsorption isotherms of the organics on: a) portlandite, b) C-S-H buffered with anexcess of portlandite and c) C-S-H with an initial C/S = 1.12. For the C-S-H systems, the organic adsorption is expressed as the number ratio of adsorbed organics to C-S-H silicon.

The adsorption isotherm of organics at C/S = 1.1 is not monotonic. Upon progressive additionof organics, it first increases to a maximum and decreases at higher organic additions. Such a behavior is not observed when C-S-H is buffered with portlandite, that is when the calcium hydroxide activity is maintained constant. Instead, in the latter the organic adsorption follows a typical Langmuir isotherm. At C/S = 1.1, there is no calcium reservoir (no portlandite excess) and the calcium (and hydroxide) activity decreases progressively with increasing the organic concentration, because of the increasing formation of calcium-organics aqueous complexes. This complex formation leads to the progressive desorption of the calcium ion from the C-S-H surface, up to the point where the calcium mediated organic adsorption reaches a maximum and finally drops. This generic behavior was well described and predictedby Turesson and co-authors (32) using Monte-Carlo simulation in the framework of the primitive model. This decrease of gluconate and sorbitol sorption under conditions

where the availability of Ca-concentration is limited as well as the lower sorption at low C/S C-S-H clearly indicates that the binding of gluconate and hexitols on C-S-H is mediated by calcium ions, in agreement with the finding of Androniuk et al. (31) on gluconate and of Labbez et al.

(33) on the adsorption mechanism of sulfate ions.

4. Conclusions

The solubility of C-S-H in the presence of three hexitols (D-sorbitol, D-mannitol, D- galactitol) and sodium gluconate has been measured. The experimental solubility data could be modeled with a speciation model for the liquid phase, while C-S-H was described based onthe surface complexation model of Haas and Nonat (23) for the solid phase using with PHREEQC.

Sorbitol, mannitol, galactitol and gluconate did not only form aqueous complexes with calcium ions, but also polynuclear complexes with silicates, with the exception of mannitol. These polynuclear complexes resulted in a significant increase in the silicate concentration ofin equilibrium with C-S-H. The increase in silicate concentration in response to organics addition was found to strengthen with the $Ca(OH)_2$ content in the solution, i.e. with the stoichiometric calcium to silicon ratio (C/S) of C-S-H. In the case of gluconate and sorbitol anincrease of up to two orders of magnitude could be observed at the highest organic concentration and C/S ratio studied. With the exception of mannitol, the complexation powerof the organic molecules with silicate aqueous species was observed to follow the same order as with calcium ions. That is gluconate > sorbitol >> galactitol > mannitol for the silicate complexation as compared to gluconate >> sorbitol > mannitol > galactitol for the calcium complexation. Interestingly, the complexation strength of the organics with silicates seems to be correlated to their observed retarding effect on C_3S hydration: gluconate >> sorbitol > galactitol > mannitol. (19), but not with complexation strength of the organics with calcium. The fact that both high pH and calcium concentration is required for the complexation of silicate by the organics was well captured with the formation of hetero polynuclear complex involving Ca and OH ions, namely $Ca_2Hex_2(H_3SiO_4)_2(OH)_2^0$, $Ca_2Hex_2(H_2SiO_4)(OH)_4^{-2}$ and $Ca_3Gluc_2(H_3SiO_4)_2(OH)_2$. These Si-complexes when combined with the organic-Ca complexes introduced in our previous work allowed us to describe very satisfactorily the solubility of C-S-H in the presence of the organics.

The adsorption of the organics on C-S-H follows the same trend as on portlandite. The organics affinity with C-S-H was found with the order gluconate >> sorbitol > mannitol ~ galactitol. A typical Langmuir isotherm was found when C-S-H is buffered with $Ca(OH)_2$. The organics adsorption was observed to drop with decreasing the C/S of C-S-H and at highorganic concentrations, typical of a calcium mediated adsorption.

Acknowledgements

We would like to thank for the financial support from Nanocem (core project 15). We are alsovery grateful for many helpful discussions with the representatives of the industrial partners L. Pegado, J.H. Cheung, V. Kocaba, P. Juilland and M. Mosquet and their interest. A special thanks to L. Brunetti, S. El Housseini, K. Alloncle and D. Nguyen for their help in the laboratory work.

References

1. Barret, P., Bertrandie, D. Fundamental hydration kinetic features of the major cement constituents: Ca_3SiO_5 and Ca_2SiO_4. Journal de Chimie Physique, 83, 765-775, 1986.
2. Yoreo, J., Vekilov, P. Principles of crystal nucleation and growth. Reviews in Mineralogy and Geochemistry, 54, 57-93, 2003.
3. Bouzouaid, L., Lothenbach, B., Fernandez-Martinez, A., Labbez, C. Portlandite solubility and Ca^{2+} activity in presence of gluconate and hexitols. Cement and Concrete Research (submitted), 2021.
4. Young, J.F. A review of the mechanisms of set-retardation in portland cement pastes containing organic admixtures. Cement and Concrete Research, 2(4), 415-433, 1972.
5. Banfill, P.F.G., Saunders, D.C. The relationship between the sorption of organic compounds on cement and the retardation of hydration. Cement and Concrete Research, 16(3), 399-410, 1986.
6. Chandra, S., Flodin, P. Interactions of polymers and organic admixtures on portland cement hydration. Cement and Concrete Research, 17(6), 875-890, 1987.
7. Ramachandran, V.S., Lowery, M.S.. Conduction calorimetric investigation of the effect of retarders on the hydration of Portland cement. Thermochimica Acta, 195(373-387), 1992.
8. Diamond, S. Interactions between cement minerals and hydroxycarboxylic-acid retarders: I, 474 apparent adsorption of salicylic acid on cement and hydrated cement compounds. Journal of the American Ceramic Society, 54(6), 273-276, 1971.
9. Khudhair, M.H.R., Elyoubi, M.S., Elharfi, A. Study of the influence of water reducing and setting retarder admixtures of polycarboxylate “superplasticizers” on physical and mechanical properties of mortar and concrete. J Mater Environ Sci, 9, 56-65, 2017.
10. Singh, N.B., Singh, S.P., Sarvehi, R. Effect of phenols on the hydration of Portland cement. Advances in Cement Research, 2(6), 43-48, 1989.
11. Zhang, L., Catalan, L.J.J., Balec, R.J., Larsen, A.C., Esmaeili, H.H. and Kinrade, S.D. Effect of saccharide set retarders on the hydration of ordinary portland cement and pure tricalcium silicate. Journal of the American Ceramic Society, 93 (1) 279–287, 2010.
12. Thomas, J.J., Jennings, H.M., Chen, J.J. Influence of nucleation seeding on the hydration mechanisms of tricalcium silicate and cement. Journal of Physical Chemistry, 113(11), 4327-4334, 2009.
13. Pourchez, J., Grosseau, P., Ruot, B. Changes in C_3S hydration in the presence of cellulose ethers. Cement and Concrete Research, 40(2), 179–188, 2010.

14. Singh, N.B. Effect of gluconates on the hydration of cement. Cement and Concrete Research, 4(6), 455-460, 1976.
15. Zhang, G. Li, G., Li, Y. Effects of superplasticizers and retarders on the fluidity and strength of sulphoaluminate cement. Construction and Building Materials, 126, 44-54, 2016.
16. Singh, N.B. Influence of calcium gluconate with calcium chloride or glucose on the hydration of cements. Cement and Concrete Research, 5(6), 545-550, 1975.
17. Lv, X., Li, J., Lu, C., Liu, Z., Tan, Y., Liu, C., Li, B., Wang, R. The Effect of Sodium Gluconate on Pastes' Performance and Hydration Behavior of Ordinary Portland Cement. Advances in Materials Science and Engineering, 9, 2020.
18. Ma, S., Li, W., Zhang, S., Ge, D., Yu, J., Shen, X. Influence of sodium gluconate on the performance and hydration of portland cement. Construction and Building Materials, 91, 138-144, 2015.
19. Nalet, C., Nonat, A. Effects of hexitols on the hydration of tricalcium silicate. Cement and Concrete Research, 91, 87-96, 2017.
20. Nalet, C., Nonat, A. Effects of functionality and stereochemistry of small organic molecules on the hydration of tricalcium silicate. Cement and Concrete Research, 87, 97-104, 2016.
21. Juilland, P., Gallucci, E. Hindered calcium hydroxide nucleation and growth as mechanism responsible for tricalcium silicate retardation in presence of sucrose. 329, 143-154, 2018.
22. Nalet, C., Nonat, A. Ionic complexation and adsorption of small organic molecules on calcium silicate hydrate: relation with their retarding effect on the hydration of C_3S. Cement and Concrete Research, 89, 97-108, 2016.
23. Haas, J., Nonat, A. From C–S–H to C–A–S–H: Experimental study and thermodynamic modelling. Cement Concrete Research, 68, 124-138, 2015.
24. Thoenen, T., Hummel, W., Berner, U., Curti, E., The PSI/Nagra Chemical Thermodynamic Data Base 12/07, PSI report 14-04, Villigen PSI, Switzerland, 2014.
25. Sjöberg, S., Nordin, A., Ingri, N. Equilibrium and Structural Studies of Silicon(IV) and Aluminium(III) in Aqueous Solution. II. Formation Constants for the Monosilicate Ions $SiO(OH)_3^-$ and $SiO_2(OH)_2^{2-}$. A Precision Study at 25°C in a Simplified seawater medium. Marine Chemistry. 10(6), 521-532, 1981
26. Pallagi, A., Sebők, P., Forgó, P., Jakusch, T. Multinuclear NMR and molecular modelling investigations on the structure and equilibria of complexes that form in aqueous solutions of Ca2+ and gluconate. Carbohydrate Research, 345(13), 1856-1864, 2010.
27. Pallagi, A., Bajnóczi, É.G., Canton, S.E., Bolin, T., Peintler, G., Kutus, B., Sipos, P. Multinuclear complex formation between Ca(II) and gluconate ions in hyperalkaline solutions.Environmental Science & Technology, 48(12), 6604-6611, 2014.
29. Kutus, B., Gaona, X., Pallagi, A., Pálinkó, I., Altmaier, M., Sipos, P. Recent advances in the aqueous chemistry of the calcium(II)-gluconate system – Equilibria, structure and composition of the complexes forming in neutral and in alkaline solutions. Coordination Chemistry Reviews. 417. 2020,
30. Glaus, M.A., Laube, A., Van Loon, L.R. Solid–liquid distribution of selected concrete admixtures in hardened cement pastes, Waste Management, 26, 741-751, 2006.
31. Androniuk, I., Landesman, C., Henocq, P., Kalinichev, A.G. Adsorption of gluconate and uranyl on C-S-H phases: Combination of wet chemistry experiments and molecular dynamics simulations for the binary systems, Phys Chem Earth, 99,194-203, 2007.
32. Turesson.M., Labbez.C., Nonat, A. Calcium mediated polyelectrolyte adsorption on like-charged surfaces. Langmuir. 27(22), 2011.
33. Labbez, C., Medala, M., Pochard, I., Nonat, A. Adsorption of multivalent ions in cementitious materials : Importance of electrostatics, in: 2nd International Workshop on Mechanisms and modelling of waste/cement interactions. Le Croisic, France, 2008.

C. Impact of gluconate and hexitol additives on the precipitation mechanism and kinetics of C-S-H

Lina Bouzouaid[1], Alexander E.S. Van Driessche[2], Wai Li Ling[3], Juan Carlos Martinez[4], Marc Malfois[4], Barbara Lothenbach[5], Christophe Labbez[1], Alejandro Fernandez-Martinez[2]

[1] ICB, UMR 6303 CNRS, Univ. Bourgogne Franche-Comté, FR-21000 Dijon, France

[2] Univ. Grenoble Alpes, Univ. Savoie Mont Blanc, CNRS, IRD, IFSTTAR, ISTerre, 38000 Grenoble, France

[3] Univ. Grenoble Alpes, CEA, CNRS, IRIG, IBS, Grenoble, France.

[4] Non-Crystalline Diffraction Beamline−Experiments Division, ALBA Synchrotron Light Source, Cerdanyola del Vallès, Barcelona 08290, Spain

[5] Empa, Concrete & Asphalt Laboratory, Dubendorf, Switzerland

Abstract

The present paper investigates the influence of gluconate and hexitol additives on the precipitation mechanism and kinetics of C-S-H. To this end, wet chemistry C-S-H precipitation experiments were performed under controlled conditions of solution supersaturation –under varying silicate concentration, while the transmittance of the solution was followed. This allowed determining induction times for the formation of C-S-H precursors in the presence and absence of gluconate and three hexitol molecules. Characterization of the precipitates was performed via small angle X-ray scattering and cryo-transmission electron microscopy experiments, which allowed the identification of a multi-step nucleation pathway also in the presence of the organics. Analysis of the induction time data in the framework of the classical nucleation theory revealed a significant increase of the kinetic pre-factor, which is associated to physical rates of cluster collision and aggregation during the nucleation process. Values of the kinetic pre-factor increase in the same order as the complexation constants of calcium and silicate with the each of the organics. This points to a retarding mechanism of crystallization related to steric hindrance of the aggregation of the early formed clusters via adsorption of the organics at their surfaces.

1. Introduction

In Portland cement, calcium silicate hydrate (C-S-H) is the principal hydration product of alite (C_3S) and belite (C_2S), playing a decisive role in the final properties of concrete (1). It is generally accepted that the formation of this hydrate follows a dissolution-precipitation process (2) (3). To control the workability and final properties of concrete, a large variety of additives are added to the cement mixture, such as setting retarders, accelerators and superplastizicers, among others (4) (5) (6) (7). These chemicals alter different processes occurring in cementitious systems, including their hydration behavior. Extensive experimental work has shown that numerous additives have a retardation effect on the hydration of C_3S (8) (9) (10) (11) (12) (13), mainly by disrupting the nucleation and/or growth process of C-S-H. In addition, it has been shown that the dissolution kinetics of cement and/or C_3S are not limited by different retarders, such as yellow dextrin and cellulose ethers (12) (14) (15) (16) (17). Thus, in order to develop more efficient cement additives, a detailed understanding of the initial formation of C-S-H in the absence and presence of these additives is needed.

In a recent work by Krautwurst et al. (18), time-resolved potentiometry coupled with transmittance measurements, small angle X-ray scattering and cryo-TEM experiments were used to study the homogeneous nucleation of C-S-H from diluted solutions. It was found that C-S-H formation follows a two-step pathway. The first step, identified by an decrease of the transmittance of the solution, corresponds to the formation of amorphous spheroids which subsequently crystallized into typical sheet-shaped C-S-H particles during a second step of transmittance decrease (18). In another study, [Plank et.al. (reference)]. TEM imaging indicated the initial presence of metastable C-S-H nanoparticles with globular morphology and sizes between 20 and 60 nm, similar to those observed by Krautwurst et al. (18). After less than one hour, those nanoparticles were observed to grow gradually into the characteristic nanofoils of early C-S-H.

These two studies described the formation of C-S-H through a so-called ‘non-classical’ nucleation pathway, which has been observed for a large variety of organic and inorganic systems, but remain a hot topic of debate and investigation due to the complex processes involved (19) (20) The formation of precursor metastable phases is predicted by Ostwald ‘s rule of stages, invoking the low energetic cost from a kinetic point of view to form the less stable polymorph (i.e. more soluble) from the supersaturated solution. Many recent observations have contributed lately to a more complete description of this rule of stages: several authors have described the formation of amorphous or nanoparticle precursors (e.g. (21) (22)), which in some cases act as the building blocks of the

crystalline phases through complex diffusion and aggregation processes which are still poorly understood (e.g. (23)). These observations have been validated for some systems, but are still far from being fully understood, and a universal law describing the full crystallization process is still far from being reached (e.g. (24)). Moreover, Plank et al. showed that polycarboxylate ether-based superplasticizers (PCEs) control the kinetics of the transition from globular to nanofoil-like C-S-H. Indeed, in the presence of those additives, this conversion is strongly delayed. It is argued that PCEs form layers around C-S-H globuli in a core-shell geometry. The authors proposed that this external layer slowed down the water diffusion into the particles' core, and consequently decreases the kinetics of dissolution and re-crystallization of the core particles. Yet, most of the commonly employed additives are small simple organics, such as gluconate, which is routinely used by the concrete industry as retarder to control the setting time of cement. (25) (26) (27) (28). Gluconate is also efficient in increasing the compressive strength to concrete (29) (30). Another saccharide derivative such as sorbitol (a neutral sugar alcohol) is also used as a set retarder for Portland cement: when added in the material at 0.40 wt%, sorbitol delays the setting of 2 days (31). Moreover, sorbitol is used as a water-reducing plasticizer, decreasing final porosity and giving greater mechanical strength and durability (32).

In overall, the case of C-S-H nucleation from diluted solutions is an archetypical case of multi-step nucleation, in which a metastable phase (amorphous spheroids) is persistent before its crystallization takes place. The aggregation of these spheroids has been suggested as a critical step, concomitant to the crystallization, but further investigations are needed to fully characterize the precipitation process, especially in the presence of additives. Therefore, the focus of this work is on the interactions of the amorphous C-S-H spheroids with different cement additives, D-sorbitol, D-mannitol, D-galactitol and of gluconate, that act as retardants of the crystallization process. The first three molecules share the same chemical formula but have different stereochemistry. Gluconate is a charged molecule known to act on the nucleation kinetics and mechanisms of C-S-H. We worked in diluted aqueous solutions and the pH of the experiments was set at the value close to the one observed in cement paste (pH 12.8). As opposed to the conditions reigning in real cement, and with the objective of simplifying the study, our goal was to study homogeneous nucleation, so the solutions were kept free from grain/impurities, in order to avoid any heterogeneous nucleation. First, the effects of additives on the nucleation kinetics of C-S-H were studied by determining the induction time as a function of supersaturation using transmittance measurements. Secondly, small angle X-ray scattering (SAXS) experiments were performed in order to characterize the size and shape distribution of the C-S-H nanoparticles formed during precipitation, in absence and in presence of additives. Finally, cryo-TEM, was used to get a clearer picture of the particle morphology in the presence and absence of organic molecules.

2. Material and methods

2.1. Materials

The different stock solutions were prepared by dissolving $CaCl_2$ $2H_2O$ (Sigma-Aldrich, ≥99% purity), sodium gluconate ($C_6H_{11}NaO_7$, Sigma-Aldrich, ≥99% purity) D-sorbitol ($C_6H_{14}O_6$, Sigma-Aldrich, ≥99% purity), D-mannitol ($C_6H_{14}O_6$, Sigma-Aldrich, ≥99% purity), and D-galactitol ($C_6H_{14}O_6$,, Sigma-Aldrich, ≥99% purity) and sodium chloride (NaCl, Sigma-Aldrich, ≥99% purity), in boiled and degassed milliQ water.

The hexitols used in this study are all isomers, sharing the formula, $HOCH_2(CHOH)_2CH_2OH$, but differ in the stereochemical arrangement of the OH groups as illustrated in Figure 1 .

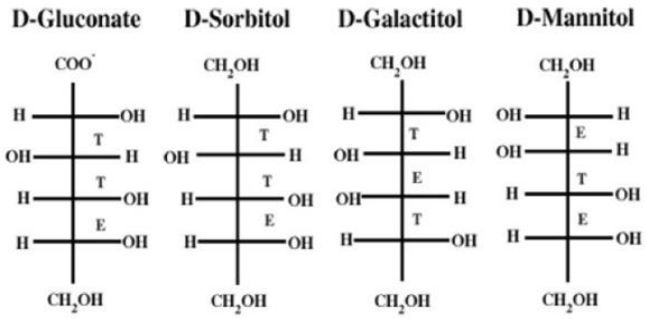

Figure 1. Stereochemistry of the different organic molecules used in this study.

2.2. Titration of Ca^{2+} with Na_2SiO_3

The precipitation of $CaO\text{-}SiO_2\text{-}H_2O$ was followed using an automated titrator instrument (Metrohm 905 Titrando) . All measurements were performed in a thermostated reactor at 23.0 ± 0.1°C. The solution in the reactor was continuously stirred with a magnetic stirrer at a constant rate of 430 rpm. A nitrogen flow circulated continuously above the solution to avoid contamination with CO_2. It was taken care that the gas did not enter the solution to avoid any disturbance of the electrodes. In the reactor, 148 mL of a solution containing 25mM NaCl background electrolyte, a fixed concentration of the organic of interest, between 0.1mM and 10mM, and 15 mM of $CaCl_2.(H_2O)_2$ After 3 minutes of equilibration time, 3ml of a titrant solution containing a silicate concentration is added. The final silicate concentrations reached were situated between 0.05mM and 0.25mM at a rate of 1.2ml/min registered in the software tiamo 2.5 (Metrohm). The addition of NaOH within the reactor allowed us to set the value of pH at 12.7-12.8, the final concentration of NaOH being fixed at 80mM.

In order to follow the formation of the first particles of C-S-H in absence and in presence of the small organics, an optical electrode (Metrohm Optrode, 6.1115.000) measuring the light transmittance of the system is added. A stable electrode signal is obtained with the use of a background electrolyte. The titrations were thus performed in 25 mM NaCl to ensure a stable signal and to limit the influence of the background electrolyte on the complex formation. One particular wavelength (among eight) using the software tiamo may be selected. For the experiment, the wavelength at 470 nm is chosen.

The calcium potential was also measured during the experiment, using the ISE Ca^{2+} electrode (Metrohm Ca ISE 6.0508.110), coupled to a reference electrode (Metrohm Ag, AgCl/3 M KCl, 6.0750.100). By plotting the measured mV against the calculated Ca^{2+} activity calculated with PHREEQC as detailed below, the calcium activity can be extracted. The pH was determined with a pH electrode (Metrohm pH Unitrode with Pt 1000, 6.0259.100), which allows reliable measurements up to pH = 14. The pH electrode was calibrated prior to the measurements with standard buffer solutions (pH 10, 12.45 and 14 from Sigma Aldrich).

2.3. Thermodynamic simulation: saturation index calculation.

The saturation index (SI) was calculated with a speciation model solved by the geochemical software PHREEQC version 3 (3.6.2-15100) using the WATEQ4f database. SI is calculated by comparing the activity product of the dissolved ions of C-S-H (IAP) with their solubility product (K_{sp}); SI = $\log(IAP/K_{sp})$.

2.4. Cryogenic Transmission Electron Microscopy

Titration experiments, as described in 2.2, were run in the presence of gluconate and sorbitol and at different time points of the reaction 4µl aliquots were retrieved from the solution in the reactor and applied to freshly glow discharged qauntifoil or lacey carbon grid and vitrified using a Thermofisher Vitrobot Mark IV system. The grids were then mounted on a Gatan 626 single-tilt cryo-transfer holder. Imaging and selected area diffraction (SAD) were performed under low-dose conditions on a Tecnai F20 microscope operating at 200 keV. Images were recorded on a Ceta CMOS camera whereas diffraction patterns were recorded on an Amsterdam Scientific Instrument CheeTah hybrid pixel camera.

2.4. Small Angle X-ray Scattering (SAXS)

SAXS experiments were performed at the NCD beamline of the ALBA synchrotron (Barcelona, Spain). The same Metrohm system described in section 2.2 was used to titrate a calcium chloride

solution containing gluconate with a sodium orthosilicate solution (see concentrations used in Table 1). The reaction took place in the same reactor used for the transmittance experiments described in section 2.2. A peristaltic pump was used to circulate the solution in a closed loop through a 1.5 mm diameter polyimide capillary that was set up at the beam position. The residence time in the tubing and capillary is in the order of ~20 seconds. The chemistry was followed using a pH electrode and a transmittance sensor (as described in 2.2). An X-ray beam of energy E = 12.40 keV (λ = 1.00 Å), calibrated using a silver behenate standard, was used. The scattered radiation was collected using a Pilatus 2M two-dimensional detector (981 × 1043 pixels, 172 × 172 μm pixel size) that was placed at 6.7 m from the sample to yield a q-range $0.03 < q < 2.00$ nm^{-1}. The scattered intensity was acquired every minute in acquisitions of 30 seconds to follow the kinetics of C-S-H nucleation.

Table 1. Conditions used for the SAXS experiments.

Additive	**[Si] (mM)**	**[Ca] (mM)**	**[NaCl] (mM)**	**[NaOH] (mM)**	**[additive] (mM)**
Pure	0.10	15	25	18	-
Gluconate	0.10	15	25	18	0.03
Gluconate	0.10	15	25	18	0.07
Gluconate	0.10	15	25	18	0.15
Gluconate	0.10	15	25	18	0.30

3. Results and discussion

Thermodynamics of C-S-H nucleation

Three curves showing the typical evolution of the transmittance over time, for the pure and the 10 mM gluconate and sorbitol systems, are shown in Figure 2. The pure system shows the same behaviour described by Krautwurst et al. (18), with two characteristic drops of the transmittance. The first drop was described as corresponding to the formation of amorphous spherical particles of ~50 nm size that act as precursors for the formation of nanocrystalline C-S-H; the second drop was described as resulting from a process of droplet aggregation and changes of stoichiometry and surface chemistry, leading to massive C-S-H crystallization (18). This behaviour is also observed in the case of sorbitol, showing two well-defined drops of the transmittance. Importantly, the case of gluconate

is notably different: the signal decrease is slower than for the pure system and for the sorbitol and no clear sign of a second drop of the signal at later times is observed.

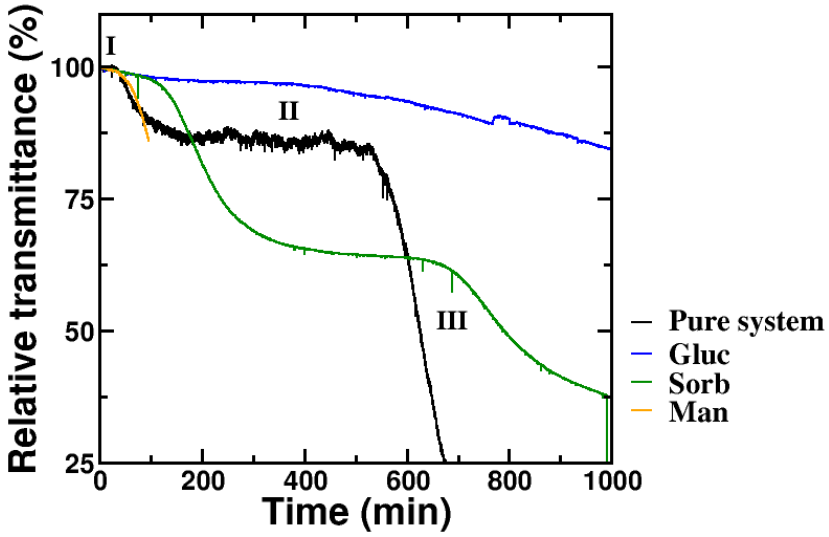

Figure 2. Evolution of the relative transmittance of the solution as a function of time for pure system of precipitating C-S-H as reference experiment (black line), and in the presence of 10 mM gluconate (blue), 10 mM sorbitol (green), 10 mM mannitol (orange), and 10 mM galactitol (pink). The final concentrations of Si is set at 0.10 mM, Ca at 15 mM. The total solution volume is set at 150 ml. After an initial drop of the transmittance (stage I) corresponding to the formation of amorphous droplets, a plateau is reached (stage II). A final decrease of the transmittance is observed (stage III), which has been assigned to C-S-H crystallization.

A detailed analysis of the initial times shows a difference between the behaviour of the pure system and that of the organic-containing systems. The neutral molecule sorbitol and the charged molecule gluconate are represented as examples (Figure 3, center and right), and compared with the reference system (Figure 3, left; data are for solutions with the same organic concentration of 10 mM and same Si_{final} = 0.15 mM and Ca_{final} = 15mM). Whereas the data from the pure system shows an initial plateau, with no changes in the transmittance until the induction time, the solutions containing organics show an initial decrease of the transmittance that takes place immediately after mixing the solutions, followed by a stabilization step prior to a second drop. This initial decrease is more pronounced in the case of gluconate than for sorbitol: in the case of sorbitol, it lasts for less than 7 minutes, and the drop in relative transmittance is less than 1%; the data from the gluconate-containing solution shows an initial decrease that lasts for ~100 minutes solution, and a drop in relative transmittance of ~2%.

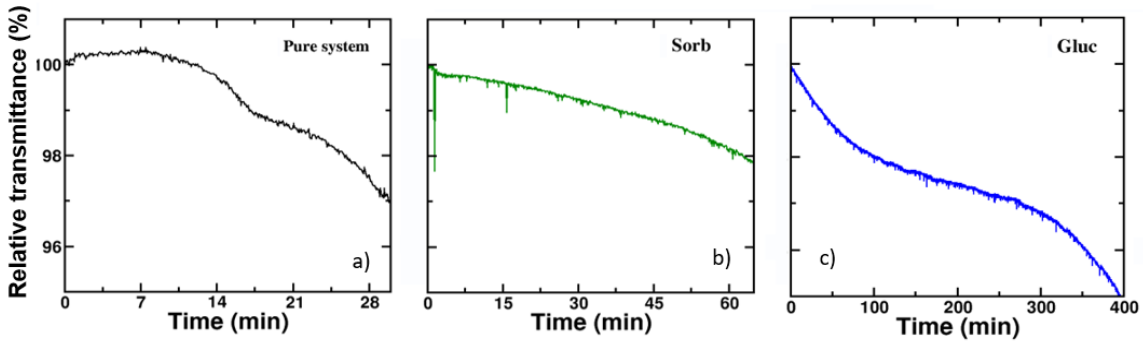

Figure 3. Enlargement of the initial part of the transmittance curves, before the first transmittance drop of stage I, with Si_{final}=0.15mM and Ca_{final} =15mM. 3.a: Transmittance as a function of the time for the pure system. 3.b: Addition of sorbitol at 10mM in C-S-H system. 3.c: Addition of gluconate at 10 mM in C-S-H system.

The presence of this first drop in the organic-containing solutions poses some questions about the interpretation of the different phenomena going on during the C-S-H nucleation in the presence of additives. In the analysis by Krautwurst et al. (18) this very initial first drop in transmittance was not observed as confirmed here, see Figure 3-a. The fact that this initial drop is not observed for the pure system allows making the hypothesis that it is related to a process of formation of aqueous Ca-Si-organic complexes. With the aim of clarifying this point, a comparison of data taken for the 10 mM gluconate system under different β-C-S-H supersaturations is presented in Figure 4 (see speciation of the supersaturated solutions in Table S1.A of the Supporting Information). The data show (Fig. 4) that all the solutions display the same trend, with an initial drop of the transmittance in the same time interval, irrespective of the supersaturation with respect to β-C-S-H. Such a behaviour differs notably from that expected for a nucleation event, in which the induction time –and its associated decrease of the transmittance– responds to changes in the supersaturation of the solution. Indeed, the initial drop is independent of the supersaturation. The associated process is thus not activated. On the contrary, the second drop in transmittance(corresponding to the first drop in the pure system), observed at around ~500 min shows a dependency with the supersaturation, with faster and more pronounced decrease at higher supersaturations. This leads us to propose that the observed the very first drop is due to the above-mentioned process of aqueous Ca-Si-organic complex formation (or complex clusters) and that the second drop at >500 min (Fig. 4b) is a true nucleation event. Note that the first two values (Si = 0.08 mM and Si = 0.10 mM) do not follow the expected trend; this behaviour, though unexpected, can be rationalized considering the stochastic nature of the nucleation process, which leads to non-negligible uncertainties in the values of the induction times, as it will be seen later.

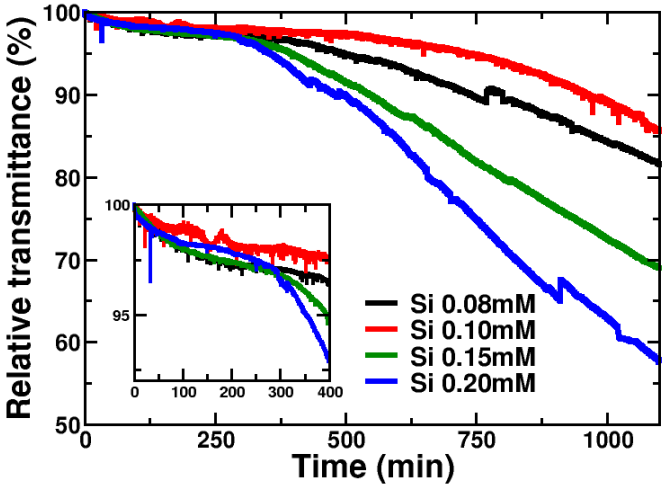

Figure 4. Transmittance as a function of time for the C-S-H system in presence of gluconate at 10mM, at different supersaturation degrees: [Si]=0.08mM, [Si]=0.10mM, [Si]=0.15mM and [Si]=0.20mM.

The data shown in Fig. 4 allows assigning the initial drop in transmittance to a process of Ca-Si-organic complex formation. It seems that the organic molecules interfere with the nuclei precipitated, or seem to induce the formation of particular nuclei that are different in shape and size, blurring the well-defined stages observed in the reference system, in particular stage I. The presence of the complexes involving calcium and the organics described in more details in our previous work (33) can be an explanation in the change of the pathways observed for the pure system, and thus can be the cause of the very first decrease of the transmittance, given that it is observed at all supersaturation degree studied (see Figure 4). The fact that, as shown in Fig. 3, this initial drop is larger for gluconate than for sorbitol is expected given the relative amount of calcium being part of multinuclear Ca-Si-gluconate complexes that form under these conditions, in comparison to the lower amount in hexitol complexes (see Table S1.B of the Supporting Information). (33).

Thus, the later drop (at ~500 min in Figure 4) can be considered as the first nucleation event occurring in the system and allows, us to perform a quantitative analysis of the thermodynamics and kinetics of nucleation using classical nucleation theory (CNT) [e.g. (34)]. To this end, all the transmittance curves were analysed by doing linear fits as explained in Figure S1 (see Supporting Information). Following the CNT formalism, the induction time (t_{ind}) can be written as a function of the solution saturation index (SI):

$$\log(t_{ind}) = C_0 + \frac{\frac{16}{3}\pi\Omega^2\alpha^3}{(k_BT)^3SI^2} \qquad \text{[eq. 1]}$$

where Ω is the molar volume of the formed phase, α is the interfacial free energy, k_B is the Boltzmann factor, and T is the temperature. C_0 is the so-called pre-exponential kinetic factor, and it is related to thermodynamic and kinetic factors such as the number of sites susceptible to act as nucleation loci, the collision rate, and the Zeldovich factor (related to the probability of successful formation of a cluster in solution). Induction times from all the experiments performed are shown in Figure 5.

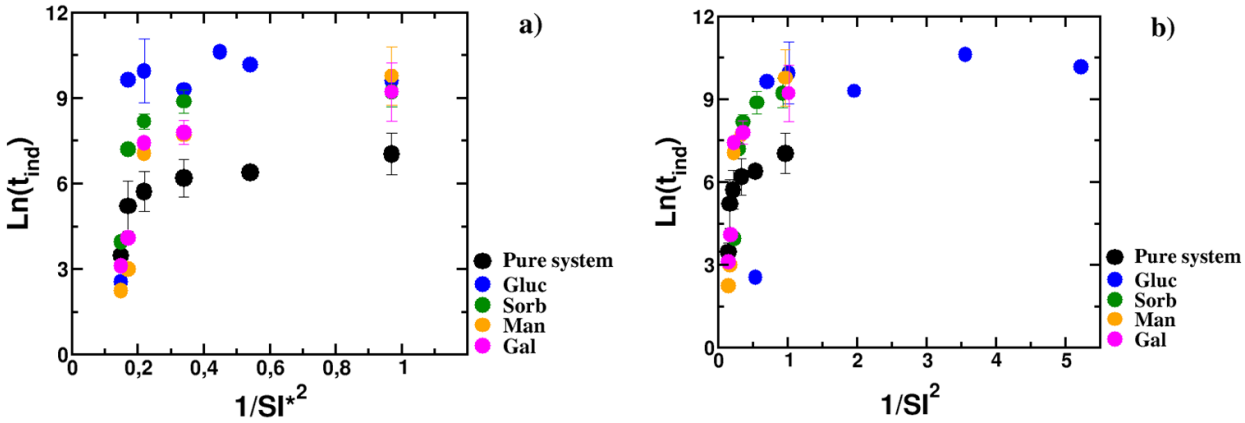

Figure 5. Logarithm of the induction time as a function of the saturation index for the pure system (black) and in presence of gluconate (blue), sorbitol (green), mannitol (orange) and galactitol (pink). The saturation index was calculated using the speciation software PHREEQC, taking into account the condition of the different precipitation experiments, including components concentrations and temperature, but also the complexes existing between calcium, silicate and the organic molecules (b). The apparent SI* was also calculated, which does not take into account the aqueous complexes involving the organics (a).

As expected, the overall trend for all the datasets is an increase of the induction time when the saturation index decreases. An overall increase of the induction times when organic molecules are added to the solution can also be observed. This increase is pronounced in the range of lower supersaturations (high $1/SI^2$ values). Data at higher supersaturations blur this effect as the induction times decrease, with the statistical error bars being more significant.

To fit these data using eq. 1 some approximations need to be made: the first one is the assumption that the nucleated phase is β-C-S-H. Indeed, the supersaturation values used to plot the data have been calculated using the solubility product with respect to that phase, and the only value for a molar volume available in the literature is that corresponding to a nanocrystalline C-S-H phase such as β-C-S-H. However, as discussed above and reported by Krautwurst et al, and as it is confirmed by our cryo-TEM data, the drop in transmittance used to determine the induction time corresponds to the formation of amorphous droplets. In the absence of precise information about the density and solubility of these droplets, the approximation is made that β-C-S-H is the nucleated phase. This implies that the values for the interfacial energies used cannot be interpreted in absolute terms, but

only relatively to each other. A second approximation made, inherent to the use of the master equation of CNT in eq. 1, is the fact that the same nature of precipitate is formed for all the supersaturation conditions. However, data fitted using all the supersaturation range and a supersaturation dependence of the pre-exponential term (C_0) shows a deviation at high supersaturation values, which probably points to a change in the nature of the precipitate at high Ca and Si concentrations (see Figure S1). A way to fix this issue is to separate the experimental data in two parts: low and high supersaturations. Here, data from low supersaturation has been fitted using eq. 1, and considering C_0 as a constant independent on the value of the saturation index, an approximation widely used in the literature.

Results of the fits yield values for the interfacial free energy or surface tension, α, and of the kinetic pre-factor, C_0 (Fig. 6). All the values of the interfacial free energies, α, fall in the range between 5 and 13 mJ/m^2, In agreement with the value (~13 mJ/m^2) obtained by Gauffinet and Nonat (35) with large uncertainties that make them indistinguishable within the error. The situation changes for the values of the kinetic pre-factor, C_0. The gluconate system shows the higher values of C_0. The systems with the hexitols sorbitol, galactitol and mannitol yield a similar value of C_0, which is still slightly higher than that of the pure system. Interestingly, this order matches that found for the complexation constants of Ca^{2+} and silicates with these organics: gluconate was found to form strong polynuclear complexes with Ca^{2+} and silicates, followed by sorbitol, which showed a weaker complexation level, and than by galactitol and mannitol, with the weakest tendency to form complexes.

The fact that the presence of the organics does not modify (within the uncertainty) the value of the interfacial free energy would suggest that the nature of the C-S-H nuclei formed –their interfacial properties remains rather the same irrespective of the presence of the organic molecules. In that case, a plausible interpretation for all the data in Fig. 6 would consist in a process by which the organics interact physically with the nucleated particles, modifying their aggregation pathways. Indeed, as suggested by Krautwurst et al. from observations with the transmittance probe, the individual, precursor particles undergo crystallization at stage III, in a crystallization process that is concomitant to the aggregation of the amorphous spheroids. This type of effect, where an organic additive imposes steric barriers to the aggregation, modifying the crystallization kinetics, has already been observed by other systems such as $CaSO_4$. (36) However, the interfacial free energy data have to be analysed carefully. The reason for this is that the nucleation rate is highly sensitive to the value of the interfacial free energy due to the cubic exponent in eq. 1. This fact makes that a small variation could change the height of the nucleation barrier (and therefore the nucleation kinetics) in a very significant way. This is exemplified in Figure 7, where a sensitivity analysis of this parameter, the interfacial free energy, is shown. Values of the height of the nucleation barrier –normalized by the thermal energy, k_BT- are given in the colour bar, and are plotted as a function of the interfacial free energy

(*x* axis) and the saturation index of the solution (*y* axis). The range of values in both *x* and *y* axes have been set to values that are used or found in the experiments reported here. The results show that the nucleation barrier can vary between very small values (< 5) where nucleation can happen spontaneously, to values in the order of ~30 at which induction times for nucleation tend to infinite. This sensitivity analysis leads us thus to make a cautionary note about the results of the interfacial free energies: the relatively large error bars precludes any detailed discussion about the implications of the values found in terms of the height of the nucleation barrier.

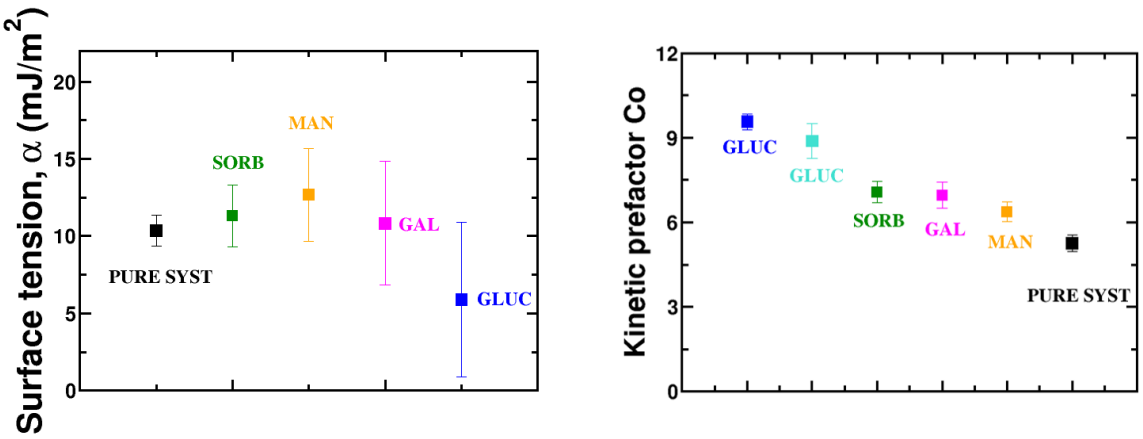

Figure 6. Left: Values of the interfacial free energies, α, obtained for the pure and organic-containing C-S-H systems. Right: Values of the kinetic pre-factor, C_0. The concentration of the organics is 10 mM. The light blue color used for gluconate in the right figure, gives C_0 as obtained for a concentration of 1 mM.

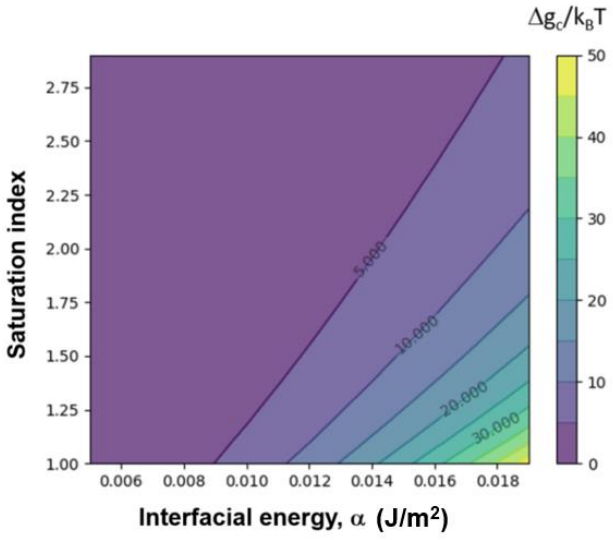

Figure 7. Height of the nucleation barrier (in k_BT units) as a function of the interfacial energy and saturation index of the solution with respect to β-C-S-H.

Physical characterization of the precipitates

Cryo-TEM images of the precipitates formed in the presence of 1mM gluconate and 5mM sorbitol, each imaged at different times during the nucleation process, are shown in Figure 8. Particles show a spherical morphology in all cases, with larger particles (~500 nm – 1 μm) formed in the presence of gluconate. The size of the particles formed in the presence of sorbitol is smaller, ~10-50 nm, similar to the sizes found by Krautwurst et al. for the pure system under identical chemical conditions of solution supersaturation (18). The electron diffraction patterns shown as insets in Figure 8 reveal that the particles formed are amorphous.

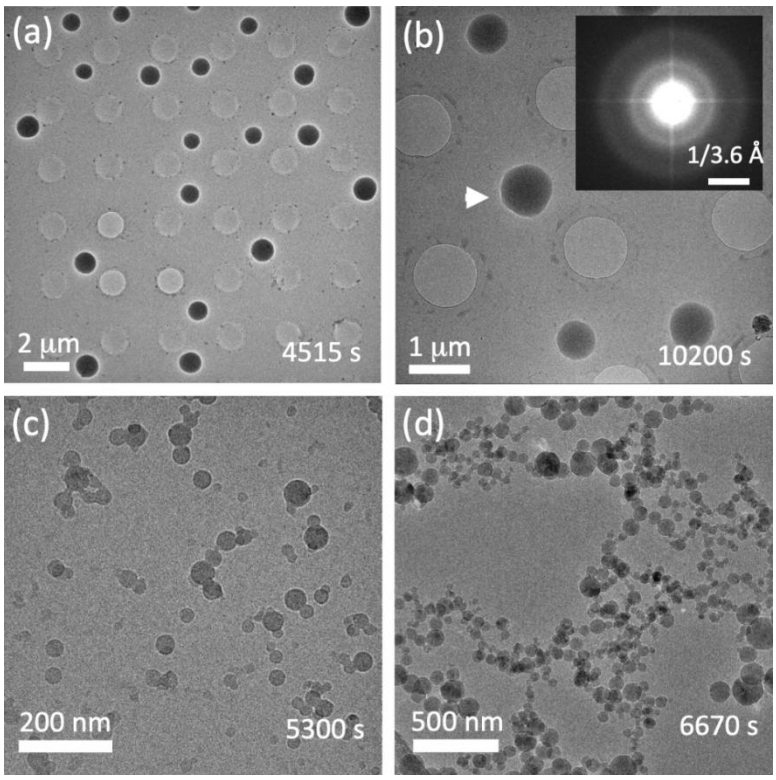

Figure 8. Cryogenic TEM images of the early stages of C-S-H precipitation in the presence of 1mM gluconate (a,b) and 5 mM Sorbitol (c,d). White arrow in (b) indicates the particle that was used for selected area diffraction (SAED) shown in the inset of (b). Times elapsed between the onset of the reaction and the cryo-quenching of an aliquot of the reacting solution.

SAXS data for some selected times are represented in Figure 9. In all cases, an increase of the intensity is observed over time. However, the pure system exhibits a clear induction time, with the intensity increasing only after 10 mins, whereas no induction time is observed for the gluconate-containing systems (see evolution of the SAXS invariant in Figure 9). This is in agreement with the turbidity data shown before, where the formation of the complexes with gluconate induced an

immediate decrease of the transmittance upon mixing of the silicate and gluconate-bearing calcium solutions.

SAXS patterns from the pure system evolve from a particle scattering characteristic of a very polydisperse system (30 mins), with no characteristic form factor, to a system where the intensity distribution follows a q^{-2} dependence, as expected for plate-like systems. It is important to keep in mind that the SAXS is sensitive to density variations, and that these can also take place within the amorphous droplets, which are very hydrated systems. A change of slope is observed at ~$3 \cdot 10^{-1}$ nm^{-1}, which is tentatively ascribed to the thickness of the plates, which would be in the order of 20 nm. However, the polydispersity of the data precludes a detailed analysis of the morphology. It is interesting to observe that the plate-like particles are observed here after ~60 mins. According to Krautwurst et al., the particles are still amorphous at this time. We make here the hypothesis that plate-like atomic arrangements are adopted by silicate molecules and calcium atoms within the amorphous spheroids (identified as silicate dimers by Krautwurst et al.), and that these happen as a preliminary step of the crystallization. The low concentrations used in these experiments made that no signal, at any point, was observed in the wide-angle detector available at the SAXS beamline.

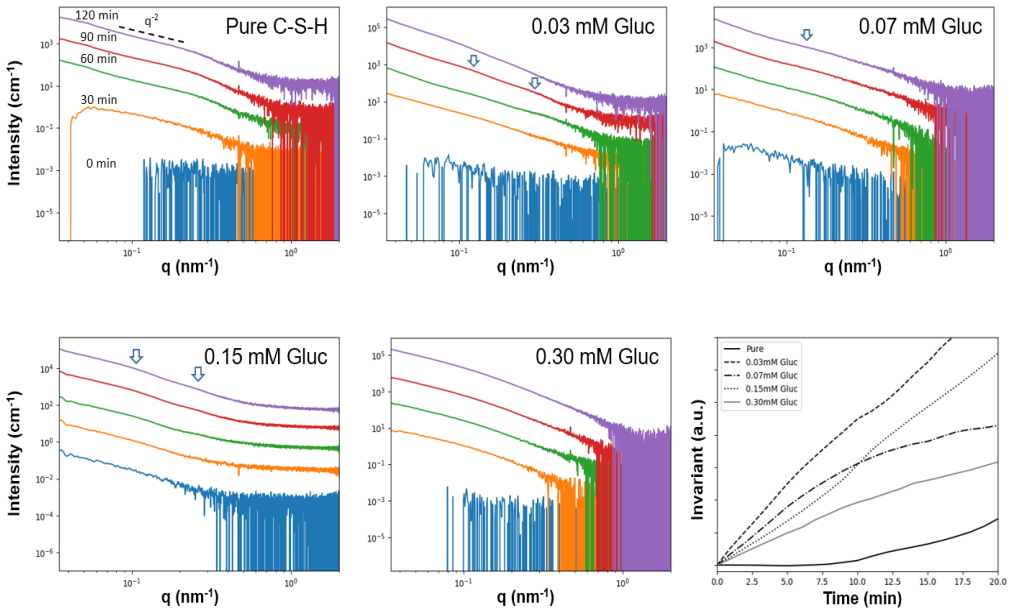

Figure 9. SAXS patterns and evolution of the SAXS invariant over time for the pure and gluconate-bearing systems. The arrows indicate bumps in the intensity coming from particle scattering within the precipitates.

Data from the systems containing gluconate are more complex. Different small bumps (see arrows in Figure 9) are observed that could indicate the presence of particles being aggregated into large networks. Indeed, the low *q* part of the data follow a power law in almost all cases (except for the system with 0.30 mM gluconate), which can be fitted using a $I \propto q^{-n}$ law, as shown in Figure S2. The

results show that the values of the exponent tend towards values higher than 2 in almost all cases, which are typically associated to mass fractals aggregates, tending to surface fractal when the values are higher than 3 (see Figure S2).. The case of the system with 0.30 mM of gluconate is different from the rest: all the data exhibit a certain degree of curvature, which again can be explained by a very polydisperse system with no particular form factor, as it was the case for the early stages (~30 mins) of nucleation of the pure system.

Another observation that is worth mentioning is the fact that the background signal is significantly higher in the system with 0.15 mM gluconate than in the rest. This could point to the presence of very small entities (sub-nm) that could be present in the solution (ion pairs, small complexes..). The nature of these cannot be ascertained from these data. In overall, the cryo-TEM and scattering data further confirm that organics do not alter the mechanism of the nucleation pathway, but rather slow down the different processes taking place en route from dissolved species to the final solid phase.

4. Conclusions

The main conclusions that emerged from this study can be summarized as follows: the precipitation and crystallization step with the characteristic drops of transmittance, already observed by Krautwurst et.al. (18) were confirmed here for the pure C-S-H and they were also found for the systems containing organic molecules. Cryo-TEM observations confirmed that a nucleation pathway through an amorphous precursor takes place also in the presence of gluconate and sorbitol. The analysis of the induction times using classical nucleation theory yields similar values for the interfacial energies, within the uncertainties. This points to similar precursor phases (not chemically different), though the results have to be taken with caution given the large error bars and the sensitivity of the induction times to the value of the interfacial energy. The analysis of the pre-exponential factor, a kinetic factor that includes terms related to the physics of the collisions between clusters formed during the nucleation process, yields an interesting observation: the values of this factor increase from the pure system to the gluconate-containing systems, and are directly proportional to the values of the complexation constants found for each of the organics with the C-S-H phase in a previous study (the paper related to the matter will be submitted to Cement and Concrete Research soon) This observation may suggest that the mechanism by which the organics delay the nucleation is related to their ability to hinder the aggregation of clusters (preventing their aggregation); or that it is related to the organics stabilization of the pre-nucleation clusters of silicate and calcium, slowing down the formation of the metastable amorphous spheroids. This is in line with the report by Krautwurst et al. (18) by which i) the amorphous spheroids are formed and ii) the processes of particle aggregation and C-S-H crystallization are intimately related. SAXS analyses bring a physical perspective about the mesoscale organization of the particles: primary particles

within the amorphous droplets are observed, adopting a plate-like configuration prior to their crystallization of pure C-S-H. This phenomenon is less clear for the organic-bearing systems, where a more complex shape of the curves suggest the formation of primary particles that aggregate forming larger clusters of sizes closer to those observed by cryo-TEM. Finally, cryo-TEM shows the formation of much bigger particles in presence of gluconate, compared to the amorphous droplets of pure C-S-H or of sorbitol-bearing C-S-H. This can be explained by the much higher complexation constant of gluconate (33) than for sorbitol, which would not be affecting the aggregation process at a large extent.

In spite of the interesting observations found here, it is unknown whether the amorphous spheroids are a requirement for C-S-H formation in real cement pastes. Experimental studies highlighted that C-S-H formation can be described as primary heterogeneous nucleation and growth (37) (38) in the real cement conditions. Indeed, given that dislocations, impurities or grain boundaries are already present in the primary materials, the nucleation process could occur more easily close to solid-liquid interfaces. Future experiments addressing this issue –multi-step pathways of heterogeneous nucleation- should be designed to give a more complete view of this complex system.

References

1. Stark, J., Wicht, B. Zement und Kalk: der Baustoff als Werkstoff. Springer-Verlag. 2013.
2. Barret, P., Bertrandie, D. Fundamental hydration kinetic features of the major cement constituents : Ca_3SiO_5 and βCa_2SiO_4. Journal de Chimie Physique, 83, 765-775, 1986.
3. Damidot, D., Nonat, A. Proc. 9th Int. Congr. on the Chemistry of Cement, New Delhi, India, 1992.
4. Paglia, C., Wombacher, F., Böhni, H. The influence of alkali-free and alkaline shotcrete accelerators within cement systems: I. Characterization of the setting behavior. Cement and Concrete Research, 31(6), 913-918, 2001.
5. Brykov, A.S., Vasil'ev, A.S., Mokeev, M.V. Hydration of portland cement in the presence of aluminum-containing setting accelerators. Russian Journal of Applied Chemistry, 86(6), 793-801, 2013.
6. Gołaszewski, J., Szwabowski, J. Influence of superplasticizers on rheological behaviour of fresh cement mortars. Cement and concrete research, 34(2), 235-248, 2004.
7. Mollah, M.Y.A., Adams, W.J., Schennach, R., Cocke, D.L. A review of cement–superplasticizer interactions and their models. Advances in Cement Research, 12(4), 153-161, 2000.
8. Peschard and A., Govin, A., Grosseau, P., Guilhot, P., Guyonnet, R. Effect of polysaccharides on the hydration of cement paste at early ages. Cement and Concrete Research, 34(11), 2153-2158, 2004.
9. Nalet, C., Nonat, A. Ionic complexation and adsorption of small organic molecules on calcium silicate hydrate: Relation with their retarding effect on the hydration of C_3S. Cement and Concrete Research, 89, 97-108, 2016.
10. Young, J.F. A review of the mechanisms of set-retardation in portland cement pastes containing organic admixtures. Cement and Concrete Research, 2(4), 415-433, 1972.
11. Nalet, C., Nonat, A. Retarding effect of organic molecules on tricalcium silicate hydration: relation with their adsorption on calcium silicate hydrates and their ion complexing power, 2015.
12. Peschard, A., Govina, A., Pourchez, J., Fredon, E., Bertrand, L., Maximilien, S., Guilhot, B. Effect of polysaccharides on the hydration of cement suspension. J. Eur. Ceram. Soc, 26, 1439–1445, 2006.

13. Singh, N.B., Singh, S.P., Sarvahi, R. Effect of phenols on the hydration of Portland cement. Adv. Cem. Res, 2(6), 43–48, 1989.
14. Poinot, T., Govin, A., Grosseau, P. Impact of hydroxypropylguars on the early age hydration of Portland cement. Cement Concrete Research, 44, 69–76, 2013.
15. Pourchez, J., Grosseau, P., Ruot, B. Changes in C_3S hydration in the presence of cellulose ethers. Cement Concrete Research, 40, 179–188, 2010.
16. Nalet, C., Nonat, A. Effects of hexitols on the hydration of tricalcium silicate. Cement and Concrete Research, 91, 87-96, 2017.
17. Thomas, N.L., Birchall, J.D. The retarding action of sugars on cement hydration. Cement and Concrete Research, 13(6), 830-842, 1983.
18. Krautwurst, N., Nicoleau, L., Dietzsch, M., Lieberwirth, I., Labbez, C., Fernandez-Martinez, A., Van Driessche, A.E.S. Two-Step Nucleation Process of Calcium Silicate Hydrate, the Nanobrick of cement. Chemistry of Materials, 30(9), 2895-2904, 2018.
19. De Yoreo, J.J., Gilbert, P.U.P.A., Sommerdijk, N.A.J.M., Penn, R.L. Crystallization by particle attachment in synthetic, biogenic, and geologic environments. Science, 349, 6760, 2015.
20. Van Driessche, A., Kellermeier, M., Benning, L.G., Gebauer, D. New Perspectives on Mineral Nucleation and Growth: From Solution Precursors to Solid Materials. Springer International Publishing, 2017.
21. Gebauer, D., Volkel, A. & Colfen, H. Stable prenucleation calcium carbonate clusters. Science 322, 1819–1822, 2008.
22. Dey, A., Bomans, P., Müller, F. et al. The role of prenucleation clusters in surface-induced calcium phosphate crystallization. Nature Mater 9, 1010–1014, 2010.
23. De Yoreo.J. A Perspective on Multistep Pathways of Nucleation. 1-17, 2020.
24. Lutsko, J. F. How Crystals Form: A Theory of Nucleation Pathways. Sci. Adv. 5, eaav7399. 2019
25. Collepardi, M., Monosi, S., Moriconi, G., Pauri, M. Influence of gluconate, lignosulfonate, and glucose admixtures on the hydration of tetracalcium aluminoferrite in the presence of gypsum with or without calcium hydroxide. Journal of American Ceramic Society, 2006.
26. Collepardi, M., Monosi, S., Moriconi, G., Pauri, M. Influence of gluconate, lignosulfonate or glucose on the C_3A hydration in the presence of gypsum with or without lime. Cement and Concrete Research, 14(1),105-112, 1984.
27. Singh, N.B. Effect of gluconates on the hydration of cement. Cement and Concrete Research, 6(4), 455-460, 1976.
28. Mota, B., Matschei, T., Scrivener, K. Impact of sodium gluconate on white cement-slag systems with Na_2SO_4. Cement and Concrete Research, 122, 59-71, 2019.
29. Suhua, M., Weifeng, L., Zhang, S., Dashun, G., Jin, Y., Xiaodong, S. Influence of sodium gluconate on the performance and hydration of Portland cement. Construction and Building Materials, 91, 138–144, 2015.
30. Li, B., Lv, X., Dong, Y., Zhou, S., Zhang, J. Comparison of the retarding mechanisms of sodium gluconate and amino trimethylene phosphonic acid on cement hydration and the influence on cement performance. Construction and Building Materials, 168, 958-965, 2018.
31. Zhang, L., Catalan, L.J., Larsen, A.C., Kinrade, S.D. Effects of sucrose and sorbitol on cement-based stabilization/solidification of toxic metal waste. J Hazard Mater, 151(2-3), 490-8. 2008.
32. Cody, A.M., Lee, H., Cody, R.D., Spry, P.G. The effects of chemical environment on the nucleation, growth, and stability of ettringite $[Ca_3Al(OH)_6]_2(SO_4)_3.26H_2O$. Cement and Concrete Research, 34(5), 869-881, 2004.
33. Bouzouaid, L., Lothenbach, B., Fernandez-Martinez, A., Labbez, C. Portlandite solubility and Ca^{2+} activity in presence of gluconate and hexitols. Cement and Concrete Research, 149, 2021.
34. Kashchiev, D. Nucleation - Basic Theory with Applications Butterworth- Heinemann. 2000.
35. Garrault-Gauffinet, S., Nonat, A. Experimental Investigation of Calcium Silicate Hydrate (C-S-H) Nucleation. J. cryst. growth, 200, 565–574, 1999
36. Nicoleau, L., Van Driessche, A.E.S., Kellermeier, M. A kinetic analysis of the role of polymers in mineral nucleation. The example of gypsum. Cement and Concrete Research, 124, 2019.
37. Gauffinet, S., Finot, E., Nonat, A. Proc. Int. RILEM Workshop. In press, Dijon, 1997.
38. Nonat, A., Lecoq, X., Gauffinet, S. Proc. X Int. Congress on Chemistry of Cement. Göteborg, Suede. 1997.

39. Vekilov, P.G. Nucleation. Crystal Growth and Design. 10(12), 5007-5019, 2010.
40. LaMer, V.K., R.H, Dinegar. Theory, production and mechanism of formation of monodispersed hydrosols. Journal of the American Chemical Society, 72(11), 4847–4854, 1950.
41. LaMer, V.K. Nucleation in phase transitions. Industrial and Engineering Chemistry, 44(6), 1270–1277, 1952.
42. Voorhees, P.W. The theory of Ostwald ripening. Journal of Statistical Physics, 38(1), 231-252, 1985.
43. Gartner, E.M., Gaidis, J.M. Hydration mechanisms, I. In: Skalny, J.P., Ed. Materials Science of Concrete. The American Ceramic Society, Westerville, 95-125, 1989.
44. Thanh, NT., Maclean, N., Mahiddine, S. Mechanisms of nucleation and growth of nanoparticles in solution. Chem Rev, 114(15), 7610-30, 2014.
45. Barthel, J., Jaenicke, R. Conway: Ionic Hydration in Chemistry and Biophysics: Studies in Physical and Theoretical Chemistry. Elsevier Scientific Publishing Company, 86(3), 264-264, Amsterdam and New York, 1982.
46. Ostwald, W. Studien über die Bildung und Umwandlung fester Körper.1. Abhandlung: Übersättigung und Überkaltung. Z. Phys. Chem, 22, 289-330, 1897.

CHAPTER IV. DISCUSSION

1. Retarding power of organic molecules on the C-S-H nucleation: relation with their ionic complexation in solution and their retarding power on the C_3S hydration

The study of nucleation of C-S-H in the presence of the hexitols and gluconate presented in paper 3 have shown that these organics molecules increase significantly the induction time of nucleation. Thanks to the speciation model developed in papers 1 and 2, the saturation index and thus the driving force for the nucleation could be determined. The analysis of those results within the framework of the classical nucleation theory revealed that the organic molecules primarily affects the kinetic prefactor, C_0. That is the rate of attachment/detachment of the C-S-H constitutive ions to the C-S-H nuclei. Figure 1 compares the retarding power of the organic molecules on the C-S-H nucleation at an organic concentration of 10 mM, expressed as C_0^m/C_0^0, where C_0^m and C_0^0 are the kinetic prefactor in presence and in absence of molecules, respectively.

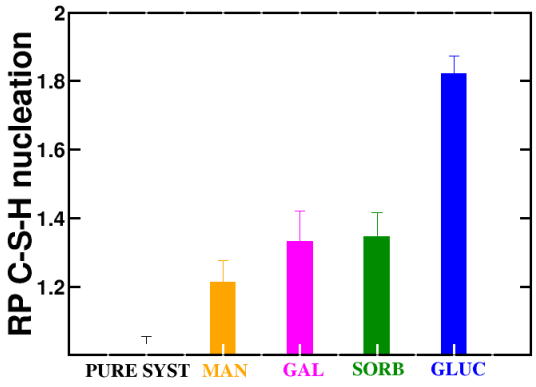

Figure 1 Retarding power of the organic molecules (RP) on the C-S-H nucleation, expressed as the ratio of the kinetic prefactor in the presence of organics (c_{org} = 10 mM) to the kinetic prefactor of the reference system (without organics).

As shown in Figure 1, the charged gluconate molecule retards nucleation the most. However, the neutral hexitols (D-mannitol, D-galactitol and D-glucitol) also induce a retardation of the C-S-H nucleation, which differs depending on the stereochemistry of their hydroxyl groups. Thus, the retarding power of organics on the C-S-H nucleation is not only a function of its charge but also varies according to the stereochemistry of its hydroxyl groups.

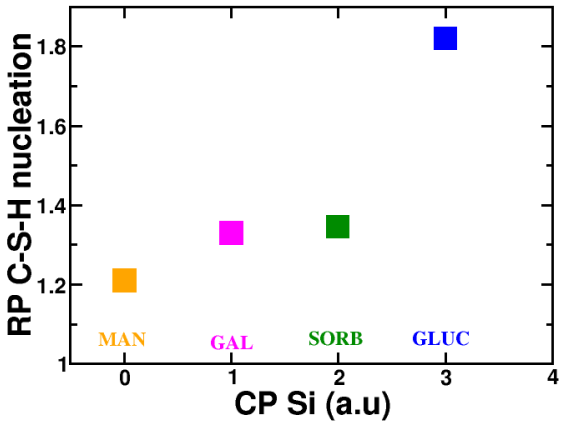

Figure 2: retarding power of the molecules (RP) on the C-S-H nucleation(C_0^m/C_0^0) as a function of the complexation power of the molecules with silicates

In paper 1 and 2, we observed that theses molecules retarding the C-S-H nucleation form complexes with calcium ions. Although gluconate is the molecule that retards nucleation the most and is observed to form the strongest complex with calcium ions, a simple rule relating the complexing power of the molecules with calcium ions and their power to retard the nucleation could not be established. Indeed, the complexing power of mannitol with calcium is superior to galactitol, however its retarding power is much lower than this last molecule. On the other hand, the organic molecules were also found to complex with silicates. Figure 2 seems to show that a correlation exists between the complexing power of the molecules with the silicates and their retarding power on nucleation. However, the retarding power of the molecules to the C-S-H nucleation is not only a function of their complexation power with the silicates. Indeed, mannitol induces a delay of the nucleation despite its very weak complexation with silicates. Moreover, the detailed analyses of the organic-ions complexes performed in paper 2 have shown that the complexation of silicates by the organics only occurs in concomitance with that of calcium ions and at high pH, through the formation of hetero-polynuclear organic complexes. In other words the complexation of the organics with calcium seems to act in a synergistic manner with the complexation of silicates by the organics on the retardation of the C-S-H nucleation.

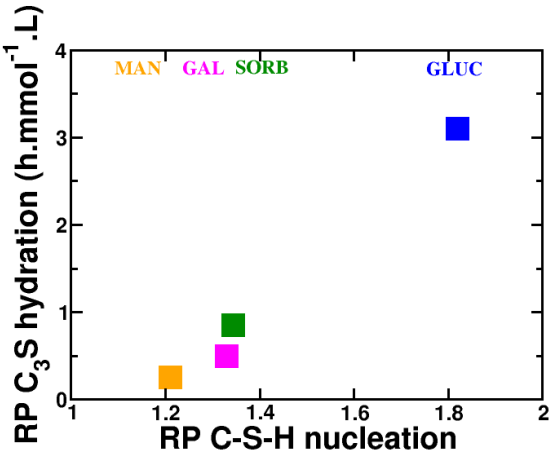

Figure 3: Retarding power of the molecules (RP) on the C_3S hydration as determined by Nalet (Chapter 1 Fig. 21) as a function of the retarding power of the molecules on the C-S-H nucleation

We were also able to confirm in papers 1 and 2 the relationship established by Nalet (1) that exists between the adsorption of organic molecules on the C-S-H and their complexation strength with calcium ions. The organic adsorption was found to increase with the complexing power of the molecules with Ca^{2+}. On the other hand, the complexation of the organic molecules with silicates does not seem to influence their adsorption. Thus, the retarding power of the organic molecules does not seem to be directly linked to their adsorption as it had been supposed previously by some authors (2) (3)

A new hypothesis can be formulated based on the observations at the very early stages of nucleation described in paper 3, the analysis of the complexes obtained in paper 2 and the pre-nucleation silicate clusters identified in the study by Krautwurst et al of the homogeneous nucleation of C-S-H in the pure system (4). Let us recall some of the results of these papers before to formulate this new hypothesis. In the paper of Krautwurst et al, the formation of silicate dimers surrounded by calcium ions, of the form $Si_2O_7^{6-}$ + 3 Ca^{2+}, were identified. These silicate dimers were further interpreted as the primitive C-S-H bricks responsible for the formation of the amorphous spheroids which eventually result in the formation of the final C-S-H crystal. In paper 2, the organics were found to form hetero-polynuclear complex involving also *two* silicates: that is $Ca_3Gluc_2(H_3SiO_4)_2(OH)_2^0$, $Ca_3Hex_2(H_3SiO_4)_2(OH)_2^0$ and $Ca_2Hex_2(H_2SiO_4)(OH)_4^{2-}$. These results thus lead us to make the hypothesis that the retarding power of the molecules on the C-S-H nucleation may be due to the stabilization of the silicate dimers in solution or the hindered formation of the same by the organics. The added effect of the Ca^{2+} complexation by the organics on the C-S-H nucleation can also be understood within the framework of this hypothesis. Indeed, the Ca^{2+} complexation would weaken the attractive correlation forces (mediated by the free Ca^{2+} ions) required for the formation of the

metastable C-S-H amorphous spheroids. In other words, the Ca^{2+} complexation by the organics would further stabilize the silicate dimers.

In all cases, the speciation of silicates in equilibrium solutions and in supersaturated conditions with respect to C-S-H appears to be a key parameter in the understanding of the nucleation of C-S-H in the presence but also in the absence of organic molecules. It would be interesting to use spectroscopic methods such as solid state NMR. In particular, the dynamic nuclear polarization technique, which allows, thanks to the principle of transferring the polarization from the electron spin to the nucleus, to overcome the low sensitivity of the NMR technique, would be a method particularly suitable.

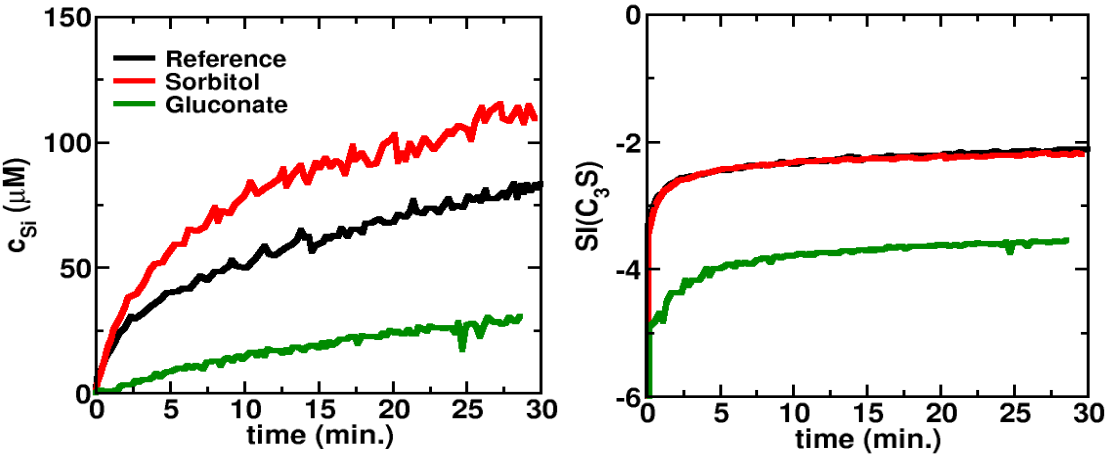

Figure 4. Comparison of the time evolution of (left) the silicon concentration and (right) the saturation index (SI) of C_3S during the pure dissolution of a C_3S grain dispersion (L/S = 10 000) in presence and in absence of organics. The solution always contains 11 mM of $Ca(OH)_2$. The organic concentration is 7.5 mM. The SI values were calculated from the ion concentrations with the speciation model developed in papers 1 and 2. The experimental data are from Nalet et al (1). The ion concentrations were measured in-situ with an ICP-AES.

The combination of the results of papers 1, 2 and 3 also showed the importance of the nucleation of C-S-H on the delay of the hydration of C_3S in the presence of organic molecules. This is illustrated in Figure 3, which shows the clear relationship between the retardation of the C_3S hydration and that of the nucleation of C-S-H induced by the various organic molecules. However, the role of the molecules on the dissolution of C_3S on the retarding effect of its hydration has to be considered. Indeed, if the hexitols have only a very limited effect on the dissolution of C_3S, this is not the case for gluconate. This becomes evident when one compares the evolution of the C_3S saturation index over time in the presence of gluconate and in the reference system. This is shown in Figure 4, where the speciation model developed in papers 1 and 2 is used to calculate the SI of C_3S from the pure dissolution measurements of C_3S performed by C. Nalet (5). Thus in the case of gluconate both the

slow down of the precipitation and the dissolution processes participates to the retardation of the C_3S hydration.

2. Impact of the retarding molecules on the pre-nucleation / nucleation process of C-S-H: comparison with the CH nucleation and implication for C_3S hydration

The influence of the gluconate and the neutral sugars alcohols on the prenucleation/ nucleation of C-S-H has been addressed in paper 3, and showed a clear influence of the organic molecules on the C-S-H precipitation. The monitoring of the C-S-H pure system precipitation via turbidity measurement showed two mains drops characteristics of the two steps nucleation mechanisms elucidated by Krautwurst et al (4).

The first drop is associated to the formation of amorphous spheroids. The second drops corresponds to the aggregation of these spheroids and the simultaneous crystallization of the calcium silicate hydrate particles. In the case of neutral molecules, this non-classical nucleation pathway was maintained, while in the presence of gluconate no second drop was observed, not even after days.

Moreover, the addition of the organic molecules in the C-S-H system interestingly showed a non activated phenomenon (contrary to nucleation) that occurred at the very beginning of the experiments, and more pronounced with gluconate: an immediate decrease in the optical transmittance. This behavior was interpreted as being due to the formation of complexes or, more probably, complex clusters between the organics and the calcium, hydroxide and silicate ions and could lead to a different nucleation pathway. The latter assumption was supported by SAXS results that highlighted a different shape and size of the nanoparticles, where the nuclei formed are more dispersed in presence of the organics, compared to the pure C-S-H. Also cryo-TEM revealed the formation of much bigger metastable C-S-H amorphous spheroids in presence of gluconate, as compared to the pure C-S-H system. Whatever it is, the very early increase of the turbidity associated with the formation of those clusters of organic-ions complexes as well as the marked increase in size of the metastable C-S-H amorphous spheroids in the presence of gluconate are indicators for the hypothesis proposed in the last section to explain the observed slow down of the nucleation rate of C-S-H.

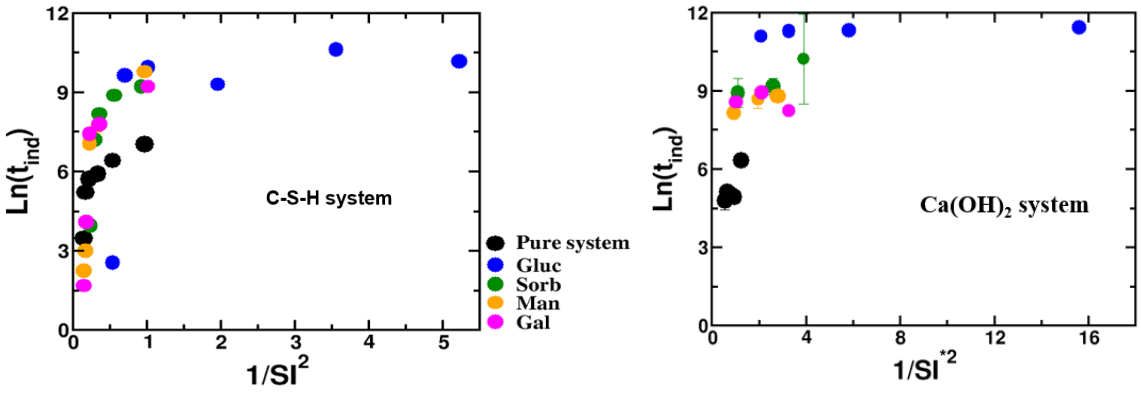

Figure 5. Logarithm of the induction time as a function of the saturation index ($1/SI^2$) for the pure system (black) and in presence of gluconate (blue), sorbitol (green), mannitol (orange) and galactitol (pink). Left figure corresponds to the C-S-H system, the right figure corresponds to the $Ca(OH)_2$ system. The organic concentration was 10 mM. The saturation index was calculated using the speciation software PHREEQC, taking into account the condition of the different precipitation experiments, including components concentrations and temperature, but also the complexes existing between calcium, hydroxide, silicate and the organic molecules.

Some authors, e.g. (6), hypothesized that the retardation of the C_3S hydration induced by retarders could be explained by the slow down of the nucleation of portlandite. Similar to the precipitation of C-S-H, the rate of formation of portlandite can indeed cause a slowing down or acceleration of the dissolution of C_3S.

The induction time of portlandite nucleation in presence of the organics was thus also measured. The results obtained are presented in Figure 5 and compared with those obtained for C-S-H with the same organic molecules at the same concentration. The induction time at which portlandite starts to nucleate is also delayed in the presence of the organics. The general trend is similar to that obtained with C-S-H, although no clear difference between the hexitols could be observed. This suggests that portlandite nucleation is probably not the main factor for the observed retardation of C_3S hydration in the presence of the hexitols. In the case of gluconate, the marked slowing down of portlandite nucleation indicates, on the other hand, that the hindered precipitation of portlandite may also contribute to the retardation of C_3S hydration.

Clearly, these preliminary results will require further measurements to elucidate both the reaction path of portlandite nucleation and its role in cement hydration in the presence of retarders. However, it may be noted that previous studies conducted in our laboratory on pure C_3S systems under controlled conditions have shown that the end of the dormant period of the hydration is not caused by the formation of portlandite, c.f. (7) (8).

References

1. Nalet, C. Influence de la stéréochimie et de la fonctionnalité de molécules organiques sur l'hydratation de composés cimentaires. Thèse de doctorat, université de Bourgogne, 2015.
2. Nalet, C., Nonat, A. Ionic complexation and adsorption of small organic molecules on calcium silicate hydrate: Relation with their retarding effect on the hydration of C_3S. Cement and Concrete Research, 87, 97-104, 2016.
3. Pourchez, J.et.al. Changes in C3S hydration in presence of cellulose ethers. Cement and Concrete Research, 40. 179-188, 2010.
4. Krautwurst, N.et.al. Two-Step Nucleation Process of Calcium Silicate Hydrate, the Nanobrick of Cement. Chemistry of Materials, 2018.
5. Nalet, C., Nonat, A. Effects of hexitols on the hydration of tricalcium silicate. Cement and Concrete Research, 91, 87-96, 2017.
6. Juilland, P., Gallucci, E. Hindered calcium hydroxide nucleation and growth as mechanism 495 responsible for tricalcium silicate retardation in presence of sucrose. 329, 143-154, 2018.
7. Damidot, D. Etude de l'hydratation du silicate tricalcique en suspension diluée par microcalorimétrie isotherme. Thèse de doctorat, Université de Bourgogne, 1990.
8. Garrault, S. and Nonat, A. Hydrated Layer Formation on Tricalcium and Dicalcium Silicate Surfaces : Experimental Study and Numerical Simulations. Langmuir, 17, 8131–8138, 2001.

CHAPTER V. CONCLUSION

The goal of this thesis was to understand how organic molecules can impact the hydration of cementitious compounds, and more precisely how they can affect the nucleation of C-S-H and portlandite. The selected molecules were organic components, neutral and negatively charged, i.e. hexitols and gluconate. Their interactions with the ions composing C-S-H have been highlighted and linked to their delaying effect, while their impact on the nucleation-precipitation of C-S-H occurring during hydration of the anhydrous compounds was also studied in the presence of these organic molecules.

The retarding effect of these molecules was quantified and correlated with the strength of complexes formed with calcium and silicon thanks to the development and application of a speciation model of the organic containing aqueous phases. The adsorption isotherms of the organics molecules on portlandite and C-S-H were determined and further compared to the strength of organic-ions complexes. The strength of complex formation with calcium decreases in the order gluconate >> sorbitol > mannitol > galactitol, which follows the same order as sorption on portlandite and C-S-H. The organic molecules were also shown to form polynuclear complexes with silicates, calcium and hydroxide ions in the typical conditions of the cement pore solution, i.e. high pH and calcium content. The strength of complexation with both calcium and silicon decreases from gluconate > sorbitol > galactitol, while for mannitol no significant formation of organic-calcium-silicon complexes was observed. In addition, a stronger complex formation was observed at higher pH values and in the presence of more calcium.

The presence of hexitols and gluconate increased the time and the maximum heat flow during the hydration of C_3S (which includes both dissolution and precipitation processes) in the decreasing order gluconate >> sorbitol > galactitol > mannitol. The complexation strength with Ca (and organic affinity with portlandite and C-S-H) cannot fully explained this sequence. This is particularly true for the hexitols for which galactitol was observed to retard more the C_3S hydration than mannitol while complexing less calcium.

The induction time of nucleation for both C-S-H and portlandite was measured in the presence and in absence of the organic molecules. The presence of gluconate and hexitols was observed to increase the induction time of C-S-H, following the same sequence as that observed for the C_3S hydration.

They were not only found to prolong the induction time, but also seems to modify the pathways of the nucleation process. In particular, SAXS revealed different shape and size of the nanoparticles, where the nuclei formed are more dispersed in presence of the organics, compared to the pure C-S-H. In addition, cryo-TEM showed the formation of much bigger particles in presence of gluconate,

compared to C-S-H without any organic. The organic also prolonged the induction time for portlandite precipitation, but the effect of the hexitols could not be distinguished.

The analysis of the induction time by the classical nucleation theory showed no strong effect of the organic on the surface tension and thus little effect on the interfacial properties of the C-S-H nuclei, but a clear impact on the kinetic prefactor.

The strength of organics to form complexes containing silicates seems to be closely related to their ability to increase the kinetic prefactor.

The results thus highlight that sorption of these organics on C-S-H and portlandite is closely related to their ability to form Ca-complexes, while nucleation in contrast depends on the ability of the organics to form ternary or quaternary complexes with silicon and calcium.

It can be speculated that the ability to form ternary or quaternary complexes with silicon will lead to an increased presence in the forming nuclei which hinder the formation of the complex structure of C-S-H nuclei, although the underlying processes are not yet completely understood and will have to be unfolded in future studies. The effect of the stereo chemical arrangement of the functional organic groups on their ability to form complexes and to interact with the nucleation of C-S-H and portlandite could be further elucidated based on molecular modelling studies. The present study concentrated on a few molecules with relatively similar structure. An extension of such investigations to different classes of organic molecules with different sizes, with different functional groups and different structural arrangement will be fundamental to generalize the knowledge gained in the present study.

ANNEXES

A. $Ca(OH)_2$ solubility and Ca^{2+} activity in presence of gluconate and hexitols

1- Solubility experiments

Table S1 : Composition of the equilibrium solutions of the experiments of portlandite solubility in the presence of organics . Experimental data were recorded after 4 weeks of equilibration at 23°C. Experiments was repeated twice, corresponding to the grey and white tables. The organic concentrations have been measured by TOC and calcium concentration by ICP-OES.

[gluconate] mM	[Calcium] mM	[gluconate] mM	[Calcium] mM	[gluconate] mM	[Calcium] mM
0.0	22.8	0,0	23.9	0	21.2
33.7	50.0	10.4	26.8	3.1	23.3
68.9	89.0	25.4	40.1	7.8	27.2
110.0	138.3	41.5	56.11	16.9	40.2
149.4	182.9	57.3	75.2	25.1	58.2
191.8	235.7	71.2	97.5	36.9	62.4
		93.2	128.6	47.4	75.6
		113.3	154.7	52.7	81.8
		133.3	179.2	68.3	101.4
		158.9	216.1		
		182.5	248.0		

[sorbitol] mM	[Calcium] mM	pH	[sorbitol] mM	[Calcium] mM	pH
0.0	23.8	12.5	2.6	22.2	12.7
35.7	29.0	12.6	42.2	27.7	12.8
77.3	33.8	12.7	85.5	33.2	12.8
115.0	39.0	12.7	122.0	38.1	12.7
146.1	46.5	12.6	159.2	45.7	12.7
207.67	54.9	12.6	205.3	55.4	12.7

[mannitol] mM	[Calcium] mM	pH	[mannitol] mM	[Calcium] mM	pH
0.0	23.3	12.6	2.4	22.2	12.7
36.7	28.7	12.6	42.8	26.9	12.7
93.8	31.9	12.7	85.2	30.6	12.6
136.9	35.8	12.7	126.7	34.4	12.7
149.2	39.1	12.7	165.9	37.8	12.7
191.0	42.8	12.7	206.1	42.1	12.7

[galactitol] mM	[Calcium] mM	pH	[galactitol] mM	[Calcium] mM	pH
0.0	23.9	12.6	1.8	24.3	12.7
34.2	28.9	12.7	46.8	26.4	12.7
87.2	32.2	12.7	86.4	30.2	12.7
90.8	32.7	12.7	110.3	31.3	12.7
96.5	31.2	12.7	110.9	30.7	12.7
98.3	31.6	12.7	145.4	31.7	12.6

2- Organic adsorption

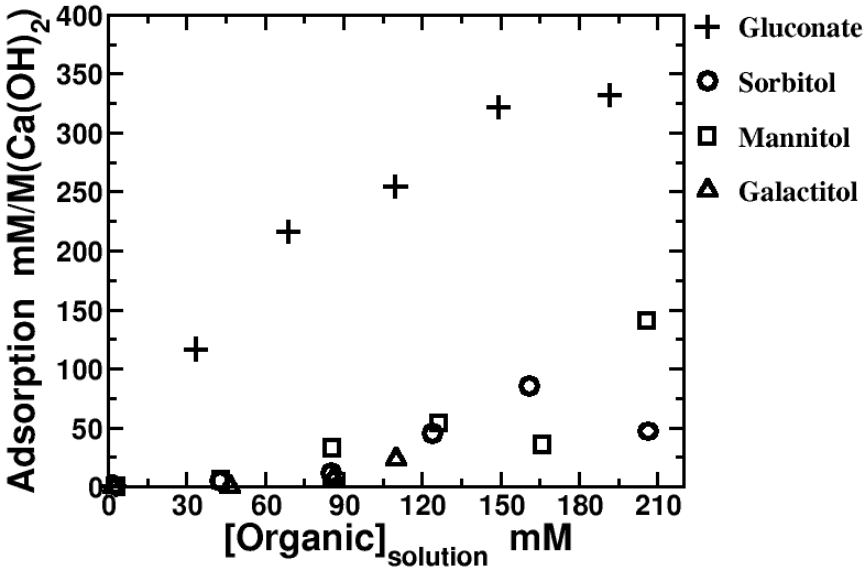

Figure S1 : Adsorption isotherm of gluconate (black crosses), sorbitol (black circles), mannitol (black squares) and galactitol (black triangles) on calcium hydroxide ($Ca(OH)_2$). The increase of the adsorption with the concentration is observed to follow a typical Langmuir isotherm. The hexitols (sorbitol, galactitol and mannitol) are observed to adsorb much less than gluconate.

3- Titrations

Table S2 Initial condition used in PHREEQC to simulate the titration experiments with gluconate, sorbitol, mannitol and galactitol at pH 13.0.

Solution 1	Potassium gluconate	Sorbitol	Mannitol	Galactitol
Temperature (°C)	25	25	25	25
pH	7 charge	7 charge	7 charge	7 charge
Density (kg/L)	1	1	1	1
Ca (mol/kg H_2O)	0.00025	0.00025	0.00025	0.00025
K (mol/kg H_2O)	0.2500	0.2500	0.2500	0.2500
NO3 (mol/kg H_2O)	0.1005	0.1005	0.1005	0.1005
Water (kg)	0.1	0.1	0.1	0.1
Solution 2	Potassium gluconate	Sorbitol	Mannitol	Galactitol
Temperature (°C)	25	25	25	25
pH	7 charge	7 charge	7 charge	7 charge
pe	4	4	4	4
redox	pe	pe	pe	pe
density(kg/L)	1	1	1	1
K (mol/kg H_2O)	0.2	--	--	--
Organic molecule (mol/kg H_2O)	0.2	0.2	0.2	0.2
Water (kg)	0.1	0.1	0.1	0.1

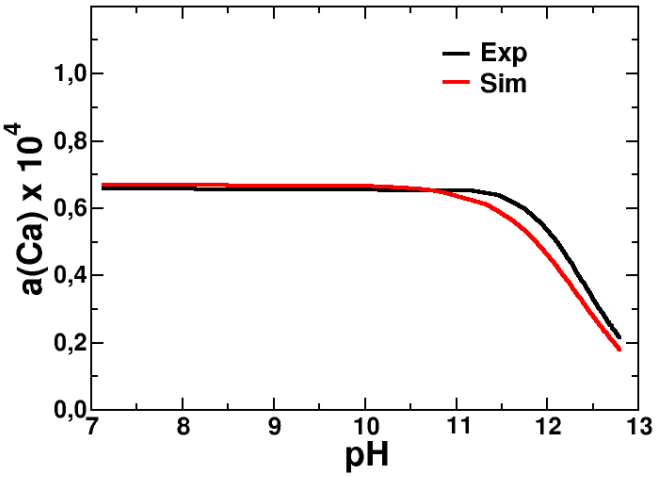

Figure S2.A: Ca^{2+} activity in a solution containing 0.25mM $Ca(NO_3)_2$, 20mM gluconate, KNO_3 at 100mM as the background electrolyte and increasing amount of 1 M KOH solution.

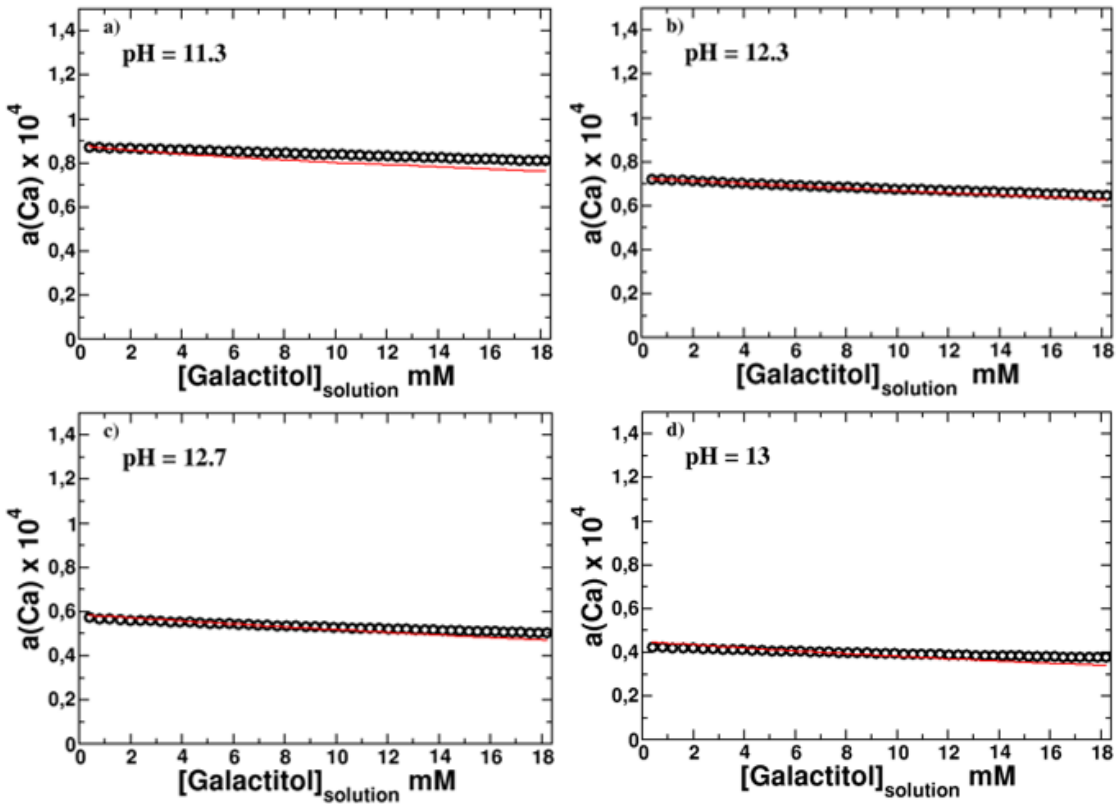

Figure S2.B: Ca^{2+} activities, a(Ca), in mM in a solution containing 0.25 mM $Ca(NO_3)_2$ and increasing amounts of 0.2 M galactitol solution at pH a) 11.3, b) 12.3, c) 12.7 and d) 13.0. The experimental points are shown by the empty circles. The red solid lines give the modeled calcium activity , based on the data compiled in Table 2.

B. C-S-H solubility in presence of gluconate and hexitols

1- Solubility experiments

Table 1.A : Composition of the equilibrium solutions of the experiments of C-S-H solubility in the presence of gluconate, sorbitol, mannitol and galactitol. Experimental data were recorded after 4 weeks of equilibration at 23°C. The organic concentrations have been measured by TOC, calcium and silicate concentration by ICP-OES.

$[CaO]_{initial}$ = 0 mM, equilibrium Ca/Si in C-S-H = 0.75

[gluconate] mM	**[Calcium] mM**	**[Silicate] mM**	**pH**
0.00	0.63	1.12	-
9.32	0.8	1.38	-
29.36	1.13	1.85	-
59.86	1.41	2.28	-
79.29	1.73	2.66	-
100.12	1.79	2.7	-
130.66	2.36	3.47	-
140.32	2.14	3.13	-
177.18	2.52	3.35	-
191.59	2.57	3.26	-
[sorbitol] mM	**[Calcium] mM**	**[Silicate] mM**	**pH**
0.92	0.85	1.39	10.61
39.49	0.85	1.33	10.6
75.36	0.8	1.49	10.55
116.94	0.95	1.57	10.49
161.81	1.02	1.65	10.48
200.49	1.03	1.74	10.48
[mannitol] mM	**[Calcium] mM**	**[Silicate] mM**	**pH**
0.89	0.79	1.54	10.59
39.41	0.81	1.55	10.51
79.10	0.83	1.52	10.48
115.49	0.9	1.56	10.48

217.29	0.89	1.45	10.49
[galactitol] mM	**[Calcium] mM**	**[Silicate] mM**	**pH**
0.94	0.84	1.51	10.69
41.77	0.92	1.38	10.7
84.05	0.95	1.43	10.72
117.05	0.93	1.46	10.72
155.94	1.04	1.48	10.72
$[CaO]_{initial}$ = 11 mM, equilibrium Ca/Si in C-S-H = 1.1			
[gluconate] mM	**[Calcium] mM**	**[Silicate] mM**	**pH**
0.00	6.73	0.03	-
9.93	7.82	0.15	-
28.46	8.32	0.4	-
60.70	9.33	0.71	-
78.24	9.6	1.03	-
98.88	10.09	1.05	-
126.94	10.89	1.51	-
152.58	11.09	1.73	-
177.58	11.69	2.01	-
195.17	11.97	2.3	-
[sorbitol] mM	**[Calcium] mM**	**[Silicate] mM**	**pH**
1.01	6.43	0.04	12.05
39.91	6.83	0.03	12.03
81.68	7.06	0.06	12
106.60	7.29	0.13	11.98
144.72	7.3	0.23	11.93
195.28	7.27	0.37	11.91
[mannitol] mM	**[Calcium] mM**	**[Silicate] mM**	**pH**
1.13	6.88	0.03	12.09
39.38	6.62	0.03	12.07
79.62	6.84	0.03	12.04
124.41	6.51	0.03	12.01
158.78	6.48	0.04	11.95
187.78	7.06	0.04	11.92

[galactitol] mM	[Calcium] mM	[Silicate] mM	pH
0.86	5.64	0.02	12.09
40.90	5.98	0.03	12.05
83.92	5.95	0.03	12.03
118.06	6.14	0.04	11.99
161.74	6.05	0.04	11.96
189.79	6.14	0.05	11.92

$[CaO]_{initial}$ = 20 mM, equilibrium Ca/Si in C-S-H = 1.3

[gluconate] mM	[Calcium] mM	[Silicate] mM	pH
0.00	13.3	0.02	-
7.99	13.2	0.07	-
50.33	14.2	0.33	-
77.22	14.6	0.54	-
95.83	15.6	0.86	-
123.33	17.7	1.31	-
141.11	18.6	1.46	-
174.44	19.5	1.65	-
175.89	19.8	1.72	-
[sorbitol] mM	**[Calcium] mM**	**[Silicate] mM**	**pH**
1.00	13.29	0.01	12.4
38.23	12.9	0.02	12.36
74.38	13.18	0.05	12.32
117.95	13.56	0.12	12.27
148.72	14.58	0.25	12.23
189.58	14.41	0.4	12.19
[mannitol] mM	**[Calcium] mM**	**[Silicate] mM**	**pH**
1.04	12.71	0.01	12.4
42.51	13.04	0.01	12.32
74.91	13.04	0.01	12.29
113.61	12.9	0.01	12.26
154.17	13.18	0.02	12.23
179.65	13.29	0.02	12.2

[galactitol] mM	[Calcium] mM	[Silicate] mM	pH
0.00	11.08	0.01	12.4
35.44	11.51	0.01	12.37
80.00	11.69	0.02	12.32
120.00	11.4	0.03	12.3
155.56	11.35	0.03	12.26
184.38	11.32	0.04	12.25

Buffered with portlandite, equilibrium Ca/Si in C-S-H = 1.5

[sorbitol] mM	[Calcium] mM	[Silicate] mM	pH
0	23.24	0	12.62
11.74	24.09	0.01	12.59
47.03	26.14	0.01	12.58
93.77	32.16	0.03	12.59
140.20	35.5	0.12	12.59
187.01	42.83	0.32	12.56
[mannitol] mM	**[Calcium] mM**	**[Silicate] mM**	**pH**
0	22.51	0	12.61
12.36	24.27	0	12.58
48.90	26.72	0	12.58
98.37	32.03	0	12.58
143.36	34.91	0	12.56
195.00	37.55	0	12.55
[galactitol] mM	**[Calcium] mM**	**[Silicate] mM**	**pH**
0	22.96	0	12.62
9.46	21.6	0	12.58
47.09	26.98	0	12.58
96.19	29.56	0.01	12.57
136.48	30.61	0.01	12.52
186.79	25.83	0.03	12.46

Table 1.B : Isotherm adsorption values of the experiments of C-S-H solubility in the presence of gluconate, sorbitol, mannitol and galactitol. Experimental data were recorded after 4 weeks of equilibration at 23°C. The organic concentrations have been measured by TOC. calcium and silicate concentration by ICP-OES.

$[CaO]_{initial}$ = 11 mM, equilibrium Ca/Si in C-S-H = 1.1

[gluconate] mM	**Org/Si**
0	0
5.53	0.05
30.29	0.18
72.21	0.23
117.75	0.17
170.36	0.04
[sorbitol] mM	**Org/Si**
0	0
11.23	0.01
46.70	0.03
91.75	0.1
139.84	0.13
191.47	0.04
[mannitol] mM	**Org/Si**
0	0
11.48	0.01
45.91	0.03
94.037	0.02
142.46	0.04
187.91	0.03

Buffered with Portlandite, equilibrium Ca/Si in C-S-H = 1.5

[gluconate] mM	**Org/Si**
0	0
2.11	0.09
18.01	0.39
44.29	0.64
76.67	0.75
109.32	0.79

[sorbitol] mM	Org/Si
0	0
7.37	0.01
37.88	0.04
77.50	0.08
115.00	0.11
154.50	0.14
[galactitol] mM	**Org/Si**
0	0
7.19	0.01
38.92	0.04
76.77	0.08
115.18	0.12
144.81	0.14
[mannitol] mM	**Org/Si**
0	0
4.58	0
33.87	0.45
75.56	0.09
120.93	0.11
162.99	0.16

Portlandite only

[gluconate] mM	Org/$Ca(OH)_2$
1.47	0
33.73	0.12
68.94	0.22
109.95	0.25
149.39	0.32
191.78	0.33
[sorbitol] mM	**Org/$Ca(OH)_2$**
2.89	0
42.84	0.05

85.41	0.01
124.00	0.05
160.98	0.09
206.52	0.05
[galactitol] mM	**Org/Ca(OH)$_2$**
2.10	0
46.60	0
86.31	0.01
110.36	0.02
[mannitol] mM	**Org/Ca(OH)$_2$**
2.98	0
43.05	0.01
85.56	0.03
126.39	0.05
165.98	0.04
205.77	0.14

2-Modeling of C-S-H solubility in presence of galactitol

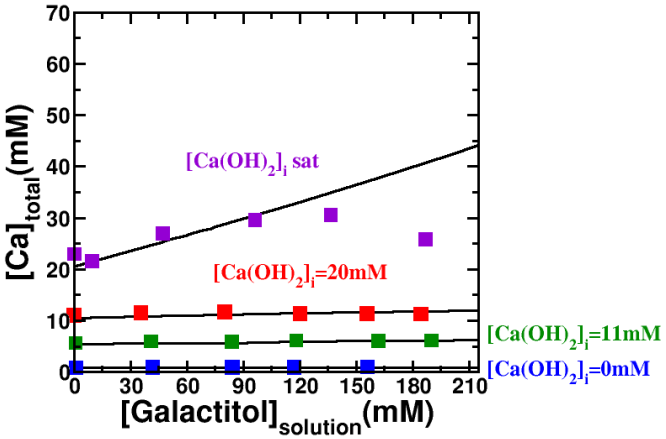

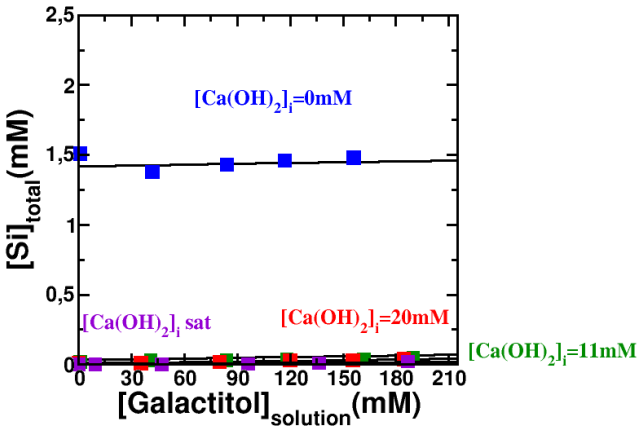

Figure 1.A: Total experimental (symbols) and simulated (lines) concentrations of aqueous calcium and silicate species at equilibrium with C-S-H (C/S 0.75) immersed in 250 mL of solution containing various initial concentrations of $Ca(OH)_2$, $[Ca(OH)_2]_i$, and varying the equilibrium concentration of galactitol.

C. Impact of gluconate and hexitol additives on the precipitation mechanism and kinetics of C-S-H

Table S1.A. Concentrations of the different complexes formed in the supersaturated solutions, obtained from the PHREEQC simulations, using a gluconate concentration of 10mM. The concentration of calcium was fixed at 15mM. Silicate concentration values were fixed at 0.08mM, 0.10mM, 0.15mM and 0.20mM.

pH	Gl	Ca	Si	Ca^{2+}	$CaOH^{+}$	GlCaOH	$Gl_2Ca_2OH_2^{2-}$	$Gl_2Ca_3(OH)_4$	$CaGl^{+}$	$Ca_3Gl_2(H_3SiO_4)_2(OH)_2$
12.63	10	15	0.08	6.09	1.62	1.81	0.05	0.00	0.26	0.01
pH	Gl	Ca	Si	Ca^{2+}	$CaOH^{+}$	GlCaOH	$Gl_2Ca_2OH_2^{2-}$	$Gl_2Ca_3(OH)_4$	$CaGl^{+}$	$Ca_3Gl_2(H_3SiO_4)_2(OH)_2$
12.63	10	15	0.10	6.08	1.62	1.81	0.05	0.00	0.26	0.02
pH	Gl	Ca	Si	Ca^{2+}	$CaOH^{+}$	GlCaOH	$Gl_2Ca_2OH_2^{2-}$	$Gl_2Ca_3(OH)_4$	$CaGl^{+}$	$Ca_3Gl_2(H_3SiO_4)_2(OH)_2$
12.63	10	15	0.15	6.07	1.62	1.81	0.05	0.00	0.26	0.03
pH	Gl	Ca	Si	Ca^{2+}	$CaOH^{+}$	GlCaOH	$Gl_2Ca_2OH_2^{2-}$	$Gl_2Ca_3(OH)_4$	$CaGl^{+}$	$Ca_3Gl_2(H_3SiO_4)_2(OH)_2$
12.63	10	15	0.20	6.06	1.61	1.80	0.05	0.00	0.26	0.05

Table S1.B Concentrations of the different complexes formed in the supersaturated solutions, obtained from the PHREEQC simulations. Simulations include experiments with sorbitol and sodium gluconate at a fixed concentration of 10mM. Calcium and silicate concentration values were fixed at 15mM and 0.15mM respectively.

pH	Sorb	Ca	Si	Ca^{2+}	$CaOH^{+}$	$CaSorb^{2+}$	$SorbCaOH^{+}$	$Sorb_2Ca_2(OH)_4$	$Ca_2Sorb_2H_2SiO_4(OH)_4^{-2}$	$Ca_2Sorb_2(H_3SiO_4)_2(OH)_2$
12.7	10	15	0.15	10.54	3.04	0.12	1.21	0.017	0.010	0.023
pH	Gl	Ca	Si	Ca^{2+}	$CaOH^{+}$	$CaGl^{+}$	GlCaOH	$Gl_2Ca_3(OH)_4$	$Gl_2Ca_2OH_2^{2-}$	$Ca_3Gl_2(H_3SiO_4)_2(OH)_2$
12.6	10	15	0.15	6.07	1.62	0.26	1.81	0.00	0.053	0.030

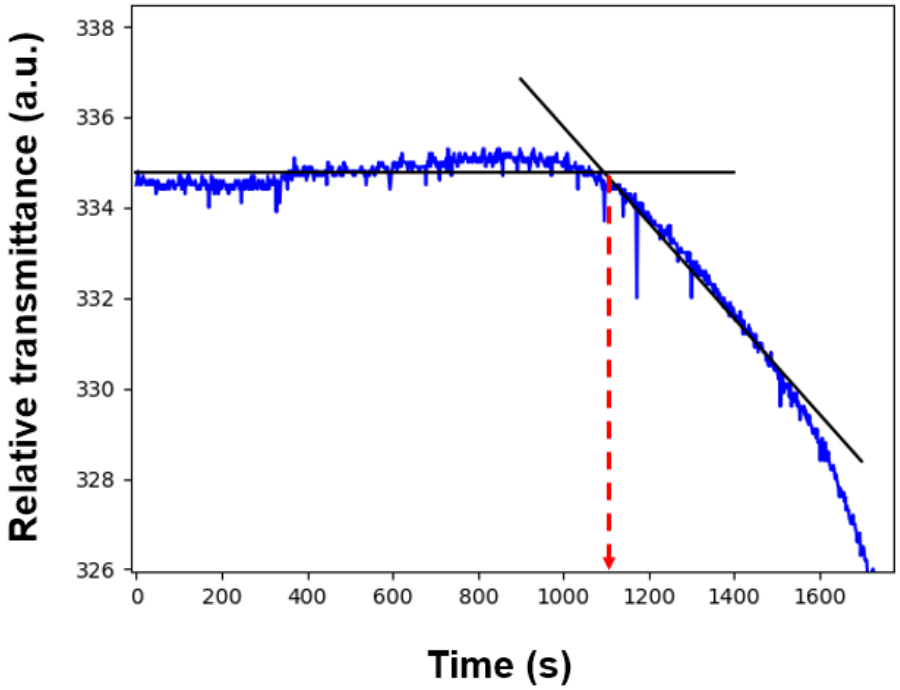

Figure S1. Method to determine the induction time from turbidity data, exemplified with the data from the pure system at [Si]=0.10mM. Two linear fits are performed to determine the point at which the transmittance of the solution starts to decay (indicated in red).

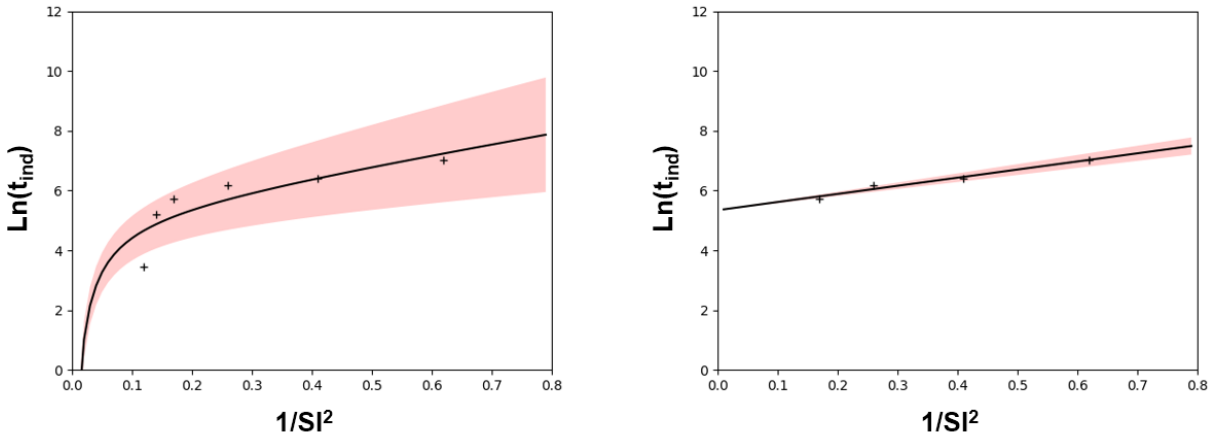

Figure S2. Left: Average values of the induction times for the pure system, together with a fit of the classical nucleation theory expression for the induction time (see eq. 1 in the main text). The equation includes a dependence of the kinetic pre-factor (C_0) with the supersaturation, which gives rise to the curvature. Right: Fit of the expression with C_0 being a constant, and using a fitting range that include only the points at lower supersaturations (i.e., high $1/SI^2$ values).

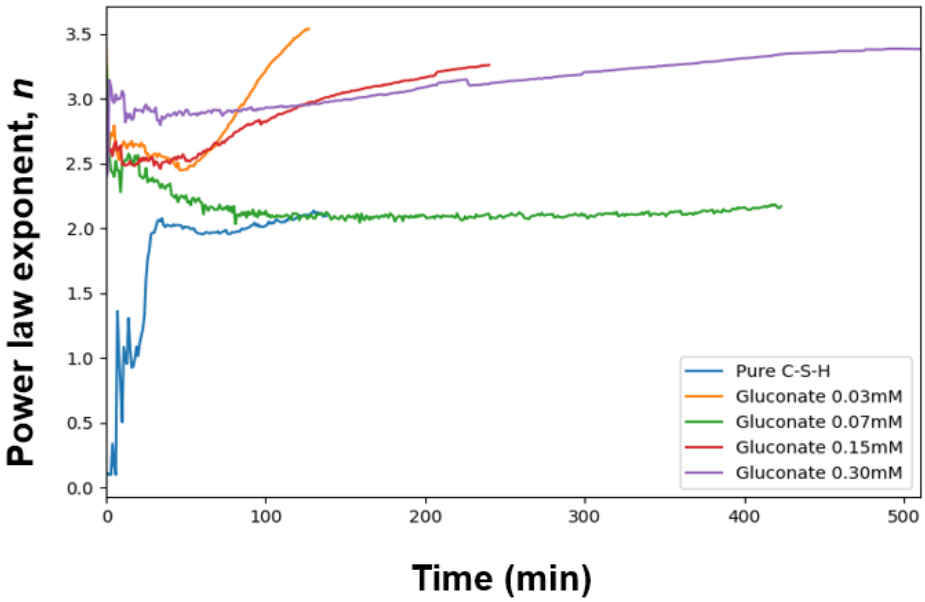

Figure S3. Values of the power law exponent used to fit low q part of the data using a $I = q^{-n}$ law.

ABSTRACT

Superplasticizers are nowadays commonly employed in concrete to improve its workability and mechanical performance. They generally have the side effect of retarding the hydration of Portland cement which results from two simultaneous reactions: the dissolution of cement grains and the precipitation of cement hydrates. The mechanisms responsible for this retardation and thus delay the setting time of cement remain however largely unexplained. The present work intended to tackle this puzzle from the perspective of cement hydrate formation and employing four small organic molecules as model for superplasticizers. In particular, the impact of these organics on the homogeneous nucleation of calcium silicate hydrate (C-S-H) was studied in detailed. The work further focused on the determination of the driving force of the nucleation (and dissolution) and thus on the determination and modeling of the ion speciation and organic complex formation with calcium, silicate and hydroxide aqueous species. The selected organics whether charged or neutral were all found to form a rich zoo of mono- and poly-nuclear complexes not only with calcium and hydroxide ions but also with silicate species. They were further successfully modeled with the speciation program PHREEQC. This allowed to compare and quantify the impact of the selected organic molecules on the nucleation rate of C-S-H. The nucleation rate was correlated to the complexation power of the organics. A modification of the C-S-H nucleation pathway induced by the organics was found for which the organic complexation with silicate and calcium ions seems to play a crucial role. More generally, the retardation power of the molecules on the hydration of alite, the main mineral phase of Portland cement, was found to correlate well with their impact on the nucleation rate of C-S-H.